NSWC TR 79-79

TRANSPARENT TUBE STUDIES OF BURNING TO DETONATION TRANSITION IN GRANULAR EXPLOSIVES I: PRELIMINARY FRAMING CAMERA STUDIES

BY HAROLD W. SANDUSKY RICHARD R. BERNECKER

RESEARCH AND TECHNOLOGY DEPARTMENT

27 OCTOBER 1980

NAVAL SURFACE WEAPONS CENTER

Dahlgren, Virginia 22448 • Silver Spring, Maryland 20910

UNCLASSIFIED

SECURITY CLASSIFICATION OF THIS PAGE *(When Data Entered)*

REPORT DOCUMENTATION PAGE		READ INSTRUCTIONS BEFORE COMPLETING FORM
1. REPORT NUMBER NSWC TR 79-79	2. GOVT ACCESSION NO.	3. RECIPIENT'S CATALOG NUMBER
4. TITLE *(and Subtitle)* TRANSPARENT TUBE STUDIES OF BURNING TO DETONATION TRANSITION IN GRANULAR EXPLOSIVES I: Preliminary Framing Camera Studies		5. TYPE OF REPORT & PERIOD COVERED Progress Sep 1976 - Dec 1977 6. PERFORMING ORG. REPORT NUMBER
7. AUTHOR(s) Harold W. Sandusky and Richard R. Bernecker		8. CONTRACT OR GRANT NUMBER(s)
9. PERFORMING ORGANIZATION NAME AND ADDRESS Naval Surface Weapons Center White Oak Laboratory, R13 Silver Spring, MD 20910		10. PROGRAM ELEMENT, PROJECT, TASK AREA & WORK UNIT NUMBERS 61152N; ZR00001; ZR01305; R0116
11. CONTROLLING OFFICE NAME AND ADDRESS		12. REPORT DATE 27 October 1980 13. NUMBER OF PAGES 99
14. MONITORING AGENCY NAME & ADDRESS*(if different from Controlling Office)*		15. SECURITY CLASS. *(of this report)* Unclassified 15a. DECLASSIFICATION/DOWNGRADING SCHEDULE

16. DISTRIBUTION STATEMENT *(of this Report)*

Approved for public release, distribution unlimited.

17. DISTRIBUTION STATEMENT *(of the abstract entered in Block 20, if different from Report)*

18. SUPPLEMENTARY NOTES

19. KEY WORDS *(Continue on reverse side if necessary and identify by block number)*

Deflagration to Detonation Transition (DDT)
Explosive
Sensitivity
Ignition
Flame Spread
Convective
Ignition
Combustion

20. ABSTRACT *(Continue on reverse side if necessary and identify by block number)*

Burning of relatively high porosity granular explosive charges, confined in transparent plastic tubes, was photographed with a framing camera. Observed luminous fronts corresponded to 1) the displacement of the charge from the ignitor by the mild gas pressure of the ignitor, 2) an increased rate of displacement once the explosive itself ignited, and 3) the propagation of flame down the charge. Luminous flame velocities were similar to convective ignition front velocities measured by

DD FORM 1 JAN 73 1473 EDITION OF 1 NOV 65 IS OBSOLETE
S/N 0102-LF-014-6601

UNCLASSIFIED

SECURITY CLASSIFICATION OF THIS PAGE *(When Data Entered)*

ionization probes in previous steel tube studies. In charges of 94/6 RDX/wax, luminous front velocities were similar to the high order compressive burning which followed the convective ignition front in steel tube studies. Although all these explosives tested previously in steel tube studies achieved a transition from deflagration to detonation, only coarse tetryl (470 μm) transited to detonation in the low confinement of the plastic tube.

FOREWORD

Burning of relatively high porosity explosive charges confined in transparent plastic tubes was photographed with a framing camera. The granular explosives (picric acid, tetryl, and RDX/wax) were among those materials in previous steel tube studies at NSWC which achieved deflagration to detonation transition (DDT). The relatively low confinement of pressure by plastic tubes is adequate for studying the early stages of DDT; the later stages of DDT were also observed in several materials and the onset of detonation was observed in one.

This research was carried out under IR 159 funded by the Independent Research Task ZR01305. The present results and conclusions from confined burning of porous explosives should be of interest in the areas of confined combustion and explosive sensitivity as well as that of safety and reliability.

Dr. Donna Price, the principal investigator for this task, provided invaluable guidance, review and encouragement. The authors thank Mr. Carl Groves for assembling and instrumenting the charges and performing much of the preparation for each shot, Mr. A. Robert Clairmont for assisting charge preparation, and Mr. Nick Vogel for maintaining the instruments. Frequent machine shop work was performed by Mr. James Deavers and Mr. Louis Reynolds. The assistance by Mr. Herman Gillum and Mr. Timothy Farrows in preparing experiments in the early stages of the program, the discussions and assistance of Dr. Peter DiBona concerning the developing flash radiography system, and the discussions with Mr. Karl Hoffman and Mr. Charles Grover about photography are appreciated.

Elihu Zimet

ELIHU ZIMET
By direction

CONTENTS

CONTENTS (Cont.)

ILLUSTRATIONS

TABLES

CHAPTER 1

INTRODUCTION

The experimental techniques used to study the deflagration to detonation transition (DDT) of explosives and propellants and the concurrent mechanistic interpretations have recently been reviewed[1]. The present work is an extension of the DDT studies at this Center. In earlier studies with porous explosives[2-8], ionization pins outlined the propagation of reaction fronts while strain gages

[1]Bernecker, R. R., "Experimental Techniques and Results for DDT of Propellants and Explosives," ONR/AFOSR Workshop on Deflagration to Detonation Transition, CPIA Publication 299, Sep 1978; pp. 187-216.

[2]Bernecker, R. R. and Price, D., "Studies in the Transition from Deflagration to Detonation in Granular Explosives. I. Experimental Arrangement and Behavior of Explosives which Fail to Exhibit Detonation," Comb. and Flame, Vol. 22, 1974, p.111.

[3]Bernecker, R. R. and Price, D., "Studies in the Transition from Deflagration to Detonation in Granular Explosives. II. Transitional Characteristics and Mechanisms Observed in 91/9 RDX/Wax," Comb. and Flame, Vol. 22, 1974, p.119.

[4]Bernecker, R. R. and Price, D., "Studies in the Transition from Deflagration to Detonation in Granular Explosives. III. Proposed Mechanisms for Transition and Comparison with Other Proposals in the Literature," Comb. and Flame, Vol. 22, 1974, p.161.

[5]Price, D. and Bernecker, R. R., "Sensitivity of Porous Explosives to Transition from Deflagration to Detonation," Comb. and Flame, Vol. 25, 1975, p. 91. See also NOLTR 74-186.

[6]Bernecker, R. R., Price, D., Erkman, J. O., and Clairmont, A. R., Jr., "Deflagration to Detonation Transition Behavior of Tetryl," Sixth Symposium (International) on Detonation, ACR-221, Office of Naval Research, U. S. Government Printing Office, Washington, D. C., 1978; pp.426-435.

[7]Bernecker, R. R., and Price, D., "Burning to Detonation Transition in Picric Acid," Proceedings of 17th Symposium (International) on Combustion, Combustion Institute, 1979; pp.55-62.

[8]Price, D. and Bernecker, R. R., "Effect of Wax on the Deflagration to Detonation Transition of Porous Explosives," Proceedings of Symposium (International) on High Dynamic Pressure in Paris, CEA, Saclay, France, 1978; pp.149-159.

monitored the build-up in pressure along explosive columns which were confined in thick-walled steel tubes. As a result of these studies, several questions have arisen: 1) what is the nature of the ignition events occurring before the response of the first ionization pin (typically located about 40 mm from the ignitor); 2) what characteristics (e.g. level of ionization or conductivity) are associated with convective ignition fronts; 3) does the convective flame front in picric acid cease to propagate before the appearance of the first detectable compressive wave and the subsequent onset of detonation; and 4) what events lead to accelerated pressure build-up shortly before the onset of detonation?

To extend our knowledge of DDT events and to answer these questions, a transparent plastic DDT tube arrangement was developed. With this system it is possible to observe photographically the progression of reaction in confined cylinders of porous explosives, from ignition to the onset of detonation, while simultaneously monitoring pressure build-up. In addition, an associated flash radiography system is nearly operational and will provide density profiles along the length of the explosive column at several discrete times in the predetonation period. The simultaneous measurement of various experimental parameters will provide a more complete understanding of the complex series of events leading to DDT.

The transparent plastic tubes cannot totally replace the steel tubes because of the lower confinement of gaseous products provided by the former. An important requirement for DDT is confinement; some explosives will not achieve a transition to detonation in a plastic tube whereas they will transit to detonation in a steel tube. Nevertheless the plastic tube experiment can provide valuable information for characterizing (delineating the nature of) the propagation of the relatively low pressure convective ignition front in addition to providing photographic recording of events just prior to detonation (when the latter does occur).

Studies of DDT in transparent configurations are not new[1]. However, there are several distinguishing features in this study. First, photographic coverage is with a framing camera rather than with a streak camera; full size frames of the side of the tube show many more details concerning the nature of the luminous zones although the streak camera defines more precisely the position of the onset of detonation. Second, the explosives which are used have exhibited in steel tubes relatively long times to detonation and long predetonation column length; it is an experimental advantage to spread out the events being studied. In this initial study the transparent tubes have been loaded with relatively porous charges (46-70% of theoretical maximum density (TMD)) of picric acid, tetryl and RDX/wax. Third, as mentioned above, several types of instrumentation are being used simultaneously.

The results of this study are expected to aid efforts in mathematical modeling of DDT in porous beds[9-11]. One deficiency in the present models, for example, is the representation of dynamic compaction of the explosive in the predetonation column. The flash radiography apparatus, when it is operational, should indicate the extent of dynamic compaction occurring in the predetonation time period. The mathematical models, as they develop, should also suggest the need for new experimental measurements.

[9]Beckstead, M. W. et. al., "Convective Combustion Modeling Applied to Deflagration-to-Detonation Transition," 12th JANNAF Combustion Meeting, Newport, Rhode Island, 11 Aug 1975.

[10]Krier, H. and Gokhale, S. S., "Modeling of Convective Mode Combustion Through Granulated Solid Propellant to Predict Possible Detonation Transition," AIAA/SAE 13th Joint Propulsion Conference, Orlando, Florida, 11 July 1977.

[11]Pilcher, D. T., Beckstead, M. W., Christensen, L. W., and King, A. J., "Comparison of Model Predictions and Experimental Results of Deflagration to Detonation Tests," AIAA/SAE 13th Joint Propulsion Conference, Orlando, Florida, 11 July 1977.

CHAPTER 2

EXPERIMENTAL ARRANGEMENT AND PROCEDURE

A. TRANSPARENT TUBE ARRANGEMENT

A schematic of the transparent tube system is shown in Figure 1. The tube (25.4 mm I.D., 75.6 mm O.D., 304.8 mm long) is machined from oil annealed polycarbonate rod made from Lexan 101-111 resin which is manufactured by General Electric. This material was selected because of its high Izod impact strength of 65-87 kg cm/cm[12] (ASTM test method D256, 3.2 mm thick notched sample). Another plastic which was considered and briefly tested is polymethyl methacrylate (PMMA); it has a lower impact strength, 1.0-1.6 kg cm/cm, and was found to fracture more readily. Although the tensile and compressive strengths of both (polycarbonate and PMMA) plastics are similar, about 0.62 kbar, it is the impact strength which better demonstrates the ability of the material to withstand rapid pressurization in the present arrangement. Even so, a polycarbonate tube provides low confinement of the gaseous products from the burning charge when compared to the steel tubes used in earlier studies.*

Lexan 101-111 has good transmittance of light (88-89%[12], ASTM test method D1003) although it is somewhat less than the 92% transmittance for PMMA. Recently it has been found that better transmittance through the Lexan could be attained by polishing the inner and outer surfaces of the tube with ethylene dichloride after machining and buffing. During this solvent polishing procedure a cloth wetted with ethylene dichloride is quickly wiped across the Lexan surfaces. There has been no evidence of surface stresses on Lexan tubes from solvent polishing (ethylene dichloride is even recommended for solvent bonding of Lexan), but excess solvent will dissolve some Lexan allowing dimensional distortions of the original surface.

As seen in Figure 1, the loaded tube is clamped between two 25 mm thick hot rolled steel plates using four threaded 19 mm diameter steel rods. The

[12]"Typical Properties of Lexan," General Electric, Publication CDC-570.

*In order to assess the effect of lower confinement of the Lexan system on DDT processes, precautions were taken to avoid drilling probe holes through the Lexan wall in the first half of the tube. Such probe holes would serve as stress concentration points and reduce even further the confinement of the system. Probe holes were drilled in the Lexan tube along the latter half of the explosive column and only for explosive systems in which a transition to detonation seemed likely.

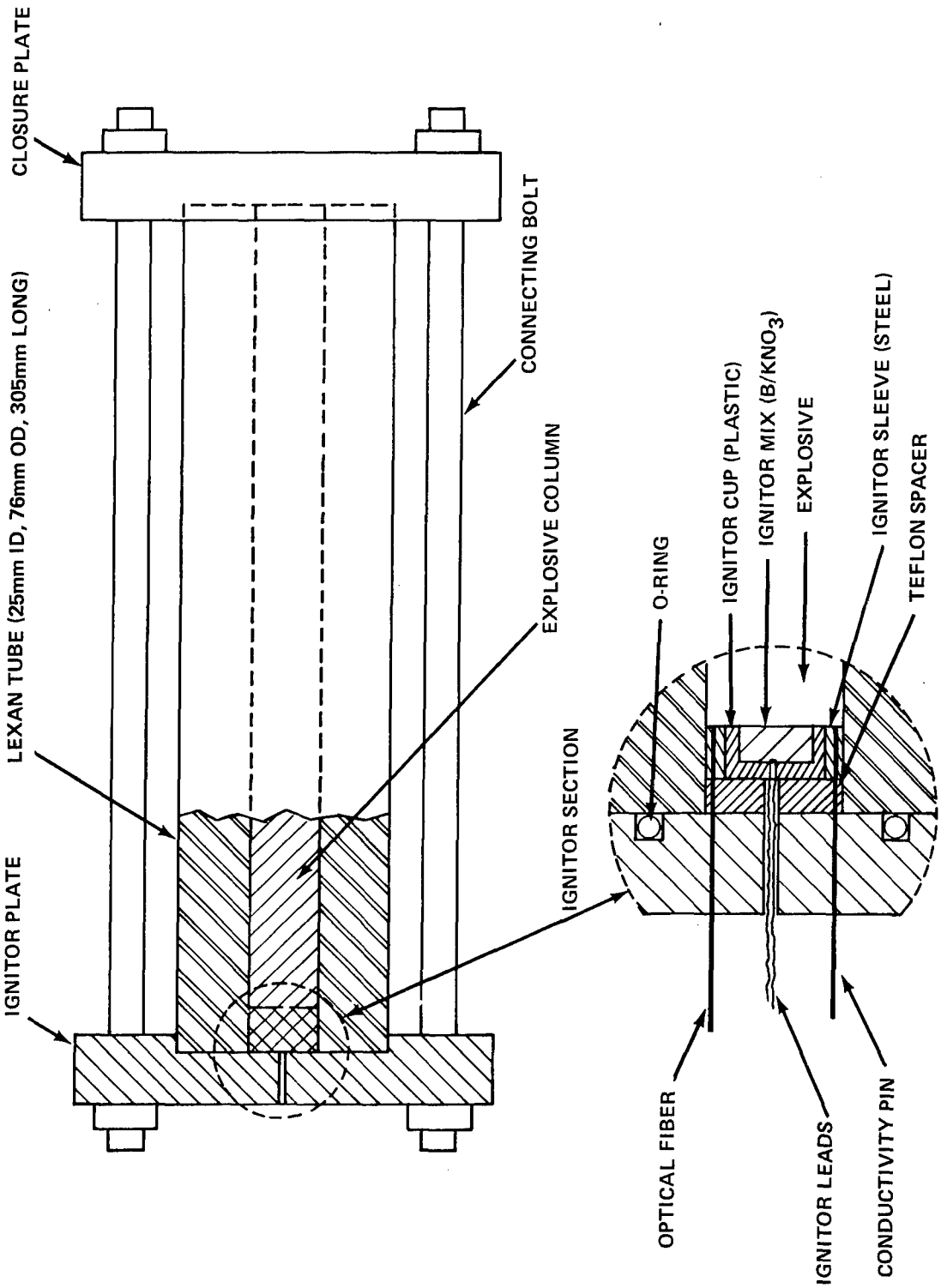

FIGURE 1 TRANSPARENT DDT TUBE

tube/closure plate interface is sealed by epoxy while the tube/ignitor plate interface is sealed by an O-ring. The ignitor section consists of a 9.5 mm long ignitor sleeve and ignitor, a 6.4 mm long Teflon spacer, and sometimes a 9.5 mm long steel spacer. The purpose of the spacers is twofold: 1) to move the zone of high pressure away from the end of the tube; and 2) to provide additional gas sealing at the end of the tube when the Teflon spacer deforms from rising pressure. Through the center of the ignitor plate and spacers there is an opening for ignitor leads; this opening is filled with epoxy when the tube is assembled. Through the entire ignitor section there are two small holes which can be used for positioning either conductivity pins or optical fibers at the explosive/ignitor interface. The pins or fibers are sealed into the ignitor plate with epoxy. In all future discussions, distances along the explosive column are relative to the ignitor/explosive interface; i.e., x = 0 at this interface.

B. REACTIVE COMPONENTS

1. IGNITOR. The ignitor is similar to that used in a steel DDT tube. About 0.75 gram of 25/75 B/KNO_3 is buttered into a thermally resistant plastic (Laminac) cup. The 6.4 mm deep cavity of the cup has a diameter of 15 mm, which is about 35% of the cross-section of the explosive column. The ignitor cup is recovered after most experiments showing little evidence of burning or melting.

To ignite the B/KNO_3, a 1 x 10 mil nichrome bridgewire in the bottom center of the cup is electrically heated by applying 30 VDC across long (~50 meter) firing leads. Current measurements in the firing leads show that the bridgewire heats up until it burns through within 1-2 ms after the voltage is applied. The average time from the first application of voltage to the appearance of luminosity at the face of the ignitor (the exposed surface of the ignitor mix which is adjacent to the explosive) varied from 5 to 25 ms, with the average being about 12 ms. A photographic study of flame penetration to the face of the ignitor is discussed in Appendix A.

2. EXPLOSIVE MATERIALS. All explosives used in this study have been used in earlier steel tube studies. The picric acid (X835) is from a commercial lot satisfying the military specifications and has an average particle size of 67μm. The coarse tetryl (X812) has an average particle size of 470μm and is also from a commercial lot satisfying military specifications. The 20μm or fine tetryl was prepared from the coarse tetryl by a turbulent mixing of its acetone solution with water to form a very fine grained precipitate. Particle size data for these three explosives are given in Appendix A of Reference 13.

The 94/6 RDX/wax (X893) and 97/3 RDX/wax (X758) were mechanical mixtures prepared from Class A RDX (X597) and carnauba wax (N134). The weight mean particle size of the wax was about 125μm while that of the RDX was 200μm (see Appendix B of Reference 14 for particle size analysis of the RDX material).

[13] Price, D., Bernecker, R. R., Erkman, J. O., Clairmont, A. R., Jr., "DDT Behavior of Tetryl and Picric Acid," NSWC/WOL/TR 76-31, 31 May 1976.

[14] Bernecker, R. R. and Price, D., "Transition form Deflagration to Detonation in Granular Explosives," NOLTR 72-202, 13 Dec 1972.

When an explosive was being loaded into a Lexan tube it was pressed in increments of 12.7 mm to insure a more uniform density along the length of the charge. Most charge densities were low enough for the tubes to be loaded by hand. The tubes with picric acid at 68% and 70% TMD were loaded with the same 300 ton hydraulic press and loading apparatus used for loading steel DDT tubes.

C. INSTRUMENTATION OF TRANSPARENT TUBES

The various instrumentation used in this study and the associated experimental data are listed in Table 1 and discussed in the following sections. The flash radiography apparatus has been used only in exploratory work. A schematic of the arrangement of this instrumentation on and around the transparent tube is shown in Figure 2.

1. OPTICAL FIBERS/PHOTODETECTORS. Optical fibers terminated by photoconductive cells are used to detect luminance from reaction of the charge for the purpose of triggering other recording instrumentation. The two probes shown in Figure 1 at the ignitor/explosive interface trigger a set of recording oscilloscopes and an electronic flash, which backlights the transparent tube apparatus. There was one optical fiber and one conductivity pin in early experiments (see next section), while in later experiments both probes were optical fibers. With two optical fibers the uniformity of luminosity across the ignitor/explosive interface is determined. Although the optical fibers are always located at the same positions on the interface, even uniform breakout of burning from the ignitor mix does not assure detection of the luminous ignitor products at the same time. The luminous gases will be cooled as well as flow into the porous explosive charges differently depending upon the characteristics (such as permeability) of the porous explosive. If a process occurs in the porous explosive (such as melting) that provides more intimate contact and absorbs more heat, then the luminosity associated with the hot ignitor gases may be delayed in arriving at the location of the optical fiber.

Another optical fiber located at 76 mm (from the ignitor/explosive interface) triggers a second set of recording oscilloscopes after burning has begun. Because this fiber is inserted only 2 mm deep into the exterior tube wall, it can be illuminated by burning or extraneous light before a luminous front has propagated to 76 mm. However, it was considered undesirable to weaken the tube by drilling a small hole through the wall and locating the optical fiber at the Lexan/explosive interface.

The optical fibers are cut to a length of 305 mm from a 1 mm diameter, single strand of Crofon, a plastic material developed by duPont. The ends are sanded flat with 600 grit sandpaper and then solvent polished. Crofon transmits light of wavelengths from 310 to 1330 nanometers with 9% light loss for each 305 mm.

Terminating the optical fibers are Model CL703 photoconductive cells manufactured by Clairex Corp., Mount Vernon, NJ. Their peak spectral response at 735 nanometers (in the near infra-red) is appropriate for the detection of burning. Their response time to light from darkness decreases as the illuminance increases. According to the manufacturer, the response time decreases from 5 ms at 10 ft-candles to 2 ms at 100 ft-candles. A 2 ms response time is too slow

TABLE 1

DATA ACQUISITION

INSTRUMENTATION	TYPE OF DATA	OBSERVED PHENOMENA
FRAMING CAMERA	LUMINOUS EVENTS	IGNITER PRODUCTS CONDUCTIVE BURNING CONVECTIVE IGNITION FRONTS COMPRESSIVE IGNITION FRONTS DETONATION WAVES
FLASH RADIOGRAPHY UNIT	DENSITY VARIATIONS, TUBE DEFORMATION	COMPACTION VOIDS
STRAIN GAGES	TUBE EXPANSION	GAS PRESSURE
CONDUCTIVITY PINS	REACTION CONDUCTIVITY	IONIZATION/CONDUCTIVITY
OPTICAL FIBERS/ PHOTODETECTORS	LUMINOUS INTENSITY	IGNITION AND BURNING, BOTH AT PERIPHERY OF AND WITHIN POROUS BED

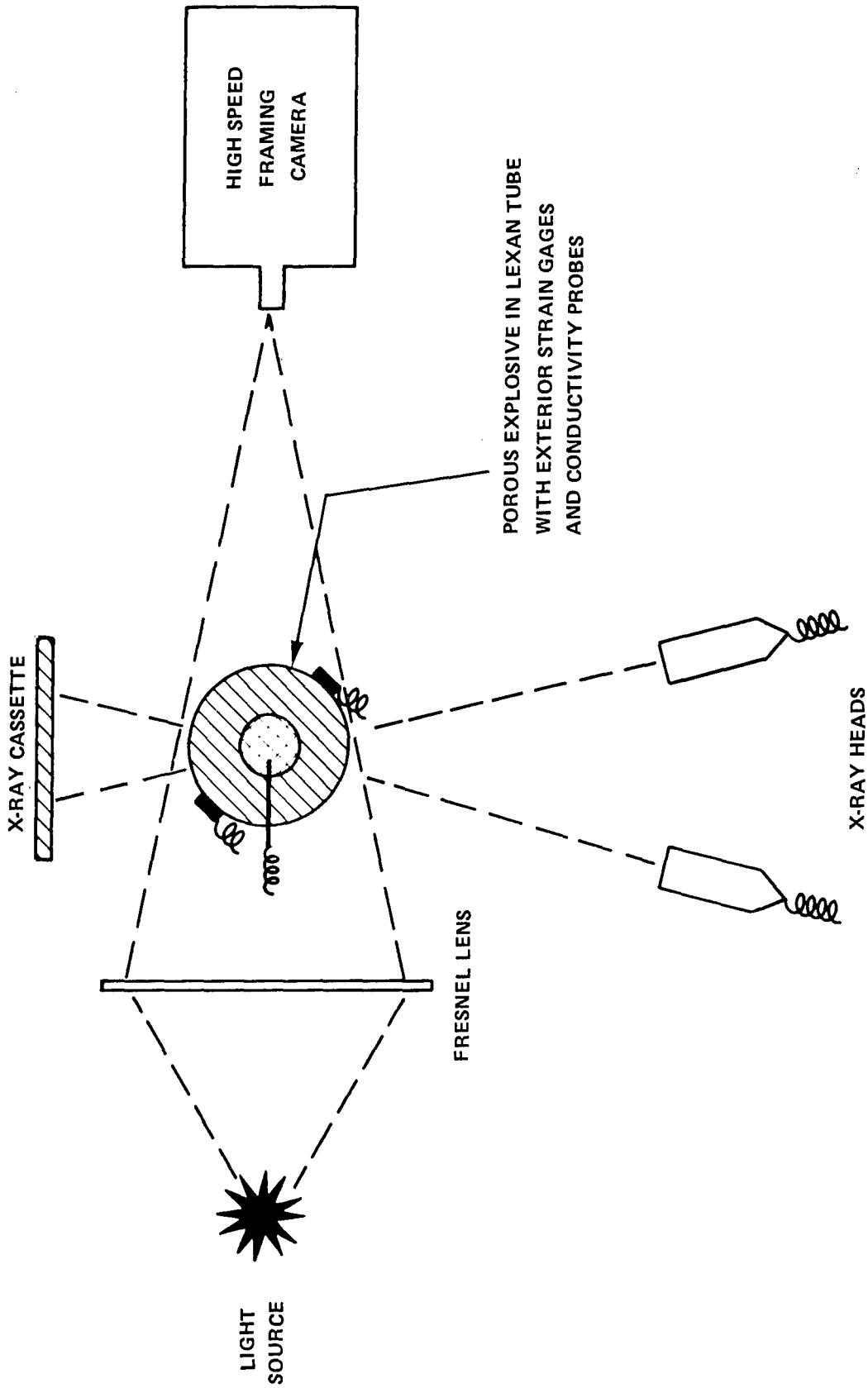

FIGURE 2 EXPERIMENTAL ARRANGEMENT

for DDT experiments; however, as described in Section C.5.b., the photocells detect luminous ignitor products before the framing camera. This indicates that the illuminance of a photocell during burning of the ignitor mix is much greater than 100 ft-candles. If the illuminance from burning of the ignitor mix is, for example, the same as that from a photographer's electronic flash several centimeters away, the photocell will respond in 10μs.

The circuitry used with the optical fiber/photocell arrangement is a 9 volt voltage divider; it consists of the photocell in series with a 10kΩ resistor, across which the output voltage is measured. In darkness the photocell resistance is at least 10MΩ and there is almost zero output voltage. As the illuminance increases, the photocell resistance decreases and the measured voltage across the 10kΩ resistor increases. For an illuminance ≥ 1000 ft-candles the photocell resistance is less than 100Ω and the output signal is essentially 9 volts.

Two varieties of these cells are used; with an illuminance of 2 ft-candles Model CL703L has a resistance of 2.7kΩ while Model CL703M has a resistance of 30kΩ. In the measurement circuitry the output signal will be 7.1 volts for the CL703L photocell and 2.25 volts for the LC703M photocell for the same illuminance of 2 ft-candles. Since triggering is set for an output signal level of usually 2.5 to 3 volts, the lower resistance CL703L photocell will trigger at lower illuminance and so is generally used. The higher resistance CL703M photocell is sometimes used with the optical fiber, in the exterior tube wall, at 76 mm in order to trigger at higher illuminance because this position is exposed to both stray light from the electronic flash backlighting and the approaching flame front (i.e., a longer delay time is desired for triggering the second set of oscilloscopes).

Since a camera can observe only the cylindrical explosive/Lexan interface, it would be instructive to implant optical fibers in the explosive charge and compare the arrival of luminous fronts inside the charge to that at the periphery of the charge. Such a study has begun and will be the subject of a future report.

2. CONDUCTIVITY PINS. Conductivity pins were used as an alternate trigger source and as a means of measuring the velocity of reaction fronts (e.g., detonation velocity). The pins are the same commercial ionization pins used in steel DDT tube studies[14] (now manufactured by Dynasen, Inc., Goleta, CA, model CA-1040). They consist of a central brass conductor surrounded by Teflon that, in turn, is encased by a brass tube with an outside diameter of 0.81 mm. These pins were used in the same 9 volt voltage divider system used for photocells. With a fixed resistor of 10kΩ, the resistance of the pin environment can be continuously measured over an effective range of 1kΩ to 100kΩ. The use of this pin with circuitry that continuously monitors conductivity can be more instructive than with circuitry that responds only to a given level of ionization. For example, the measurement of conductivity might serve to distinguish a convective ignition front from a compressive ignition front.

In charges which are expected to detonate, conductivity pins have been inserted through the Lexan tube and into the explosive column in order to get an accurate measurement of detonation velocity along the latter part of the charge and help locate the onset of detonation. Since the framing camera minimum interframe time is 40μs, it is not likely that two successive frames showing the detonation wave will be obtained to provide even an average detonation velocity before the wave reaches the end of the explosive column. Likewise, the camera frames preceding and following the onset of detonation can only roughly bracket the location of the onset.

In early work a conductivity pin at the ignitor/explosive interface was used, in conjunction with an optical fiber/photocell, for triggering the recording oscilloscopes and electronic flash. This pin, in the conductivity mode, did not reliably respond to the reaction causing the luminance detected by the optical fiber/photocell and hence its use as a trigger device was discontinued.

3. STRAIN GAGES AND PISTON GAGE. Generally five pairs of strain gages (SG) are mounted on the exterior of the Lexan tube along the predetonation column in order to monitor continuously the build-up of pressure. The type of strain gages used in this study as well as their Wheatstone measuring circuits are described in Reference 14.

The sensitivity of the strain gages on the exterior of a Lexan tube to internal pressure is about one hundred times that for a steel tube. In Reference 5 the strain gage response for a steel tube was statically determined to be 112 microstrain units (με) per kbar, up to the elastic limit of 2.2 kbar. For the Lexan tube the strain gage response is calculated to be 10,790 με/kbar up to an elastic limit of only 0.28 kbar (Young's modulus of elasticity = 23.8 kbar). A static calibration up to only .034 kbar agreed with the calculated strain gage response on a Lexan tube; higher pressure static (and also dynamic) calibrations are planned.

When reporting strain gage data (i.e., strain as a function of time), no correction has been made for the transit time of a pressure change through the Lexan tube wall. For a sound velocity of 2.22 mm/μs[15] in polycarbonate at room temperature, the transit time through a 25 mm thick wall is 11.3μs. This time is small compared to the total time during which events are occurring in the predetonation column of Lexan tube experiments. However, when correlating pressure (strain) with a luminous front, this correction will be significant when front velocities are high (e.g., ≥1mm/μs) or when rates of pressurization are high (e.g., ≥ 0.01 kbar/μs).

Sometimes a piston gage is inserted between the explosive column and the closure plate in order to observe directly the pressure build-up at the end of the column. The schematic of a prototype piston gage in Figure 3 shows it to be essentially a Lexan cylinder with two axially mounted strain gages. The strain gages, which measure compression of the Lexan cylinder, have tape wrapped over them for isolation from hot gases. Since the length of the piston gage is too short for uniform strain across the cylinder at the strain gage locations, each piston gage is calibrated prior to use. Rather than try to seal the

[15]Phillips, D. W. et al., "Ultrasonic Studies of Polycarbonate, Polysulfone, and Polyether Sulfone," Journal of Applied Polymer Science, Vol. 21, 1977, p.1859.

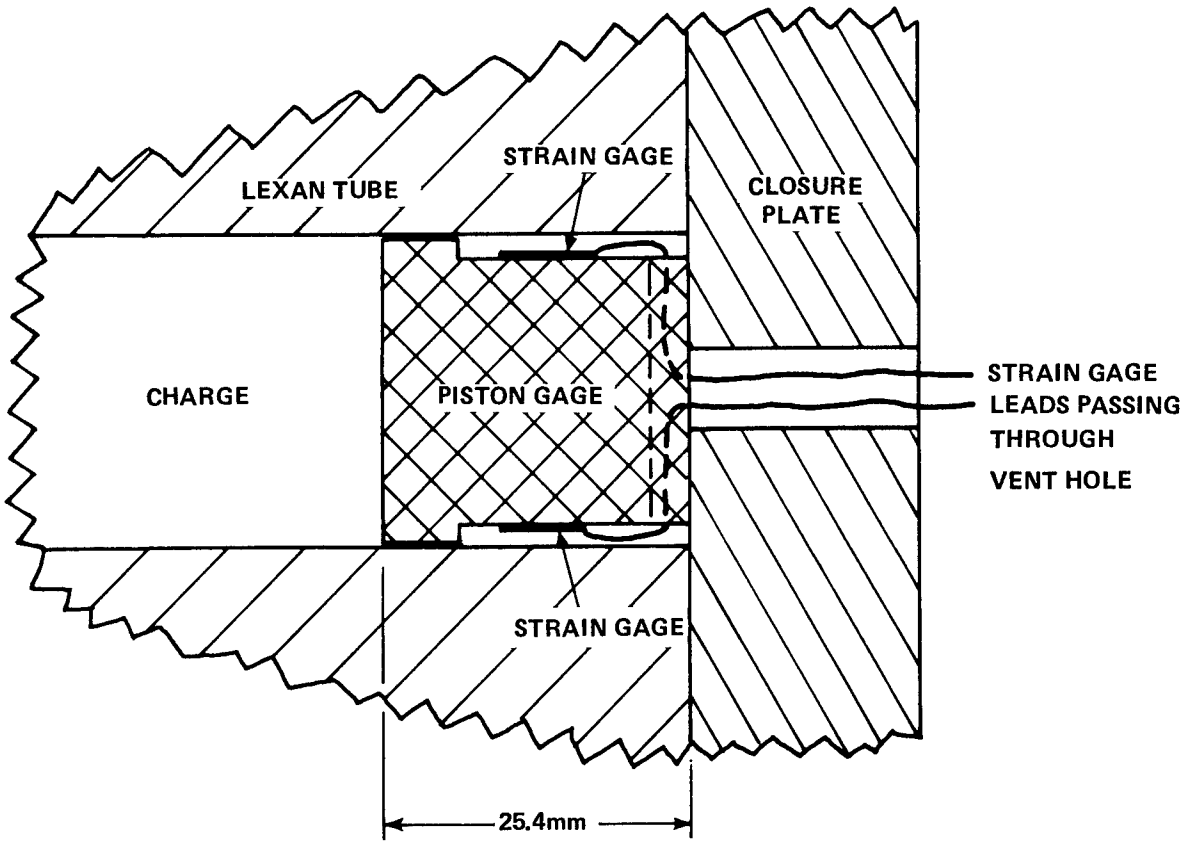

CROSS-SECTION OF GAGE IN TUBE ASSEMBLY

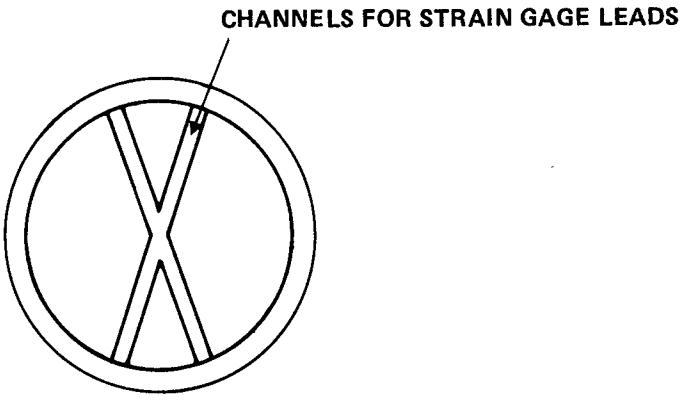

VIEW OF GAGE FROM CLOSURE PLATE

FIGURE 3 LEXAN PISTON GAGE

interface between the tube and the outer diameter of the piston, any combustion gases are allowed to pass by the piston and vent through the hole in the closure plate through which the strain gage leads pass.

4. RECORDERS FOR PROBES AND GAGES. The responses from photocells, conductivity pins and strain gages are recorded on as many as eight oscilloscopes and a Probe Sequence and Time Interval Recorder (IPR). Six of the oscilloscopes are dual beam Tektronix model 5444's, one is a dual beam Tektronix model 556, and the other is a Tektronix model 454. The IPR, which was designed and built at NSWC/WOL (see Appendix C), will display the order of a sequence of eight events and measure the time interval between them.

A range of sweep rates for the oscilloscopes are required for recording the widely different rates at which events proceed during the DDT mechanism. For the relatively slow ignition and initial burning processes, several oscilloscopes recording the strain gage and probe traces of interest with slow sweep rates are simultaneously triggered during the ignition process by an output pulse from the IPR. This output pulse is generated when any input first triggers the IPR; usually this is the detection of luminance at the ignitor/explosive interface by an optical fiber/photocell. For the rapid events occurring late in the DDT mechanism, other oscilloscopes with rapid sweep rates are often internally triggered near the onset of these events. The "A^{+}Gates" of these oscilloscopes are connected to input channels of the IPR. Thus the response time of all probes and the triggering times of the oscilloscopes are precisely known to a tenth of a microsecond relative to each other.

5. HIGH-SPEED PHOTOGRAPHY. The present arrangement for photography of luminous reactions in the Lexan tubes is simply a framing camera viewing the backlighted Lexan tube through a window in the firing chamber (see Figure 2).

a. Cameras. Any camera is limited to viewing the cylindrical interface between the Lexan tube and the explosive column. A streak camera continuously observes this interface along only a single axis, thus yielding no information about irregular flame front propagation. With the full view frames of the framing camera nearly one half of the interface is visible, and with mirrors or another camera, the entire lateral surface of the explosive charge is visible. The streak camera has the advantage of being able to follow continuously the progress of reaction fronts. For example, a continuous access streak camera precisely records the position of the onset of detonation whereas this event will probably occur between frames of the framing camera.

A better, and also more difficult, arrangement for photographic recording is to use simultaneously framing and streak cameras. Thus far only a framing camera has been used but a new continuous access streak camera is now available and will on occasions be used with the framing camera in future experiments, especially for the more energetic explosives.

A Beckman and Whitley Model 326 Dynafax framing camera is currently used to record luminous events. This is a continuous access, rotating drum camera which will record 224 frames of 16mm size at a maximum rate of 25,000 fps. The continuous access feature is required for these experiments because the time at which ignition of the explosive occurs, once the ignitor is energized, cannot be

predicted within the available writing time of any camera requiring synchronization with the event. Unfortunately, the continuous access feature does permit the camera to overwrite after 9 ms at the maximum framing rate. Hence, for charges which can be luminous for as long as 9 ms, such as the relatively slow burning picric acid, the camera views the change via a mirror which is broken by a detonator before overwriting can occur.

Often the density on our high speed camera films from luminous fronts was so weak that interpretation and data reduction from the films was difficult. Some of the reduced data from our camera films may suggest areas where there is no luminosity and it would appear there should be. In addition, in reducing data from camera films there were occasions when a luminous peninsula appeared; the front of this peninsula was plotted, despite the nonplanarity of this more forward luminous front.

b. Backlighting and Time Reference of Film with Other Instrumentation. The transparent tube apparatus is backlighted with an electronic flash which is located near the focal point of a Fresnel lens. During an explosion only the xenon tube of the electronic flash is destroyed; the flash circuit is located nearby in a protective box. The energy for the flash is stored in a 1000μf capacitor at 350 VDC. A 5 ohm resistor in series with the xenon tube lengthens the light pulse to about 5 ms and reduces the peak light intensity which otherwise overexposes the film.

The backlighting serves several purposes. First, the silhouette of the apparatus provides a spatial frame of reference for the luminous fronts. Second, the silhouette of the tube shows any expansion of the exterior tube wall from internal pressure. Third, the first appearance of backlighting establishes a time reference for the images on the camera film with data from other recording instruments. The electronic flash circuit is triggered at a known time relative to the other recording instruments by the "A^{+}Gate" of one of the oscilloscopes. For data reduction the first appearance of backlighting on the film is arbitrarily taken as the trigger time. Therefore, the time origin of the film data lags the time origin of the oscilloscope data by as much as 50μs, the interframe time (40μs at the maximum framing rate) plus the response time of the electronic flash (~10μs).

For these experiments the source of the trigger pulse for the electronic flash has been the detection of luminance at the ignitor/explosive interface by an optical fiber/photocell. (This probe (see Section 2.C.4.) started the IPR which in turn triggered oscilloscopes, one of which triggered the electronic flash.) Even neglecting the delay in the appearance of backlighting on the film discussed in the previous paragraph, the backlighting generally preceded by at least 40μs the first appearance on the camera film of luminous gases from burning. Thus, the first appearance of luminous gases on the film cannot be assumed to be the beginning of reaction as detected by an optical fiber/photocell or a probe. In establishing a time reference between a camera film and other recording instruments, a precise marker, such as an electronic flash, must be imaged on the camera film.

There are several reasons why the optical fiber/photocell responds at a different time from that of the appearance of luminous gases on the camera film. The first is that the response of the optical probe and the camera film to the same luminous gases will be different. Second, the optical probe does not view exactly the same luminous gases. Note that in Figure 1 the end of the fiber at the ignitor/explosive interface is about 1 mm from the inner tube wall viewed by the camera. Despite this short distance, luminous gases propagating across the ignitor/explosive interface at even a relatively rapid rate, 0.10 mm/μs, would require an additional 10μs to get from the end of the optical fiber to the inner tube wall. In addition, the luminance of the gases will be declining as they propagate between the room temperature porous explosive and steel ignitor sleeve.

c. Types of Film and Processing. Several types of high speed film are being used in the framing camera. The best results have been obtained with Kodak 2484, a moderately coarse panchromatic film, when processed in Kodak D-19 developer. Since burning is being observed, high speed films with extended red sensitivity (Kodak 2475) and near infrared sensitivity (Kodak 2481) were tried but showed no improvement over the panchromatic film (Kodak 2484). Some experimenting was done with Kodak Ektachrome 5241 color film but the image quality was poor after "pushing" the development process "2½" stops. Another color film (Kodak EPD 404) will be tested in the future. It is planned to improve the film quality by replacing the diamond stops, which control the shuttering of the framing camera, with rectangular stops which will effectively double the light exposing each image. This will allow the use of finer grain black and white film and reduce the need to "push" the color film during processing.

6. FLASH RADIOGRAPHY. Flash radiograms will indicate relative density along the length of the porous bed and tube deformation at various discrete times during the DDT process. With the available equipment two radiograms can be taken during an experiment in conjunction with photography and instrumentation on the tube. Each radiogram requires a separate x-ray head, but as shown on Figure 2, one x-ray cassette can be used with each x-ray head exposing approximately half of the film.

The flash radiography equipment consists of Field Emission Corporation Model 235 x-ray heads and pulsers. The 100-150 kilovolt pulsers have a pulse width of 0.1μs. Because the x-ray heads are in the firing chamber about a meter from the optical tube, each head is encased in an aluminum canister for protection. In addition, the section of each high voltage cable that is in the firing chamber is in a canvas hose for protection.

Kodak X-Omat XRP-5 film is used with DuPont Cronex Quanta II intensifying screens for image amplification. The film and screens are placed in a cardboard folder whose edges are sealed by black tape. The film folder is packed in an open faced steel box made from 12.7 mm thick plate. In front of the film holder there is 6.4 mm of glass (facing the charge), 6.4 mm of Lexan, 12.6 mm of Celotex (a fibrous wall board or ceiling tile material), 6.4 mm of Lexan, and another 12.6 mm of Celotex. Behind the film holder there is 38.1 mm of Celotex and corrugated cardboard with a 3.2 mm lead sheet in the bottom of the box. A lid, with an opening in the center for the x-rays, clamps the protective layers and film holder in the steel box. The face of the steel box (the glass layer) is

located 30.5 cm from the center of the charge if it is expected to transit to detonation. Since moving the x-ray film away from the charge and placing solid material in front of the film both reduce x-ray intensity, a balance must be found between protecting and still adequately exposing the film.

Flash radiograms were successfully obtained when no film protection was used during a dynamic compaction experiment in which the tube did not rupture (see Appendix B). Since the end of the study being reported here, successful flash radiograms were obtained of charges which transited to detonation using the above procedure for protecting the film.

CHAPTER 3

EXPERIMENTAL RESULTS

Since the initial objective of this experimental program was to determine the feasibility of this transparent tube apparatus to study the mechanism of transition to detonation, a variety of explosives were tested generally at a single packing density. These experiments are summarized on Table 2 and discussed in detail in the following sections.

A. PICRIC ACID

In steel tube experiments picric acid[7], at packing densities from 62.7 to 70.9% TMD, exhibited a decelerating convective flame front which failed to propagate to the end of the tube. Following a delay period of as long as 650μs, accelerated pressure build-up did occur near the ignition region, leading to the propagation of compressive waves and a transition to detonation. Picric acid has been studied here in Lexan tubes at 60, 68, and 70% TMD to determine if convective flame front failure, as outlined by ionization pin responses in steel tubes, can be observed photographically.

1. PICRIC ACID AT 59.7% TMD (SHOT S41). The highest density that 67μ picric acid could be hand loaded in a Lexan tube was found to be 1.05 g/cc (59.7% TMD). It was anticipated that the experimental results would be similar to the lowest density, regular steel tube tests at 62% TMD[7] in which a failing convective front reaches the end of the tube prior to a transition to detonation. In these steel tube tests the pressures behind the burning front, prior to reaching the end of the tube, are low enough to preclude rupture of the Lexan tube; therefore, the effects from the lower strength of the Lexan should be minimal.

The progress of the luminous front for the 59.7% TMD (1.05 g/cc) picric acid experiment as recorded by the framing camera is shown in Figure 4. In this distance-time plot, as well as all following ones, distance is relative to the ignitor/explosive interface and time is relative to the first detection of light by an optical fiber/photocell at the ignitor/explosive interface. As is usually the case, the first detection of light by an optical fiber/photocell preceded the first appearance of luminosity within the tube (as seen on the framing camera film); in this case the time interval was 158μs. A relatively slow luminous front, which will be called an ignitor front, propagated first at 0.041 mm/μs for 750μs and then at 0.026 mm/μs for the next 700μs. By 2000μs the progress of the ignitor front had stopped at 48 mm; subsequently, the luminous zone between the ignitor and the front began to fade in intensity and was no longer visible after another 500μs indicating cessation of burning.

TABLE 2

SUMMARY OF TRANSPARENT DDT TUBE EXPERIMENTS

SHOT NUMBER	MATERIAL	DENSITY (g/cc)	DENSITY (%TMD)	V_{IF}[b] (mm/μs)	V_{CIF}[b] (mm/μs)	COMP. VEL. (mm/μs)	ℓ (mm)	COMMENTS
S41	Picric Acid	1.05	59.7	.041	f	0.62[a]	f	Burning front failed after ignitor front
S51	Picric Acid	1.20	68.2	.023	0.33	d	f	3 ms delay between end of ignitor front and burning
S43	Picric Acid	1.23	69.9	.037	0.23-.52	1.20[a]	f	1 ms delay between end of ignitor front and burning
S42	20μm Tetryl	0.80	46.2	.056	0.4	*	≥280	Possible transition to detonation at end of charge
S49	470μm Tetryl	1.00	57.8	.038	0.45	1.14[a]	150-200	Definite transition to detonation
S37	94/6 RDX/Wax	1.20	69.8	.013	*	0.85[b]	f	Lexan tube ruptured behind .85 mm/μs compressive front
S40	94/6 RDX/Wax	1.20	69.8	.013	*	0.85[b]	f	16.8 mm ID tube ruptured behind .85 mm/μs compressive front
S52	97/3 RDX/Wax	1.15	65.3	.010	0.4	~1.0[c]	f	Lexan tube ruptured behind .4 mm/μs convective front

V_{IF} = Ignitor front velocity

V_{CIF} = Convective ignition front velocity

Comp. Vel. = Compressive front velocity

ℓ = Predetonation column length

a = Strain gage records
b = Film record
c = Conductivity Pin data
d = Insufficient data
f = Failure
* = Not observed

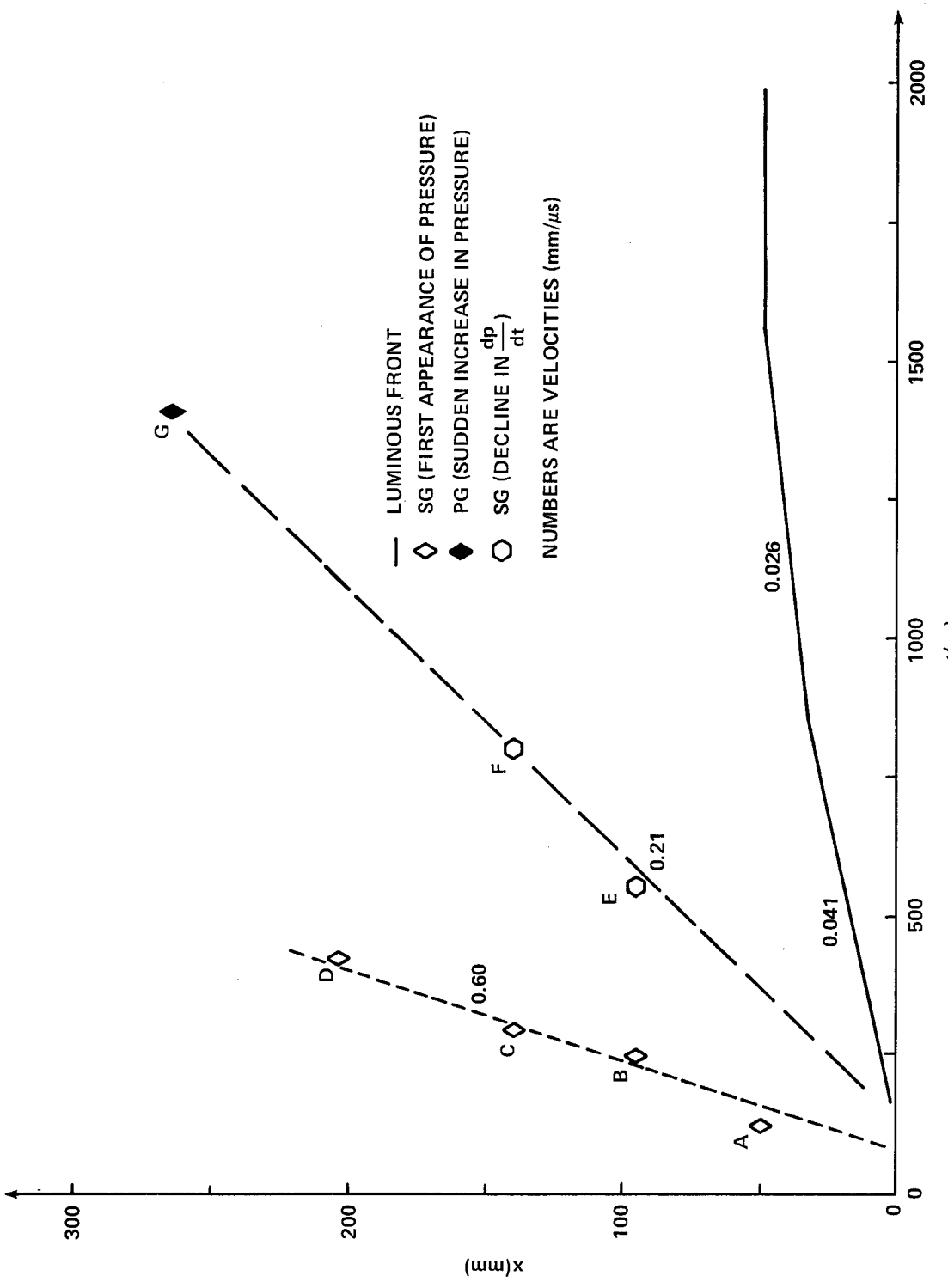

FIGURE 4 DISTANCE-TIME DATA FOR PICRIC ACID (59.7% TMD), SHOT S41

There were four strain gages (SG) along the tube and a piston gage (PG) at the end of the picric acid column. The traces from these gages are in Figure 5; the letters in Figure 5 located at changes in the rate of strain are the same letters associated with the diamonds in Figure 4.

About 75μs before the first appearance of light on the film a pressure front with a velocity of 0.60 mm/μs began propagating from the ignition zone. As this pressure wave propagated down the charge the succeeding strain gages had a lower $\frac{d\varepsilon}{dt}$ following the first appearance of strain. Thus, it appears that a weak compressive wave was associated with the ignitor front, but the rate of burning in the ignition zone was not sufficient to maintain the compressive wave's strength as it propagated from the ignition zone. The piston gage detected one sudden change in pressure about 1000μs after the postulated compressive wave should have arrived. It is interesting to note that the pressure leveled off rather abruptly at the 95 and 140 mm gage locations and that the times at which $\frac{d\varepsilon}{dt}$ declined can be plotted along with the response of the piston gage to generate a 0.21 mm/μs front originating from the ignition zone at the same time as the first appearance of light on the film. This may be a front of longitudinal compaction.

All gages recorded peak pressures at about 2 ms; thereafter, the pressure at each gage location remained nearly constant for the remaining 8 ms of the recording period (only the first 3 ms of the recording period is shown on Figure 5). The nearly constant pressure after the ebbing of luminosity indicates that a sudden loss in pressure was not responsible for the extinction of burning. After 2 ms the pressure recorded by the strain gages were also relatively uniform over the length of the charge, but the pressure recorded by the piston gage was significantly lower. (The conversion from strain to pressure is discussed in Section 2.C.3.) The location of each gage and its maximum pressure measurement (at about 2 ms) were:

Gage	Position (mm)	Pressure (kbar)
SG	51	0.18
SG	95	0.15
SG	140	0.14
SG	203	0.14
PG	267	0.04

Since the pressure in the tube had remained low, the tube was recovered intact. There was a void between the ignitor and the picric acid column about 40 mm long in the center of the tube cross-section and about 48 mm long near the inner tube wall, which corresponds to the 48 mm long zone of luminosity seen on the camera film. Some of the picric acid near the ignitor had been melted; across the center of the picric acid column there were large particles, several millimeters in diameter, of resolidified picric acid and patches of resolified picric acid over the remaining visible cross-section. The x-ray of the recovered tube in Figure 6 shows nonuniform density between 40 and 82 mm from the ignitor. (The distance between numbers on the scale of the x-ray corresponds to 23.7 mm.) This nonuniform density, which indicates channels and voids throughout the picric acid column, extends 8 mm before and 34 mm beyond the

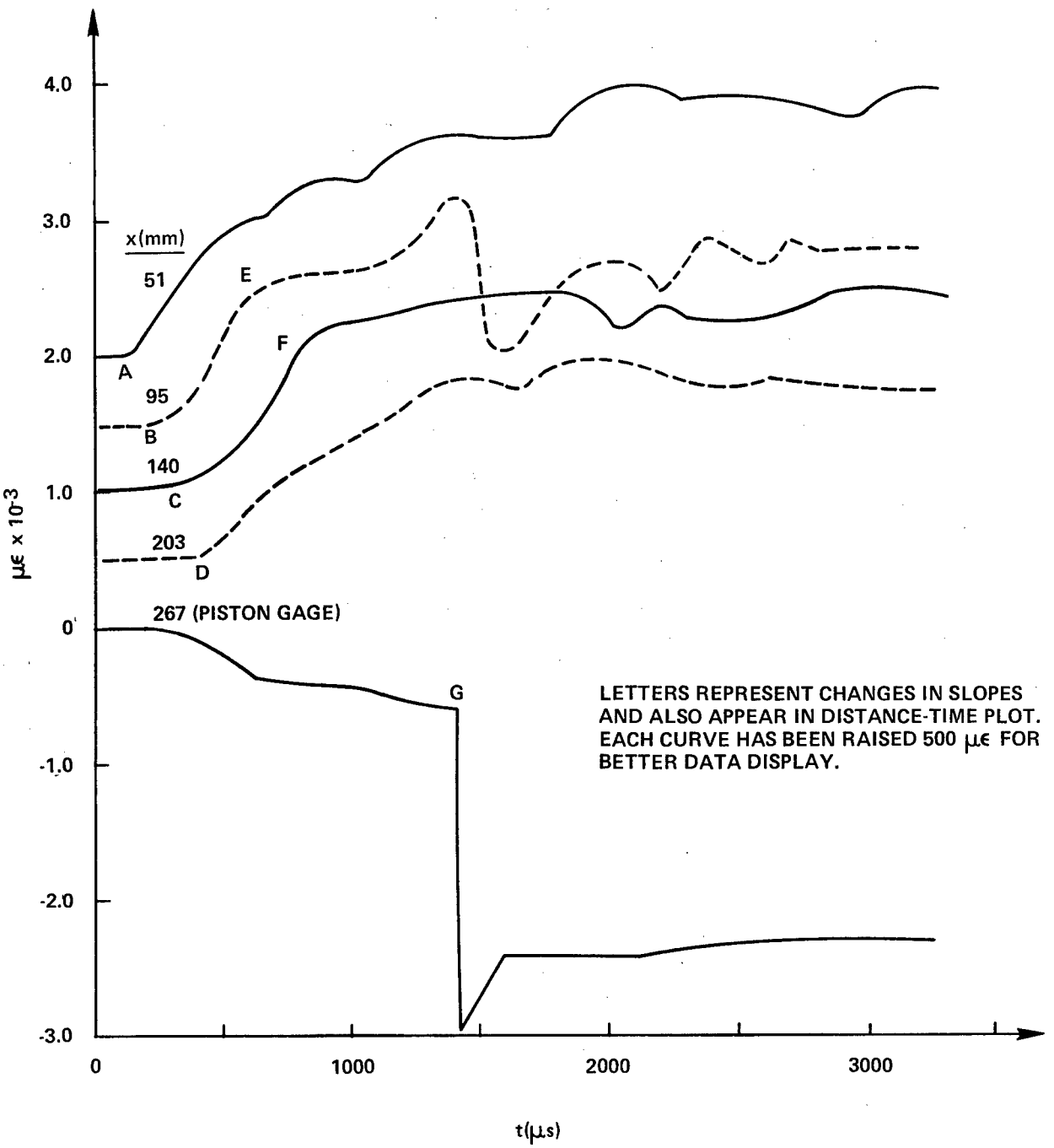

FIGURE 5 STRAIN VERSUS TIME FOR PICRIC ACID (59.7% TMD), SHOT S41

observed luminous front. This could be a case in which the view of the camera at the tube interface was not representative of the entire picric acid column; that is, reaction distribution on the surface and in the interior of the charge are somewhat different. However, some of the nonuniformity in density may result from the depressurization of the charge after the cessation of burning.

Before and after the charge was fired the interface between each increment was visible. There were originally twenty-one increments, each 12.7 mm long. In the recovered apparatus twenty of the increments were still visible. Most of the increments were 10.2 mm long with the increment closest to the ignitor measuring 10.7 mm. The x-ray of Figure 6 shows voids within the first several increments, and so the movement of the visible increment boundaries at the tube interface is not an accurate indication of compaction for those increments. But, assuming that the remaining increments are compacted uniformly, the visible increment boundaries indicate a nearly uniform compaction to 73% TMD. Some of this compaction may have occurred after the 2000μs during which luminosity was recorded.

2. PICRIC ACID AT 68.2% TMD (SHOT S51). Picric acid was hydraulically pressed in a 280 mm long Lexan tube to a density of 1.20 g/cc (68.2% TMD). As with the 60% TMD charge, an ignitor front propagated from the ignitor at a slow rate and then stopped. But, in this case, about 3500μs after the first detection of light a luminous burning front originated just beyond the ignition zone and propagated to the end of the charge.

Enlargements (10X) of some frames from the camera film are shown in Figures 7a, b, and c. On all these photographs the two parallel luminous bands are the result of the backlighting penetrating the space between the Lexan tube and the connecting bolts (see Figure 1). Ignition starts near the left side of the photographs. If the luminous zone at some time (as in the frame at 3128μs) moves to the left, it is because luminous gases have occupied a space between the ignitor sleeve and the inner tube wall which results from expansion of the inner tube wall.

An x-t diagram of the luminous fronts with corresponding changes in the rate of strain is plotted in Figure 8. The strain-time traces from strain gages located at 89 and 152 mm are shown on Figure 9.

For the first 1350μs after the detection of luminance by an optical fiber/photocell a luminous ignitor front propagates at the rate of 0.023 mm/μs. Both strain gages first detect pressure at 300μs. The gage at 89 mm detects a higher rate of pressurization to a local maximum of 0.15 kbar at 760μs, whereas the gage at 152 mm has a local maximum of 0.14 kbar at 860μs. Both gages then detect a mild decline in pressure to 0.11-.12 kbar at 1280μs.

Once the ignitor front stops propagating the luminance declines (compare the frames at 1503, 1909, 2316 and 2722μs on Figure 6a) while both gages record the same mild increase in pressure to 0.17 kbar at 3120μs. Then at 3120μs both gages begin to record the same moderate rate of pressurization as seen in Figure 9. Correspondingly, the frames from 3128 to 3535μs show an increase in luminance for the luminous zone although it is not expanding.

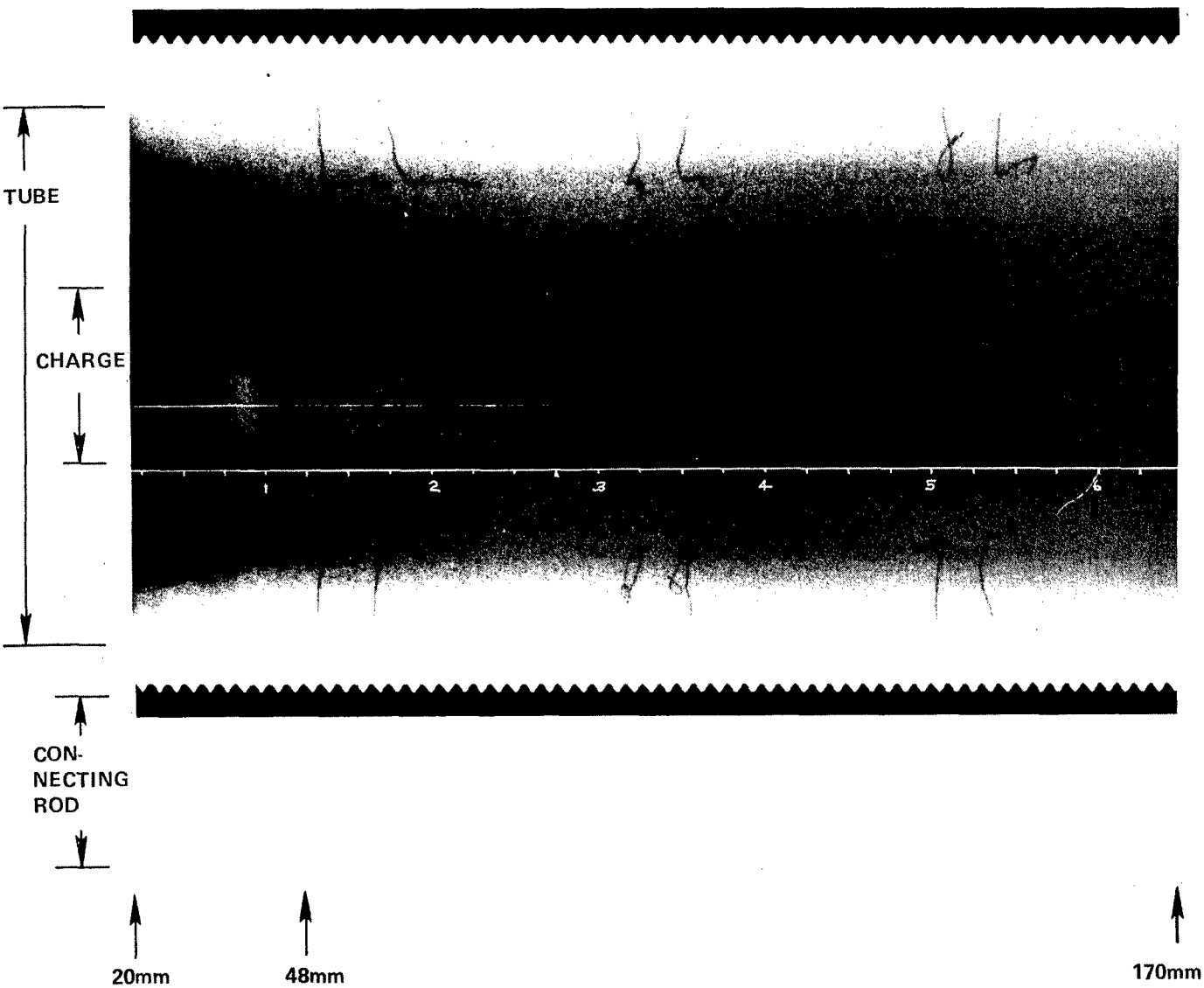

FIGURE 6 X-RAY OF TRANSPARENT DDT TUBE FOLLOWING EXPERIMENT WITH PICRIC ACID (59.7% TMD), SHOT S41

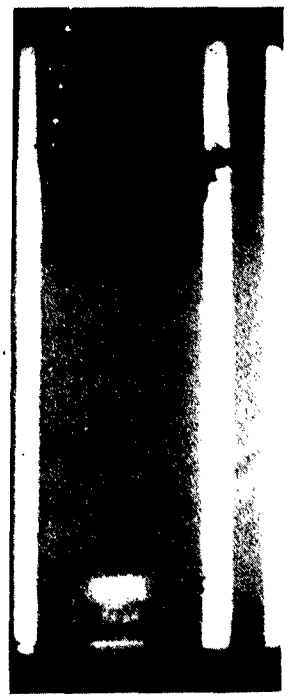

2316 μs

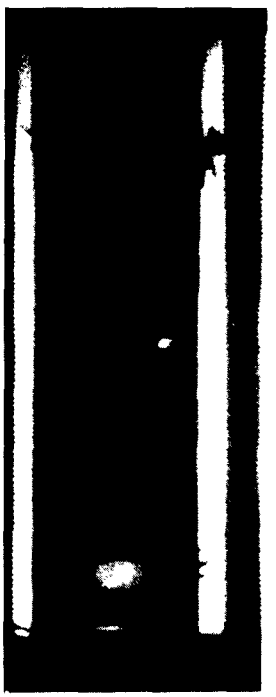

2722 μs

3128 μs

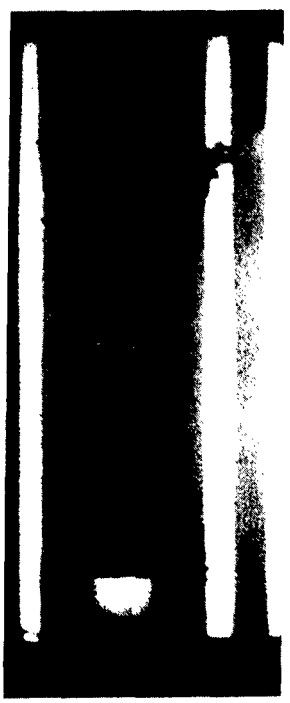

1097 μs

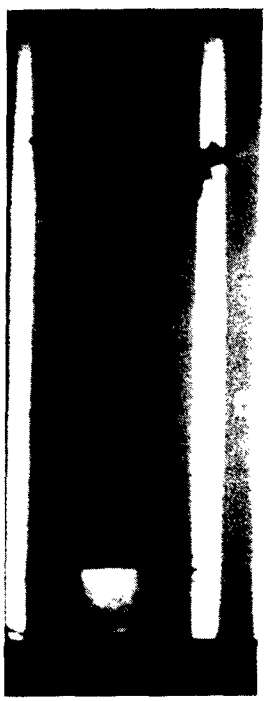

1503 μs

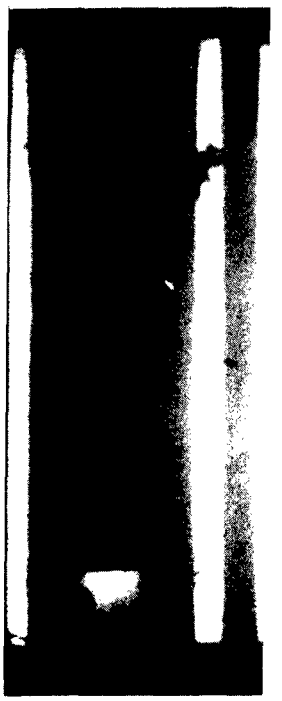

1909 μs

FIGURE 7a PHOTOGRAPHS OF BURNING IN PICRIC ACID (68.2% TMD), SHOT S51, SHEET 1 OF 3

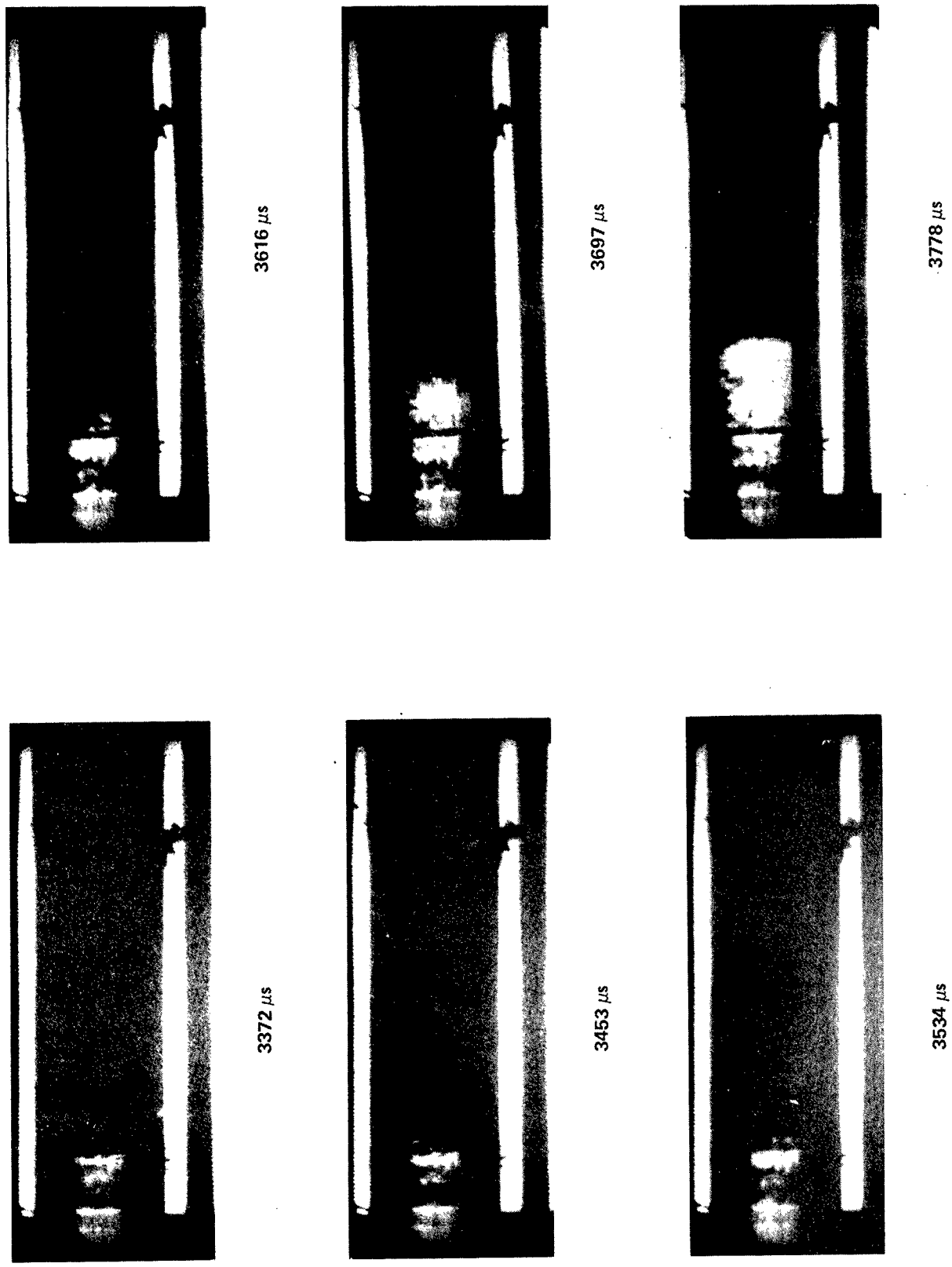

FIGURE 7b PHOTOGRAPHS OF BURNING IN PICRIC ACID (68.2% TMD), SHOT S51, SHEET 2 OF 3

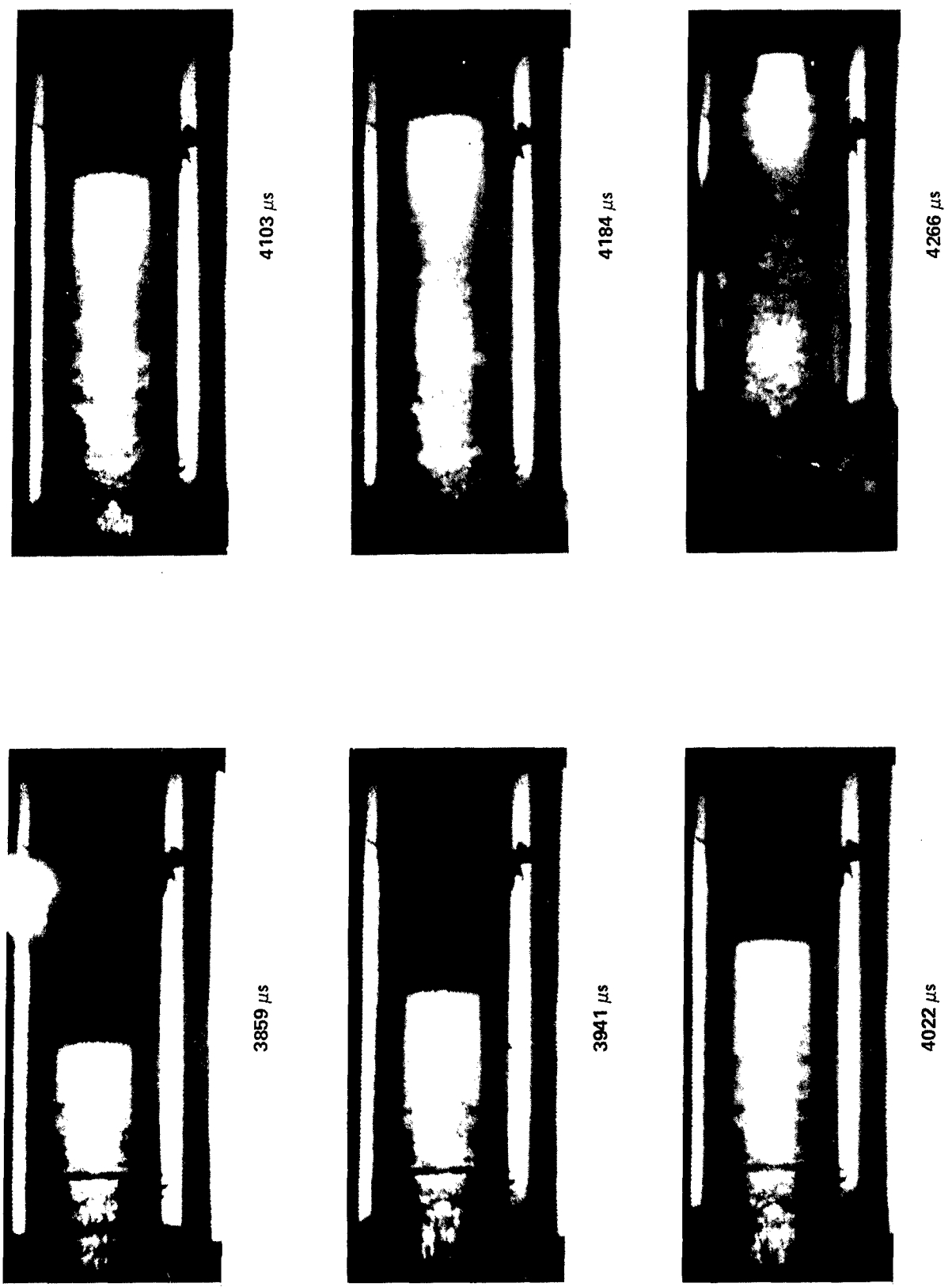

FIGURE 7c PHOTOGRAPHS OF BURNING IN PICRIC ACID (68.2% TMD), SHOT S51, SHEET 3 OF 3

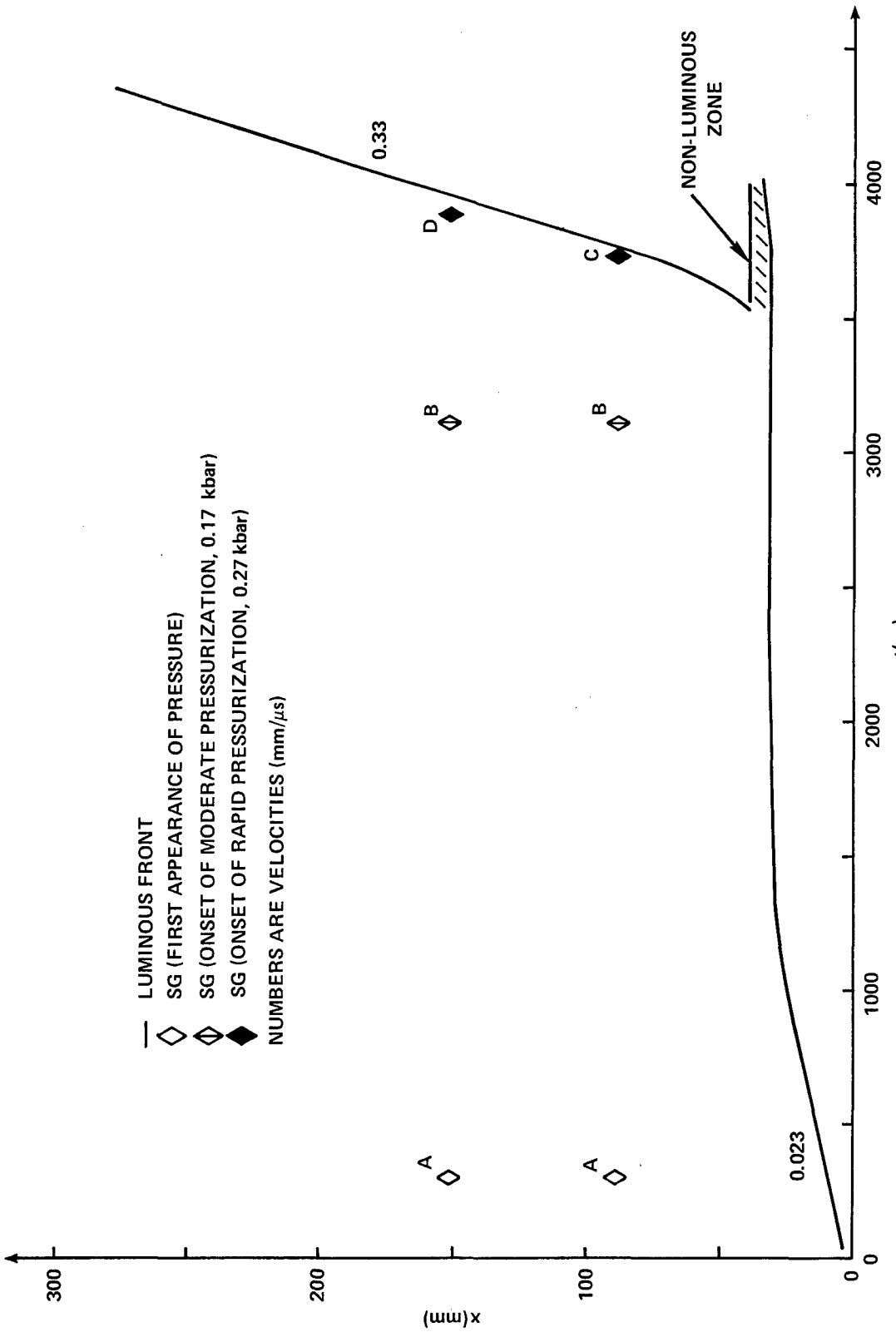

FIGURE 8 DISTANCE-TIME DATA FOR PICRIC ACID (68.2% TMD), SHOT S51

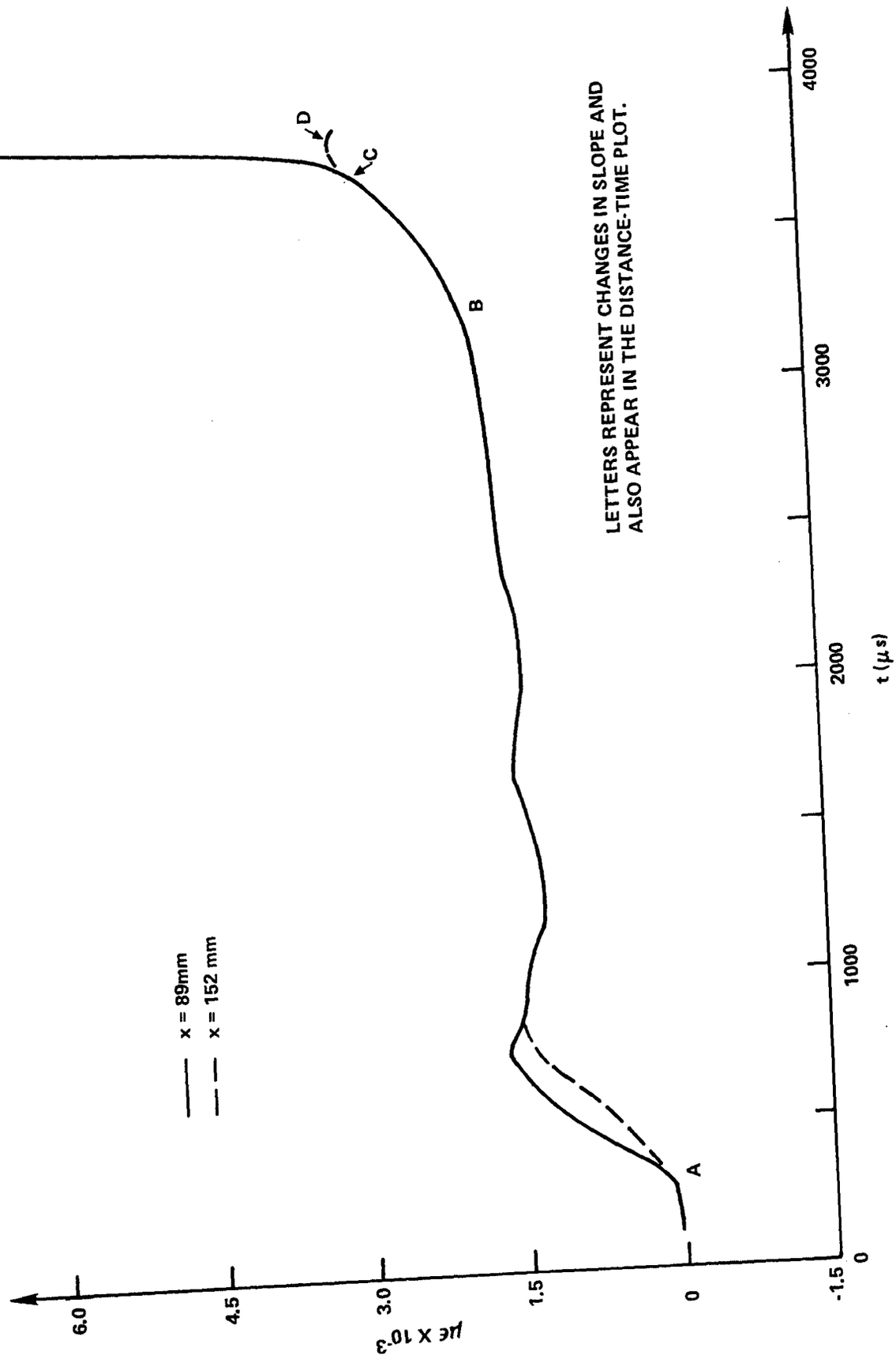

FIGURE 9 STRAIN VERSUS TIME FOR PICRIC ACID (682% TMD), SHOT S51

A second luminous zone begins to develop at 3524μs. Until 3778μs, the second front is irregular and accelerating, but from 3778 to 4266μs, the luminous front remains planar and propagates at a constant velocity of 0.33 mm/μs. This latter front appears to be a convective ignition front. Note in the frames from 3616 to 4022μs there is a dark band about 5 mm long between the two luminous zones. This band could be a remnant of melted and/or compacted material (from the failing of the ignitor front) which is next to the Lexan tube wall, or the band could represent a relatively impermeable plug that inhibits (but does not prevent) the transition to convective burning, or it could be an interface phenomenon.

Both gages experience a rapid increase in rate of strain just prior to the arrival of the burning front. The pressures at this time are very near the elastic limit of 0.28 kbar (3021με) for the Lexan tube; therefore, the rapid increase in strain may be due, in part, to plastic deformation of the tube in addition to combustion. At 4266μs, which is the last frame before tube rupture, all but the last third of the tube is plasticly deforming.

All of the frames in Figure 7c show the burning front and the zone extending several centimeters behind it to be the most luminous zone in the tube. Instead of being an indication of reactivity, it could simply mean that the surface of the inner tube wall near the front has been perturbed less by burning than zones further from the front. Also, these brightly luminous zones appear to have a larger diameter, but magnification is an optical characteristic of the tube. There is both an image of the inner diameter which is relatively true and also a 1.6X magnified image (refractive index of Lexan is 1.586) which becomes dominant at high luminance.

3. PICRIC ACID AT 69.9% TMD (SHOT S43). Picric acid was hydraulically pressed in a Lexan tube to a density of 1.23 g/cc (69.9% TMD). The results were similar to those from the experiment at 68.2% TMD, however, there was a leak from the ignitor end of the charge which had an undetermined effect on the results. The photographs were partly obscured by the leaking gases and are not of sufficient quality to reproduce here. However, the luminous fronts and changes in the rate of strain at five gage locations are plotted on the x-t diagram in Figure 10. The strain-time traces from strain gages located at 41, 95, 130 and 190 mm and a piston gage at 257 mm are shown in Figure 11.

The luminous events following the first detection of light in this experiment are different from those of the two lower density charges. A weakly luminous 0.14 mm/μs front propagated ahead of a more luminous 0.04 mm/μs front, which should be the usually observed ignitor front. As in the case of the 60% TMD charge (see Figure 4), the origin of the luminous fronts appears to have been the origin of a pressure wave which propagated the full length of the charge, in this case with a velocity of 1.20 mm/μs.

By 500μs the luminous fronts and the pressurization near the ignition region had both stagnated. Downstream from the ignition region the pressure was relatively uniform, but it oscillated with a period of about 600μs. Noting that the piston gage indicates pressure by compression while the strain gages indicate pressure by tension, all records are in phase as they oscillate. To a lesser extent, the records in the 68% TMD charge also showed oscillations (see Figure 9); therefore, the oscillation cannot be entirely attributed to the leak at the ignitor plate.

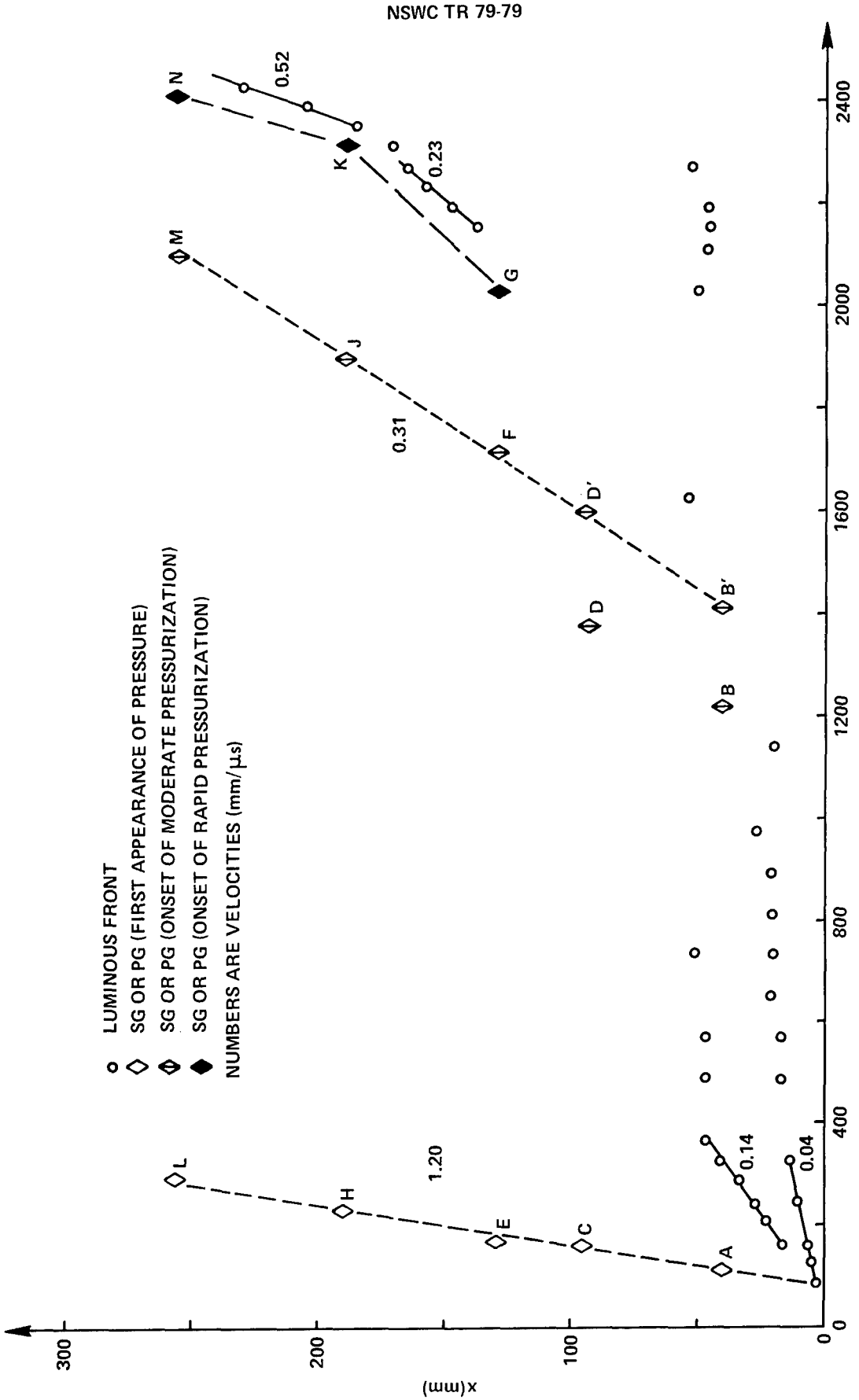

FIGURE 10 DISTANCE-TIME DATA FOR PICRIC ACID (69.9% TMD), SHOT S43

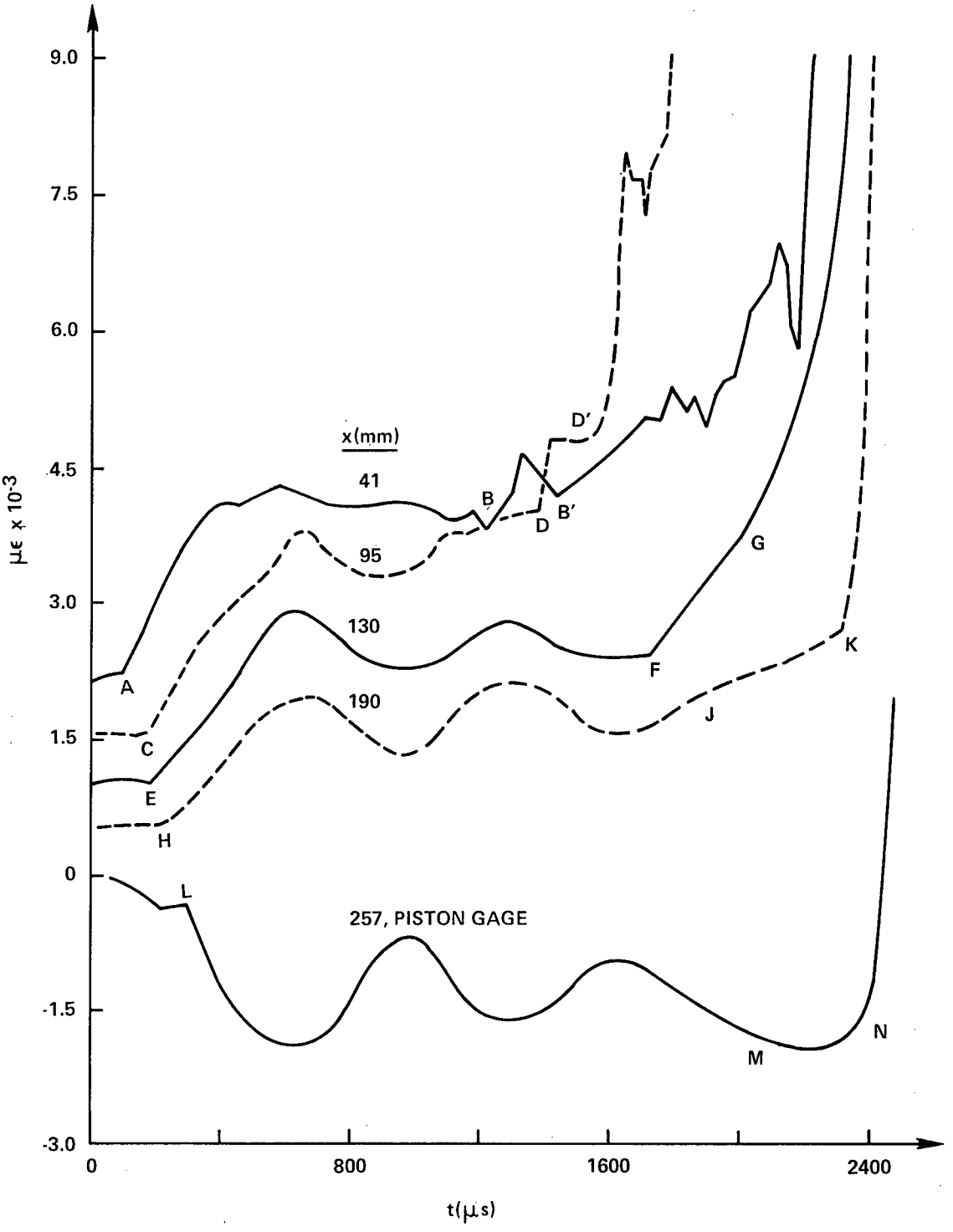

FIGURE 11 STRAIN VERSUS TIME FOR PICRIC ACID (69.9% TMD) , SHOT S43

(KEY OF FIGURE 5)

Following the stagnation of the 0.14 mm/μs luminous front at 50 mm, another luminous front was not detected until almost 2 ms later at 140 mm. When propagating from 50 to 140 mm this front was either not luminous enough to expose the camera film, or it was masked by the leaking gases, or it propagated in only the core of the charge. This new luminous front (a convective ignition front) propagated at 0.23 mm/μs for 50 mm and then accelerated to 0.52 mm/μs before it reached the end of the charge and the piston gage.

Even though the 0.23 mm/μs luminous front was not visible until 140 mm, the SG's and PG indicate the build-up in pressure (dotted line through diamonds B', D', F, J, M) which precedes such a front. These points are selected from the gage traces in Figure 11 for the following reasons. For the 41 and 95 mm gages the end of the pressure stagnation following ignition appears to be at points B and D. Note that for the 41 mm gage the strain increases after point B but later declines to almost the original level before increasing again at point B'. For the 95 mm gage the strain increases at point D but quickly stagnates until point D' where it increases again. So points B' and D' are chosen to indicate the end of the pressure stagnation at the 41 and 95 mm locations because the strain continues to increase after these points. For the remaining gages, the end of the oscillating pressure stagnation is where the oscillation begins to be disrupted. This point obviously occurs at point F for the 130 mm gage. But for the 190 mm gage it appears that at point J the pressure begins to rise whereas the oscillation should have reduced it. Also for point M on the PG trace, the strain begins to decrease (pressure increases) whereas the oscillation should have increased it.

Just before the luminous front reached the PG it recorded a rapid increase in tension instead of compression beginning at point N. This probably does not mean that the pressure rapidly decreased; the upstream gages certainly recorded a rapid increase in pressure just before the luminous front reached their positions (Points G and k). Perhaps the pressure caused the SG's on the piston gage to fail or the gage leads to short. It is doubtful that the SG's could have been heated rapidly enough by gases passing by the piston to cause an apparent strain of the magnitude recorded.

B. TETRYL

Coarse (470μm) tetryl and to some extent fine (20μm) tetryl were difficult to study in steel tubes[6] because the ionization probes were not consistently triggered by the initial reaction fronts. Also, tetryl differs from other explosives in that the origin of accelerated pressure build-up in the DDT mechanism lies closer to the onset of detonation than to the ignition region. Fine tetryl at 46.2% TMD and coarse tetryl at 57.8% TMD were studied in Lexan tubes in order to observe both the initial reaction fronts and the source of accelerated pressure build-up.

1. FINE TETRYL AT 46.2% TMD (SHOT S42). This 0.80 g/cc (46.2% TMD) charge is the highest density charge of 20μm tetryl which could be hand packed; it is almost the same density as the most porous steel tube charge (Shot 1209, 45.8% TMD)[6], which had a predetonation column length of 147 mm. Enlargements (10X) of some frames from the camera film are shown in Figures 12 a,b,c,d, and e. There are two x-t diagrams; in Figure 13a the complicated luminous fronts are displayed, while in Figure 13b a summary of the luminous fronts along with changes in the rate of strain at five locations are displayed. The strain-time traces from strain gages located at 64, 102, 140, 165 and 190 mm are shown in Figure 14.

Simultaneously with the appearance of a luminous 0.056 mm/μs ignitor front a 0.17 mm/μs pressure front began propagating from the ignitor/explosive interface. (Discussion refers to Figure 13b except where noted.) Within 100μs a slightly accelerating (0.17-0.21 mm/μs), low pressure, weakly luminous front began propagating to the end of the charge. This front is essentially planar but the luminous zone behind it is irregular with varying luminosity (see Figure 13a). The pressures associated with this front are low, <0.07 kbar, much lower than the pressures associated with convective ignition fronts in other explosives confined in Lexan tubes. Also, the extent of conductivity of the combustion products was insufficient to cause response of the conductivity pins at 235 and 260 mm. Because this front is weak and because following passage of the luminous front the rate of pressurization sharply declined, as shown by the dashed line A-C-E, it is termed a "transient ignition front."

Following the decline in the rate of pressurization there is essentially a plateau in pressure that persists for 400μs in the vicinity of the first strain gage. The plateau ends with a moderate rate of pressure rise along a 0.32 mm/μs front (points B,D,F,G). In the meantime, the ignitor front appears to have continued to propagate at its original velocity. From 1000 to 1200μs, just following the origin of the 0.32 mm/μs pressure front, the ignitor front almost stops and the length of its luminous zone shrinks (see Figure 12c and d.) But it regains luminous intensity and propagates at its original 0.056 mm/μs velocity until at 1320μs the velocity increases to 0.42 mm/μs. This velocity is based on the dashed line shown in Figure 13a; note that as shown in Figure 13a and in the 1320μs and 1361μs frames in Figure 12, there are small zones of intense luminosity ahead of the dashed line. In any case, following the 0.32 mm/μs pressure front by about 300μs there is an approximately 0.4 mm/μs luminous front; these fronts are possibly associated with convective ignition.

In the vicinity of the 0.42 mm/μs luminous front, the 1526μs frame in Figure 12e shows that the upper edge of the Lexan tube has expanded slightly. This indicates a pressure ≥0.28 kbar at that position in the tube, but the entire first half of the tube might have yielded if there had not been a gas leak at the ignitor plate. The 0.42 mm/μs luminous front existed for only about 200μs before the transient ignition front reached the end of the charge between the 1485 and 1526μs frames. The 1526μs frame shows near the end of the charge an intensely luminous zone that is associated with the transient ignition front reaching the end of the charge. The closure plate was dented on the side adjacent to the charge and had some spalling on its outer surface. It is unlikely that this damage occurred following the 1568μs frame since this frame shows the tube rupturing near the closure plate and thus releasing the pressure. It is also unlikely that the impact of the low pressure transient ignition front on the closure plate would damage it. Possibly because of the reflected pressure of

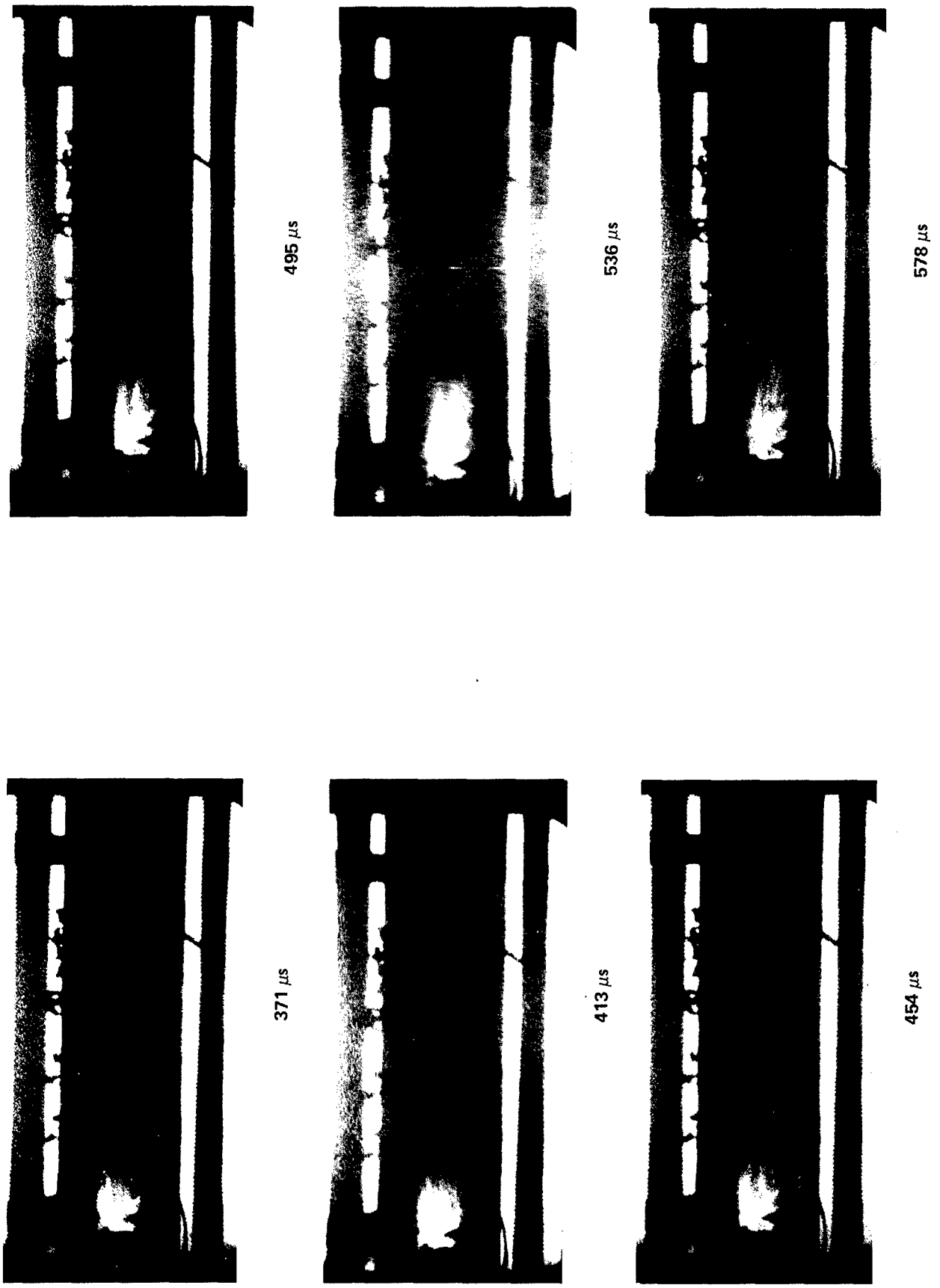

FIGURE 12a PHOTOGRAPHS OF BURNING IN FINE TETRYL (46.2% TMD), SHOT S42, SHEET 1 OF 5

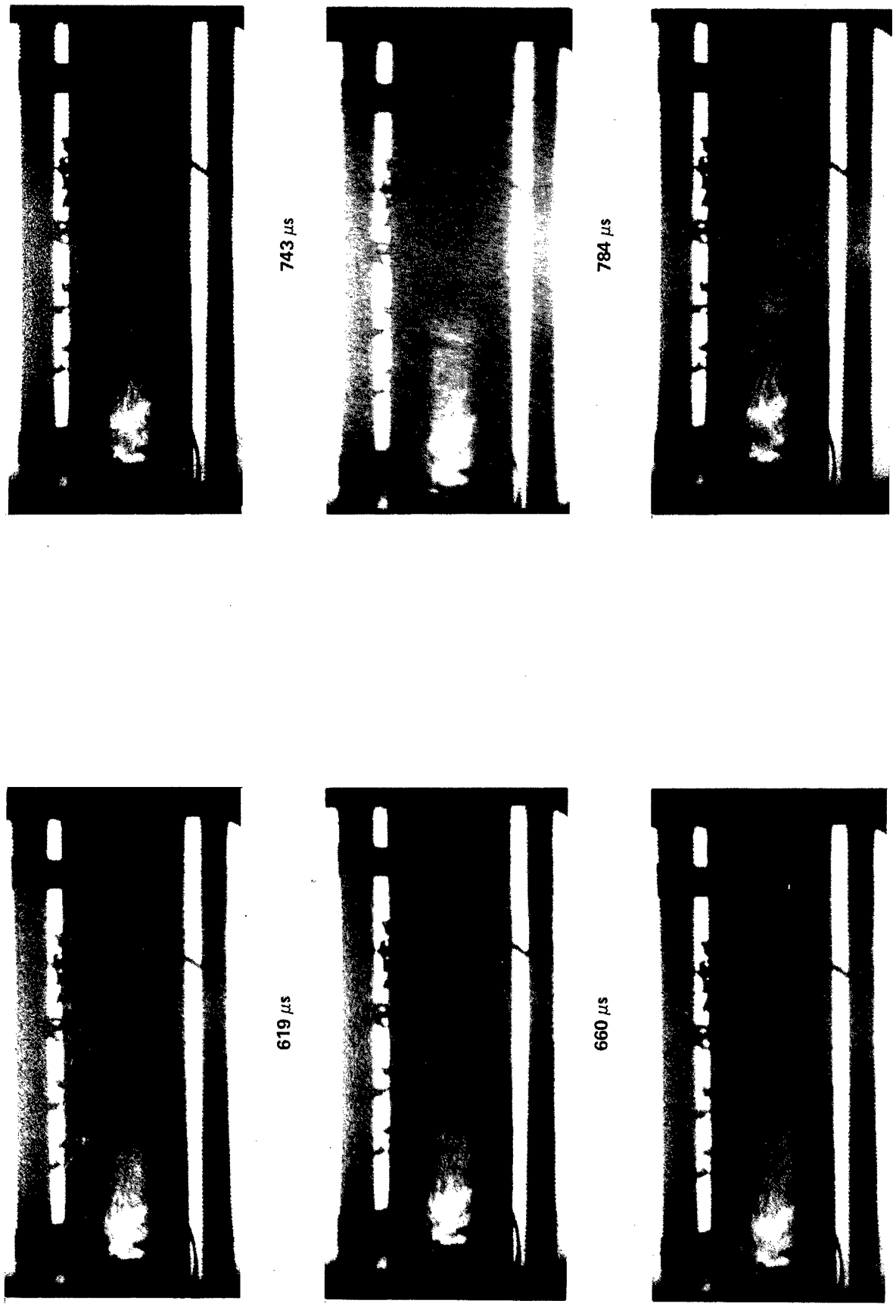

FIGURE 12b PHOTOGRAPHS OF BURNING IN FINE TETRYL (46.2% TMD), SHOT S42, SHEET 2 OF 5

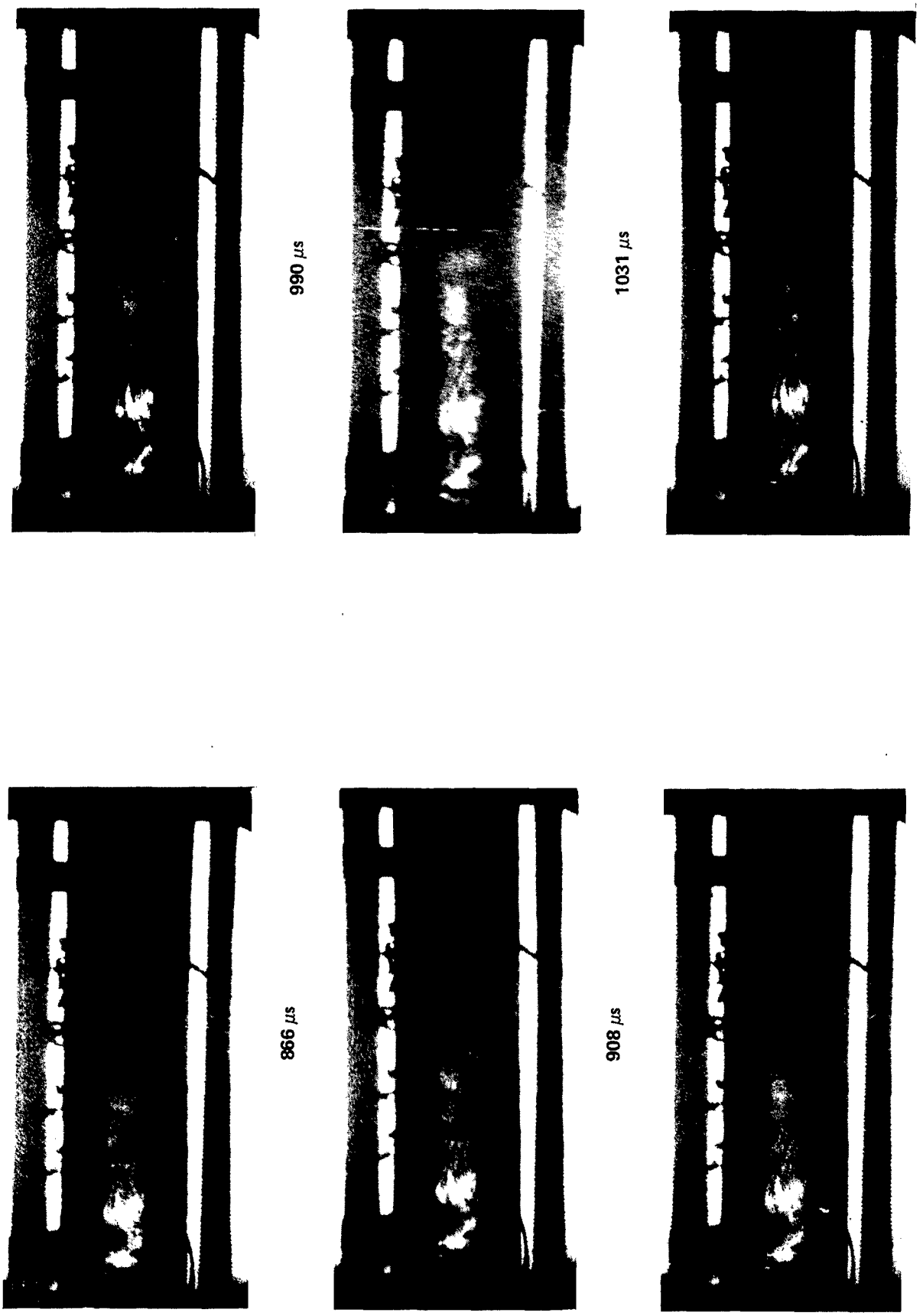

FIGURE 12c PHOTOGRAPHS OF BURNING IN FINE TETRYL (46.2% TMD), SHOT S42, SHEET 3 OF 5

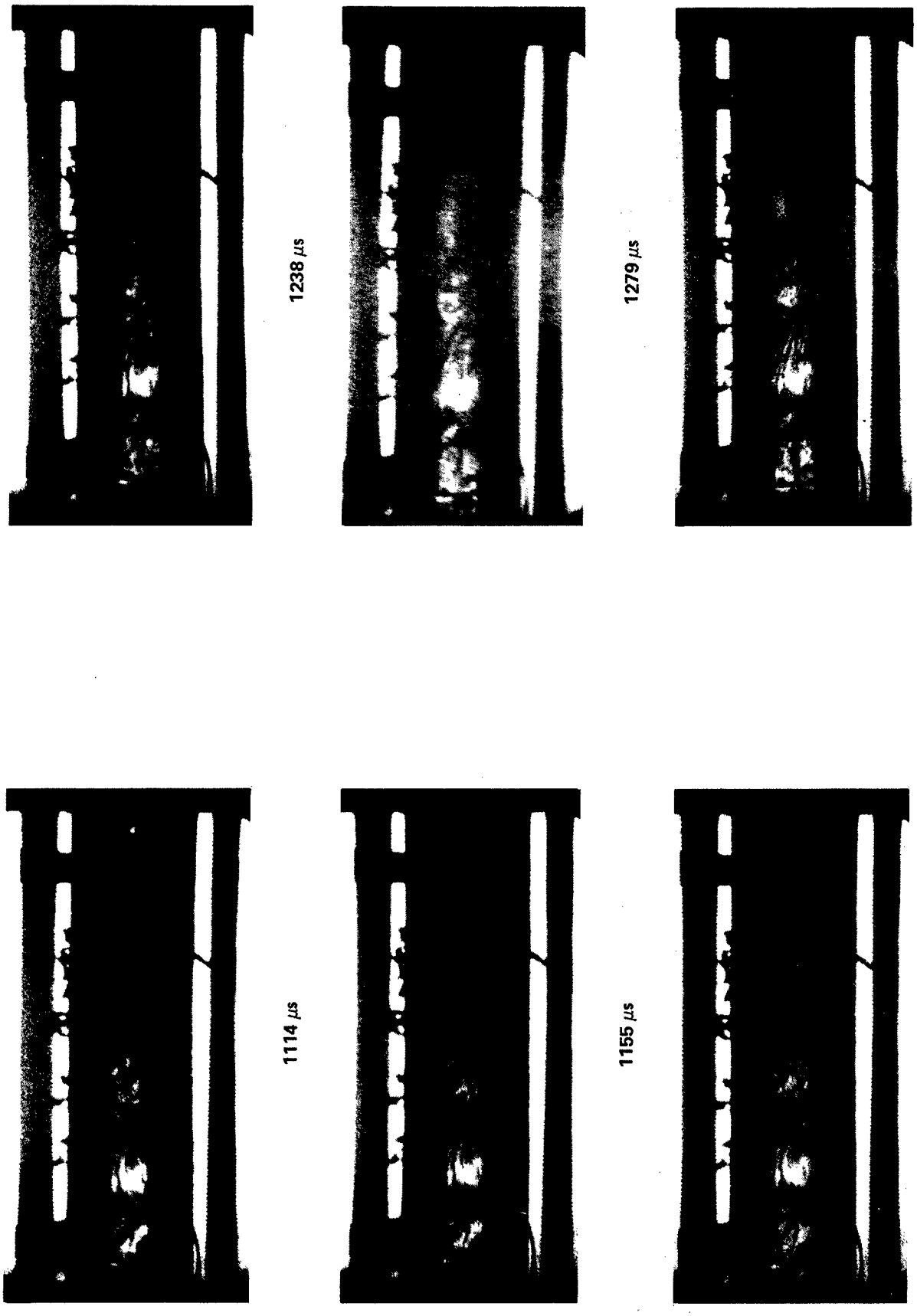

FIGURE 12d PHOTOGRAPHS OF BURNING IN FINE TETRYL (46.2% TMD), SHOT S42, SHEET 4 OF 5

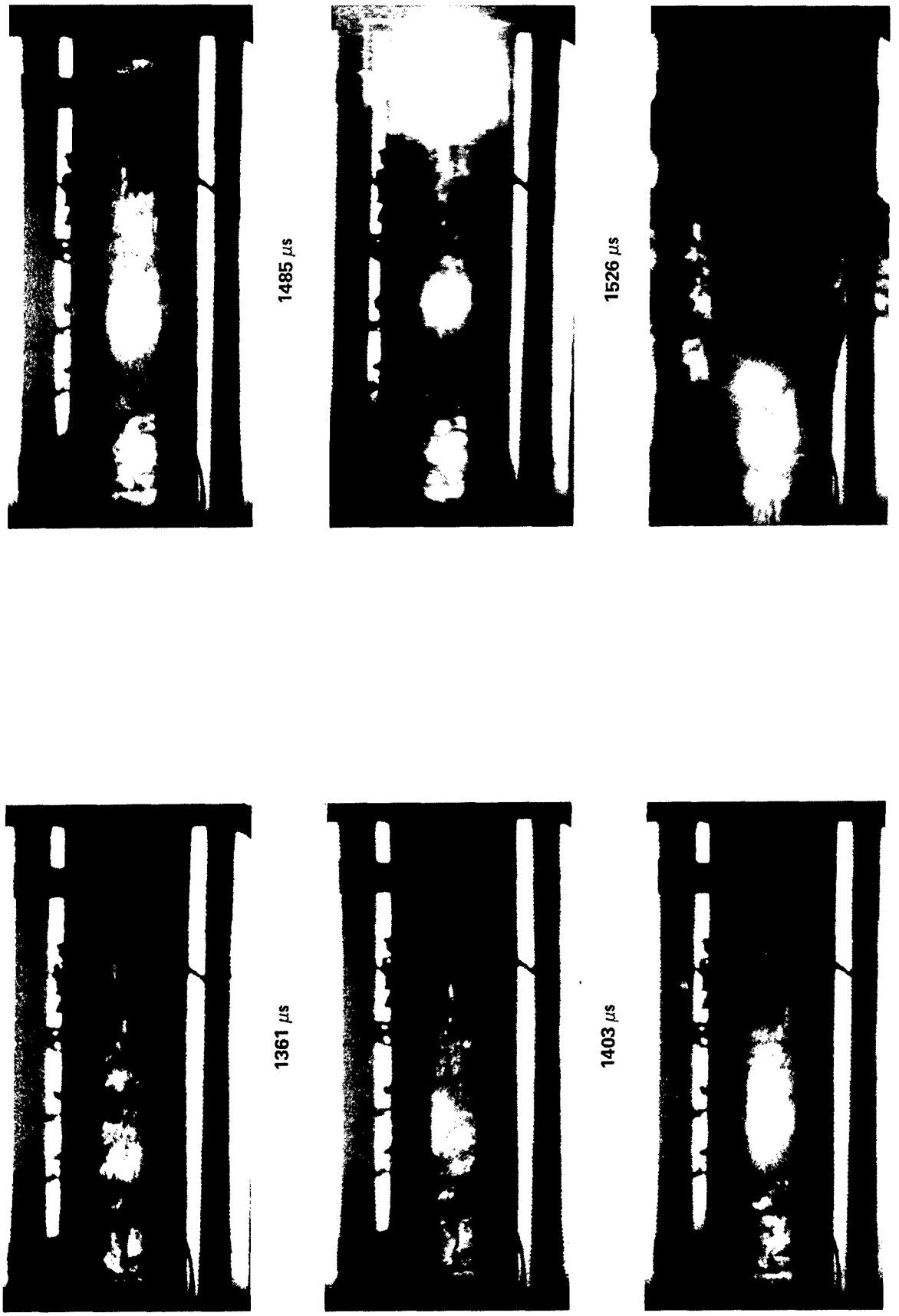

FIGURE 12e PHOTOGRAPHS OF BURNING IN FINE TETRYL (46.2% TMD), SHOT S42, SHEET 5 OF 5

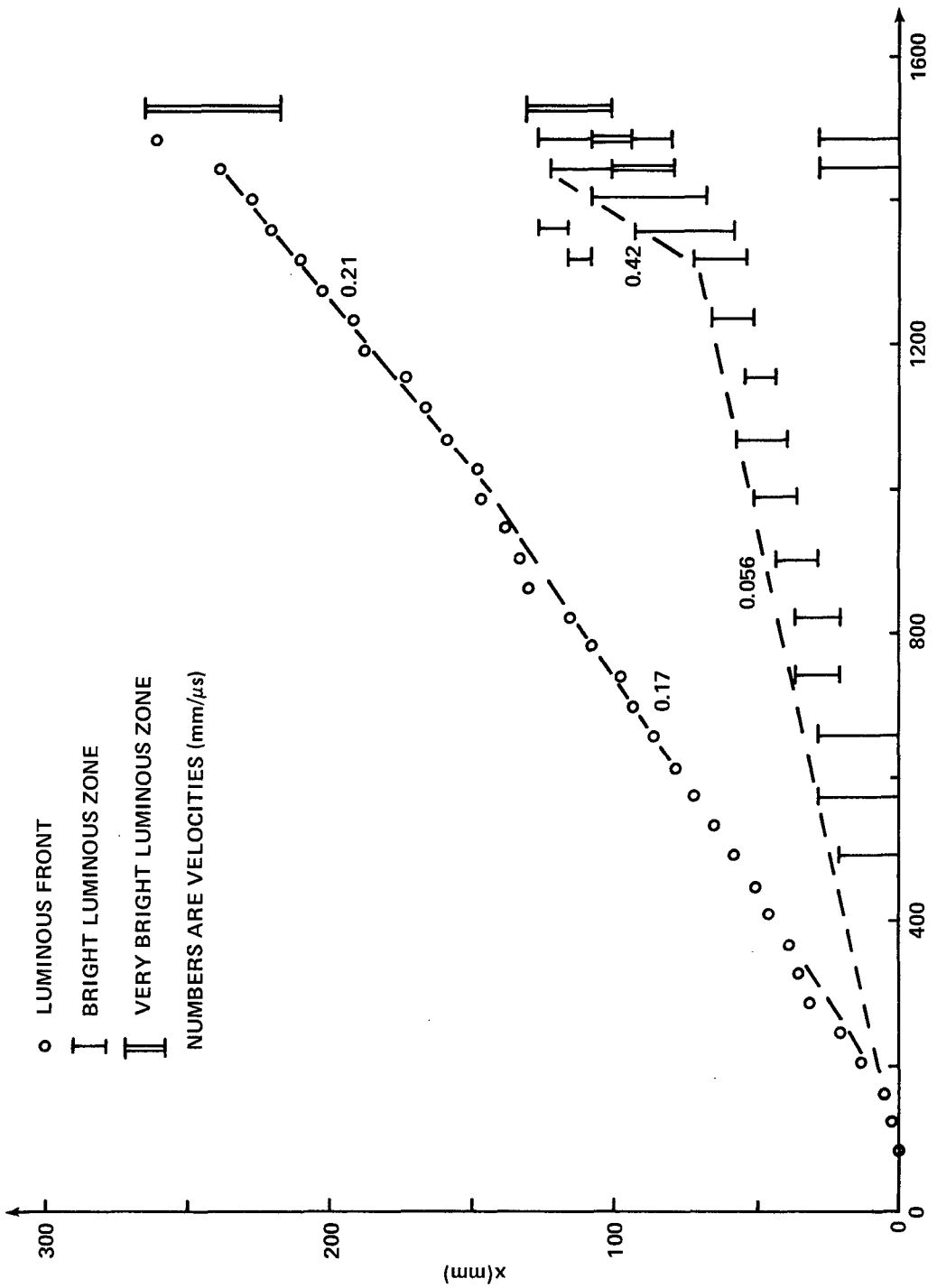

FIGURE 13a CAMERA RECORD FOR FINE TETRYL (46.2% TMD). SHOT S42

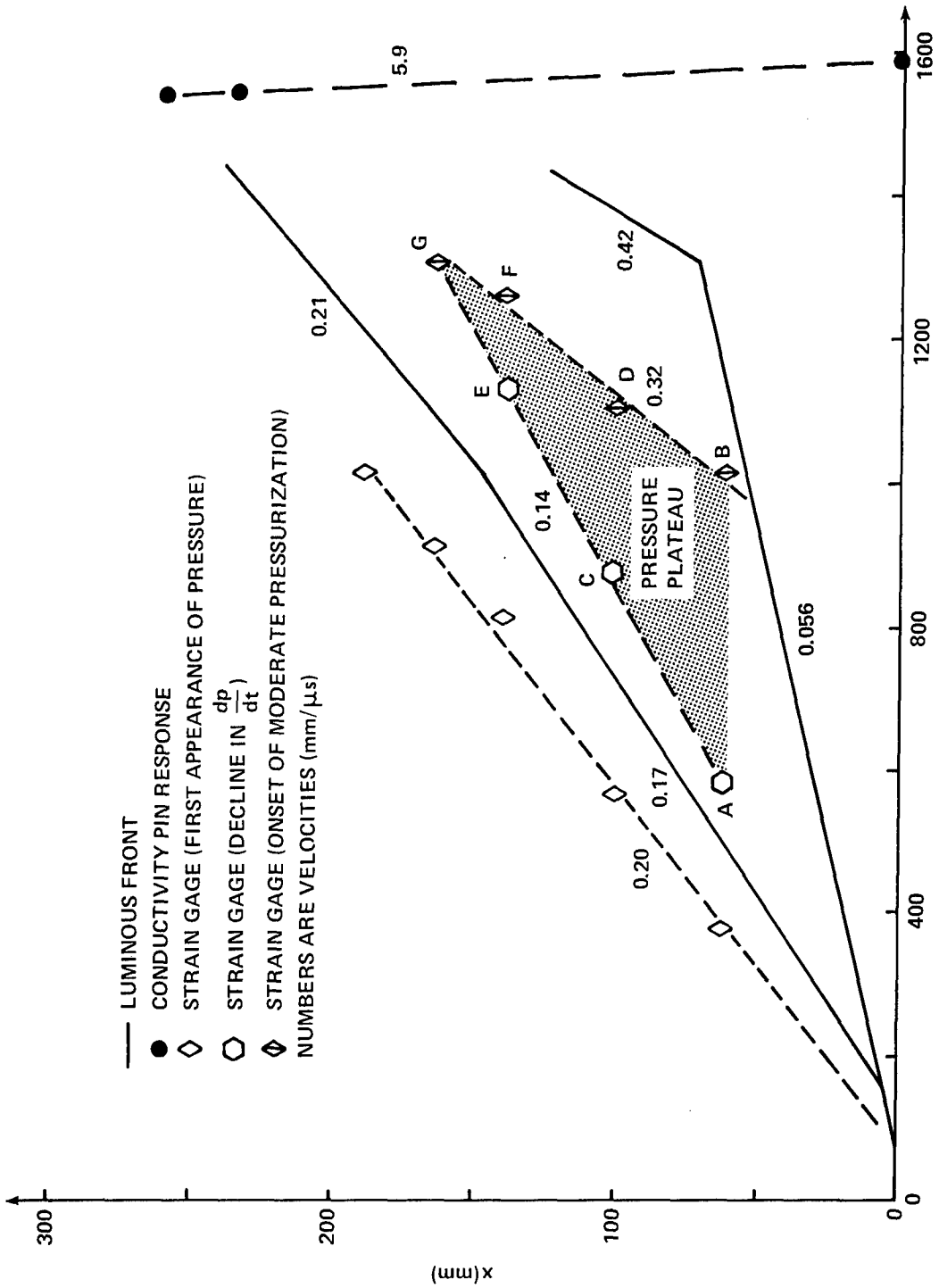

FIGURE 13b DISTANCE-TIME DATA FOR FINE TETRYL (46.2% TMD), SHOT S42

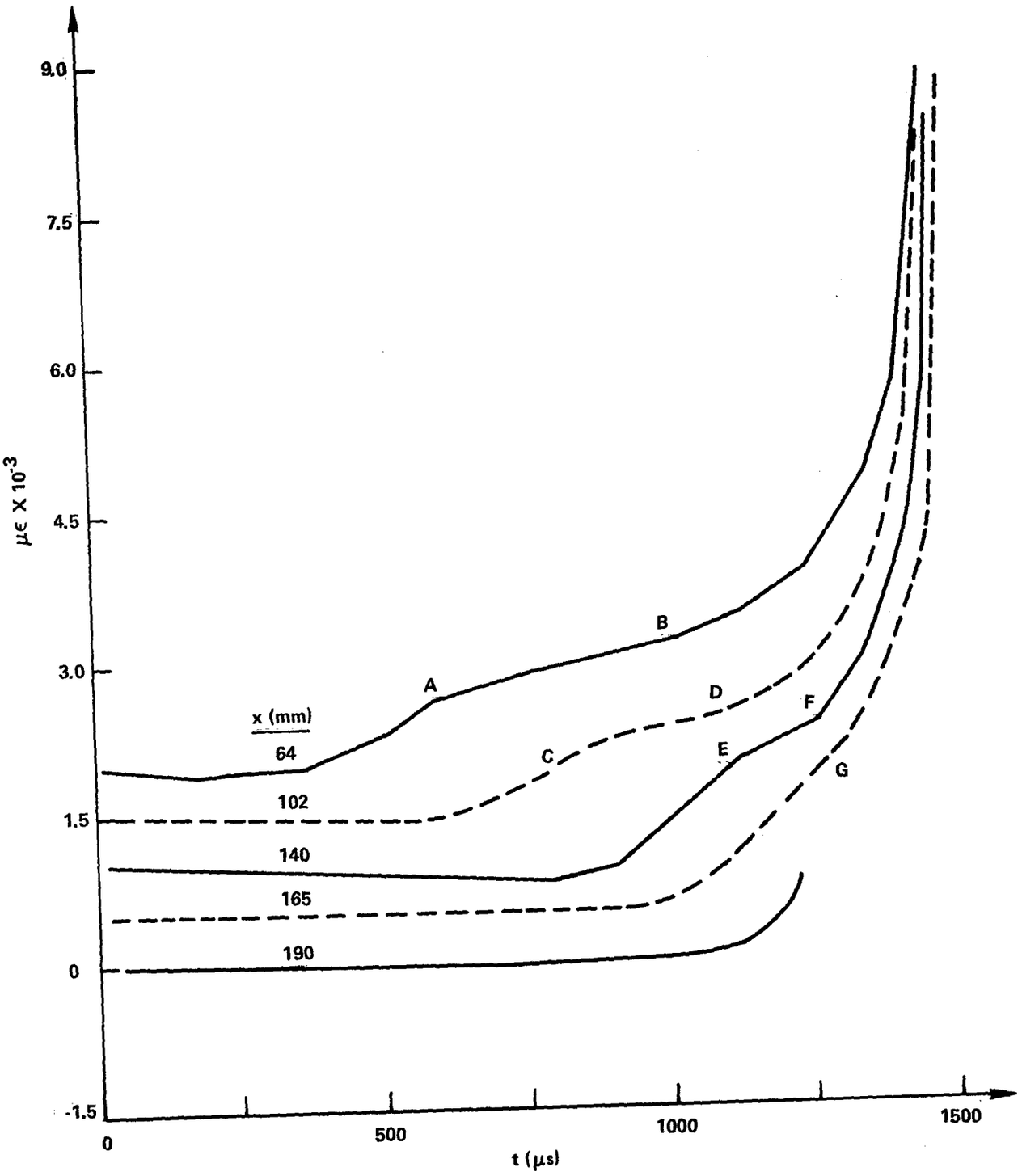

FIGURE 14 STRAIN VERSUS TIME FOR FINE TETRYL (46.2% TMD), SHOT S42

(KEY OF FIGURE 5)

the transient ignition front, it appears that a transition to detonation was about to occur or did occur at the end of the charge. In fact, the conductivity pins near the closure plate and the one at the ignitor recorded what appears to be a rearward 5.9 mm/μs front, which is a reasonable velocity for a detonation wave. However, a rearward detonation wave should have damaged the ignitor plate even though there would be a column of gas between the end of the explosive column and the ignitor. The apparent response of the two conductivity pins near the closure plate about 25μs after the appearance of the bright luminous zone is probably the error in synchronizing the camera with the recording oscilloscopes, as discussed in Section 2.C.5.b.

2. COARSE TETRYL AT 57.8% TMD. This 1.00 g/cc (57.8% TMD) charge is the highest density charge of 470μm tetryl which could be hand packed; it is somewhat more porous than the most porous steel tube charge (Shot 607, 63.2% TMD), which had a predetonation column of 75 mm[6]. In the present experiment a transition to detonation occurred between 150 and 200 mm, as best as can be determined from conductivity pin responses and the camera film. The detonation wave punched a 75 mm diameter hole in the closure plate. Although the fragments from steel DDT tubes are useful in locating the onset of detonation, the Lexan tube fragments do not show any distinguishing markings from the detonation wave.

Enlargements (10X) of all but the first few frames from the camera film are in Figures 15 a and b. The gray speckled appearance of the 578 and 660μs frames is due to preparing the film for loading into the camera. The propagation of luminous fronts and the times at which there are changes in the rate of strain at five gage locations are plotted on the x-t diagram in Figure 16. The strain-time traces from the gages at 38, 76, 114, 152 and 216 mm are shown in Figure 17.

There is a considerable delay of 250μs between the first detection of ignition by the optical fiber/photocell at the ignitor interface and the first light on the camera film. From then to the frame at 495μs, the camera film shows the propagation of a weakly luminous, decelerating ignitor front. However, by redrawing in Figure 16 the initial portion of this front to reflect a uniform velocity, then this ignitor front almost extends backward to 100μs with an average velocity of 0.038 mm/μs. This feature may reflect the difficulty in detecting and measuring the first light on the film. Extrapolation of this ignitor front backward in time (the lower dashed curve in Figure 16) shows that the ignitor front could be associated with the propagation of the first pressure wave, points, A, C, E.

Beginning with the frame at 495μs the luminous front velocity increases to 0.10 mm/μs, and in the next frame at 536μs the luminous intensity behind the front markedly increases. If the pressure front passing through points D, E, G, J in Figure 16 is extrapolated back toward the ignitor it intersects with the ignitor front at about 450μs. Therefore, it appears that at about 450μs the reaction rate at the ignitor front increases resulting in a 0.70 mm/μs pressure wave and an increased luminous front velocity. Perhaps as a consequence of the increased reaction rate, beginning with the 454μs frame there is a perturbation on the bottom side of the nearly planar front, labelled the "flame peninsula" in Figure 16, which is propagating somewhat faster than the planar front.

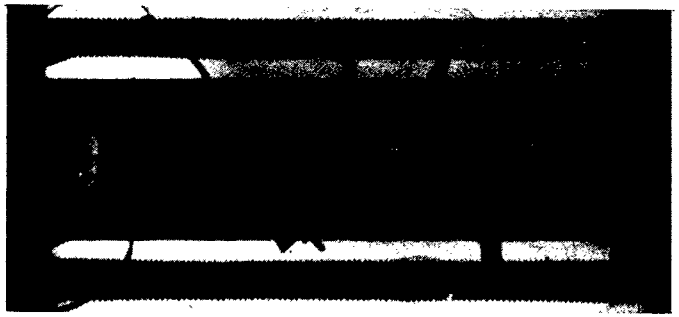

413 μs

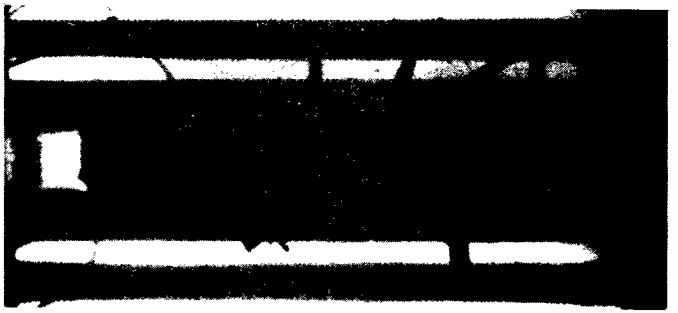

536 μs

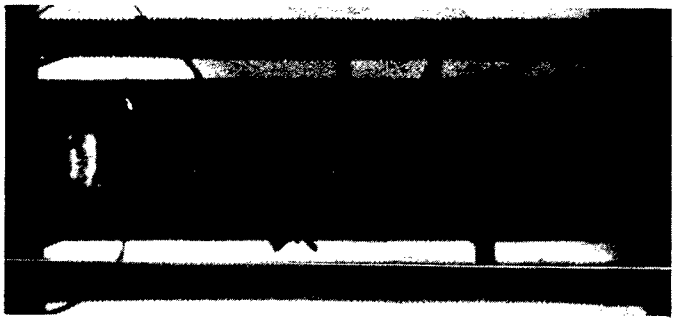

454 μs

578 μs

495 μs

619 μs

FIGURE 15a PHOTOGRAPHS OF BURNING IN COARSE TETRYL (57.8% TMD), SHOT S49, SHEET 1 OF 2

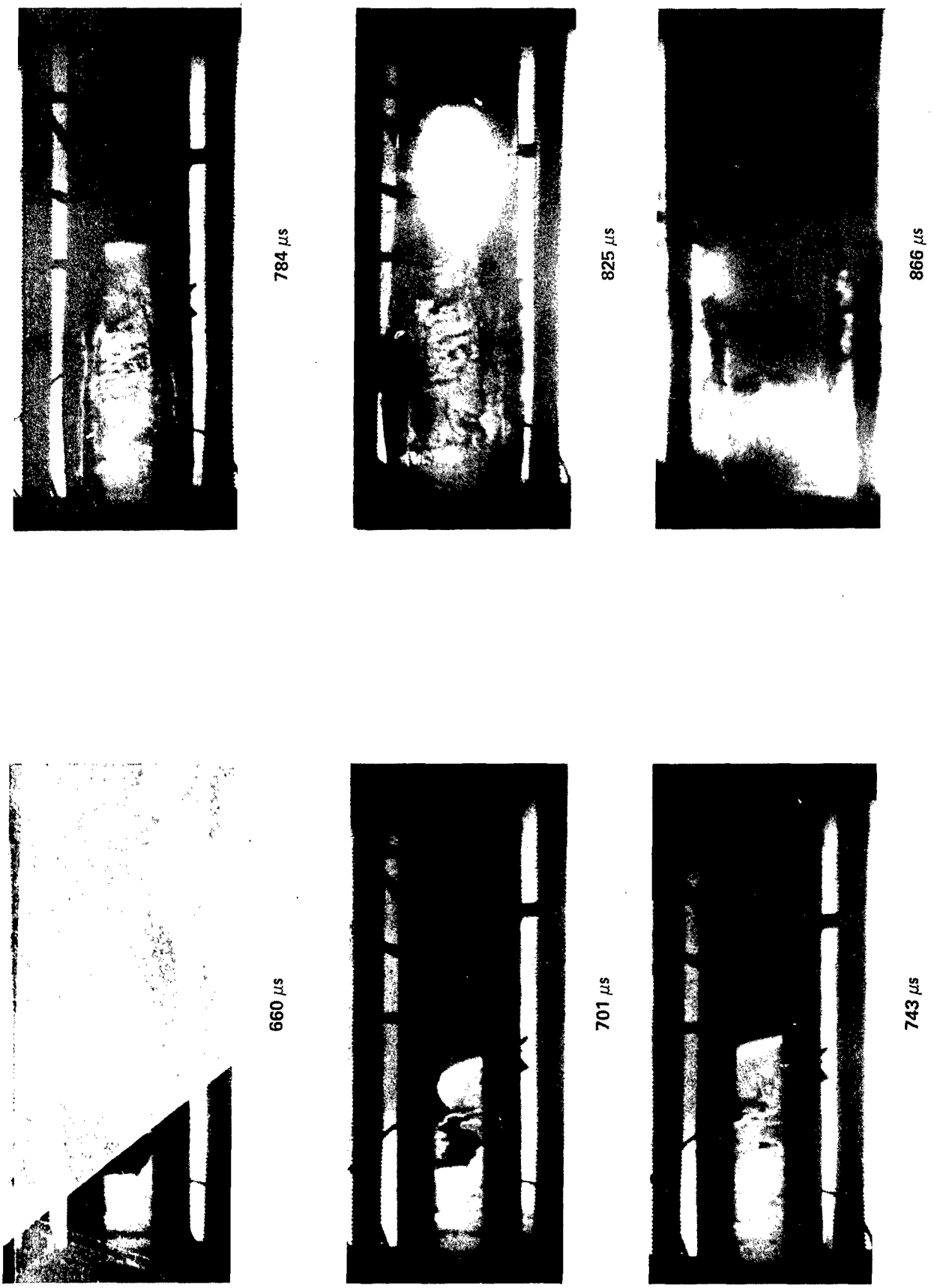

FIGURE 15b PHOTOGRAPHS OF BURNING IN COARSE TETRYL (57.8% TMD), SHOT S49, SHEET 2 OF 2

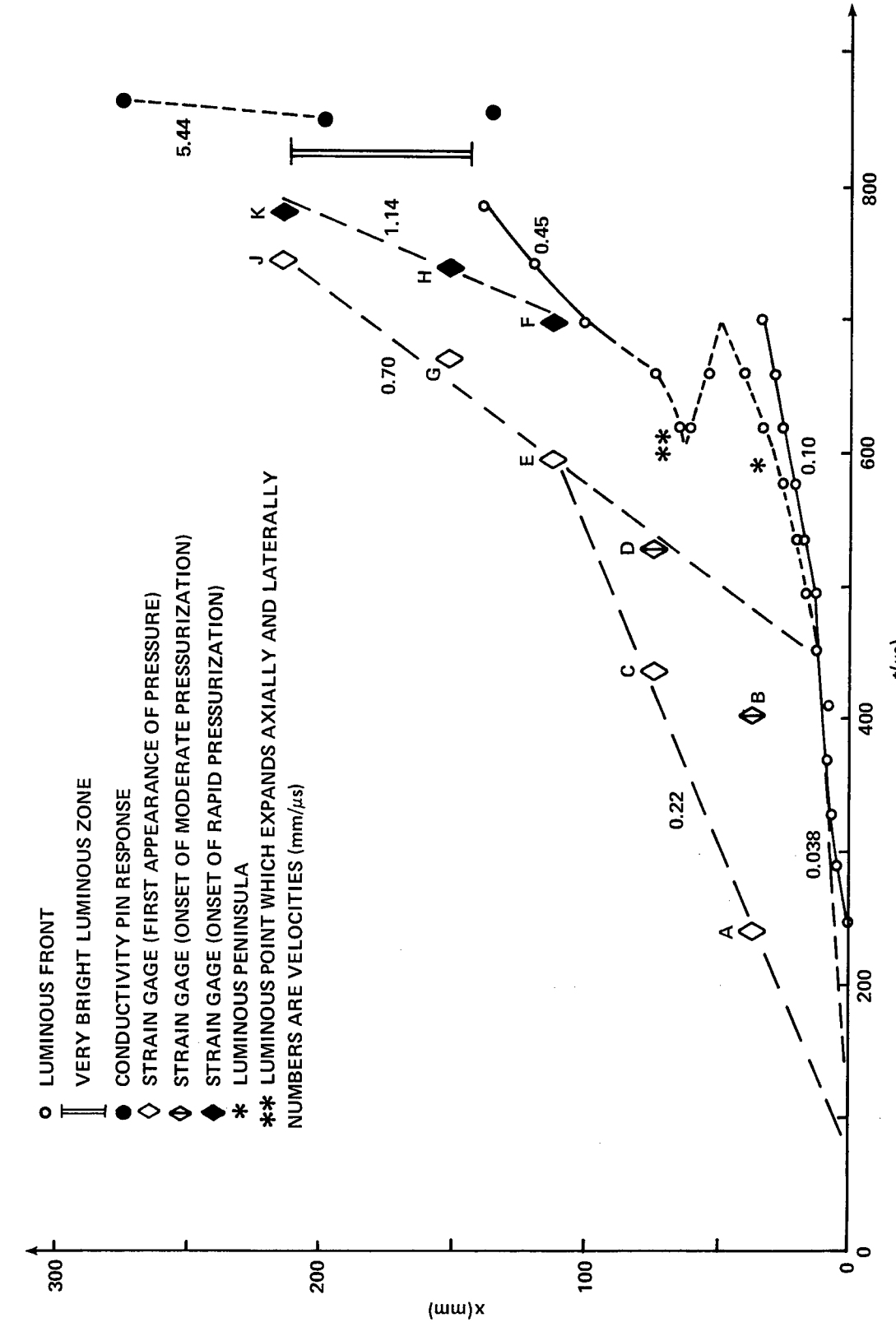

FIGURE 16 DISTANCE-TIME DATA FOR COARSE TETRYL (57.8% TMD), SHOT S49

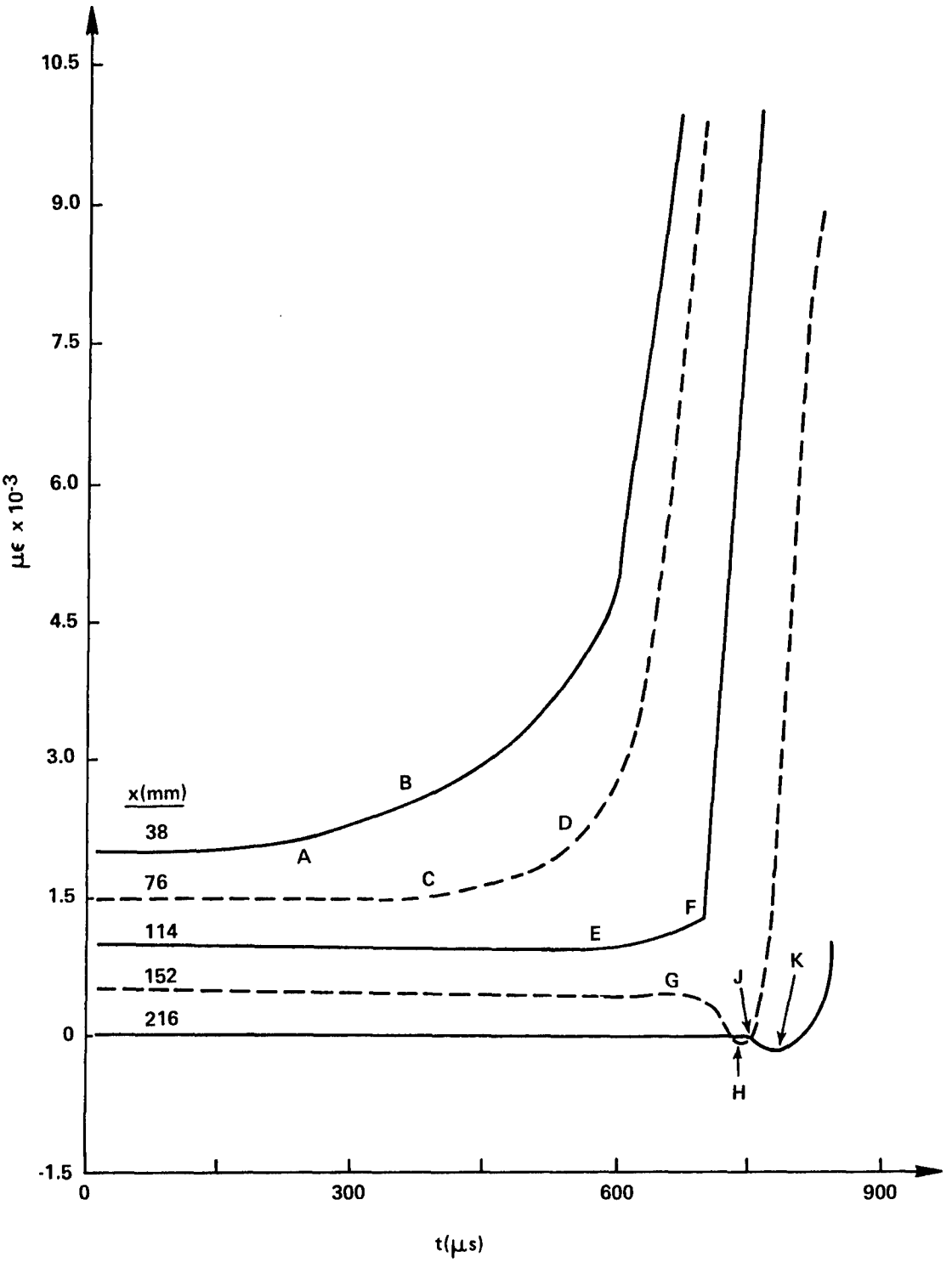

FIGURE 17 STRAIN VERSUS TIME FOR COARSE TETRYL (57.8% TMD), SHOT S49

(KEY OF FIGURE 5)

Note in the 619μs frame that a point of luminosity appears 30 mm ahead of the flame front. This point of luminosity may be burning caused or enhanced by pressure build-up ahead of the wide luminous front. It may also be propagation of burning ahead of the wide luminous front through a channel in the charge not visible to the camera. In any case, this point of luminosity quickly expands until a planar front, propagating at 0.45 mm/μs, appears in the 743μs frame. At approximately the same time when and location where the planar front develops, there originates a 1.14 mm/μs pressure front (points F, H, K in Figure 16) that is followed by high strain rates. The pressure associated with the 0.45 mm/μs luminous front is nominally 0.7 kbar, and hence exceeds the elastic strength of the Lexan tube. Despite the relatively high pressure, the front was only weakly luminous and did not trigger the conductivity pin at 136.5 mm.

The SG records in Figure 17 show negative excursions for the 152 and 216 mm locations. This is the first time such pronounced negative excursions have been observed in the Lexan system. These excursions have been extensively observed in the steel DDT tube system during the propagation of strong compressive waves and also prior to the onset of detonation. In those cases, the strain gages were located close to the onset of detonation and/or relatively far from the ignitor.

As seen in the 784μs frame of Figure 15b, the first half of the tube is expanding from the high internal gas pressure. In the next frame at 825μs this section of the tube is rupturing while an intensely luminous detonation wave propagates in the second half of the tube. The apparent 25μs delay between the luminous detonation wave and the conductivity pin responses in Figure 16 is fictitious as discussed in Section 2.C.5.b.

The triggering of conductivity pins at 200 and 276 mm indicate a detonation velocity of 5.44 mm/μs. The pin at 136.5 mm triggered after the pin at 200 mm possibly because of a rearward travelling shock wave. In a steel tube (which has an ID of 16.7 mm), the detonation velocity for a 63.2% TMD 470μm tetryl charge (Shot 607) was 5.82 mm/μs. Considering the differences in effective confinement and porosity, the detonation velocities in the two systems are in good agreement.

C. RDX/WAX

Various mixtures of RDX/wax ranging from 0 to 15% wax have been investigated in steel tube studies[3,8]. All mixtures exhibited the same mechanism for DDT as proposed in the original study of 91/9 RDX/wax[3]. In this initial study in Lexan tubes, the more energetic mixtures, which are more likely to transit to detonation in a low confinement system, were investigated.

1. 94/6 RDX/WAX AT 69.8% TMD (SHOTS S37 and S40). In a steel tube test, 94/6 RDX/wax at 70.3% TMD, Shot 401[8], exhibited DDT and had a predetonation column length of 130 mm. This material was investigated here at a similar porosity in two different Lexan experiments. The first experiment (Shot S37) was conducted with a standard Lexan tube except the length was 254 mm instead of 305 mm. In this shot the tube

ruptured just behind a 0.85 mm/μs luminous front 130 mm from the ignitor. Consequently, in the second experiment (Shot S40, also with a 254 mm long tube) the inside diameter was reduced from the standard 25.4 mm to 16.8 mm in order to increase the confinement slightly; any diameter effects on DDT in a Lexan tube might also be indicated. (This smaller inner diameter tube contained a smaller ignitor identical to those used in 16.7 mm inner diameter steel tubes[2].) The smaller inner diameter tube also ruptured just behind a 0.85 mm/μs luminous front, but the front was farther downstream (180 mm) at the time of rupture.

Enlargements (10X) of some of the frames from the camera film from the first experiment (Shot S37) are shown in Figures 18 a, b. In both Shot S37 and S40 the connecting bolts were so close to the tube that the view of the top and bottom edges of the outer diameter of the tube are blocked by the bolts. Since it is desirable to observe the expansion of the outer diameter of the tube, tabs of paper which projected beyond the connecting bolts were attached to the first tube (see Figure 18). This was not done for Shot S40, but for all subsequent experiments the bolts were moved further from the tube as shown in Figure 1.

For Shot S37 the luminous fronts and changes in the rate of strain at two gage locations are shown on the x-t diagram in Figure 19. The first luminous event was a 0.013 mm/μs ignitor front which propagated to about 10 mm, where a faster 0.08 mm/μs luminous front began. The planar 0.08 mm/μs front transited, at about 40 mm, to an irregular, less luminous 0.85 mm/μs front. The velocity of the 0.85 mm/μs front declined beginning at 115 mm due to tube deformation just before it ruptured.

The strain gage traces for gages at 25.4 and 76.2 mm are shown in Figure 20. Moderate pressurization occurred about 300μs ahead of the luminous front for both gages. Just before the arrival of the 0.08 mm/μs luminous front at the 25.4 mm gage location, there was a momentary pressure spike and then a return to the previous rate of pressurization. These traces end at 1000μs because that was the maximum recording time chosen for the oscilloscopes. Gages beyond 76.2 mm recorded essentially no change in strain within the 1000μs recording time.

Enlargements (10X) of some of the frames from the camera film from the second experiment (Shot S40) are shown in Figures 21 a, b, and c. The luminous fronts from this experiment are plotted on the x-t diagram in Figure 22 with the luminous fronts from Shot S37 to show that results of both Lexan tube experiments are quite similar. In Shot S40 (the smaller I.D. Lexan tube) the ignition process was much slower; consequently, the luminous front data from Shot S37 are shifted 1300μs in positive time on Figure 22 for comparison with the data from Shot S40. The smaller inner diameter of the tube in the second experiment apparently was conducive to the propagation of the 0.85 mm/μs luminous front another 50 mm before the tube ruptured.

In the earlier steel tube work the first ionization pin was usually at 41 mm; hence the zone in which the 0.013 mm/μs and the 0.08 mm/μs fronts propagated in the Lexan tube was uninstrumented. In the steel tube experiment (Shot 401), the first four ionization pins (at 41, 67, 92 and 105 mm) were discharged by a 0.38mm/μs convective ignition front; and about 100μs after the 41 mm pin discharged, the strain gages detected a 0.9 mm/μs postconvective (compressive) wave. So in the

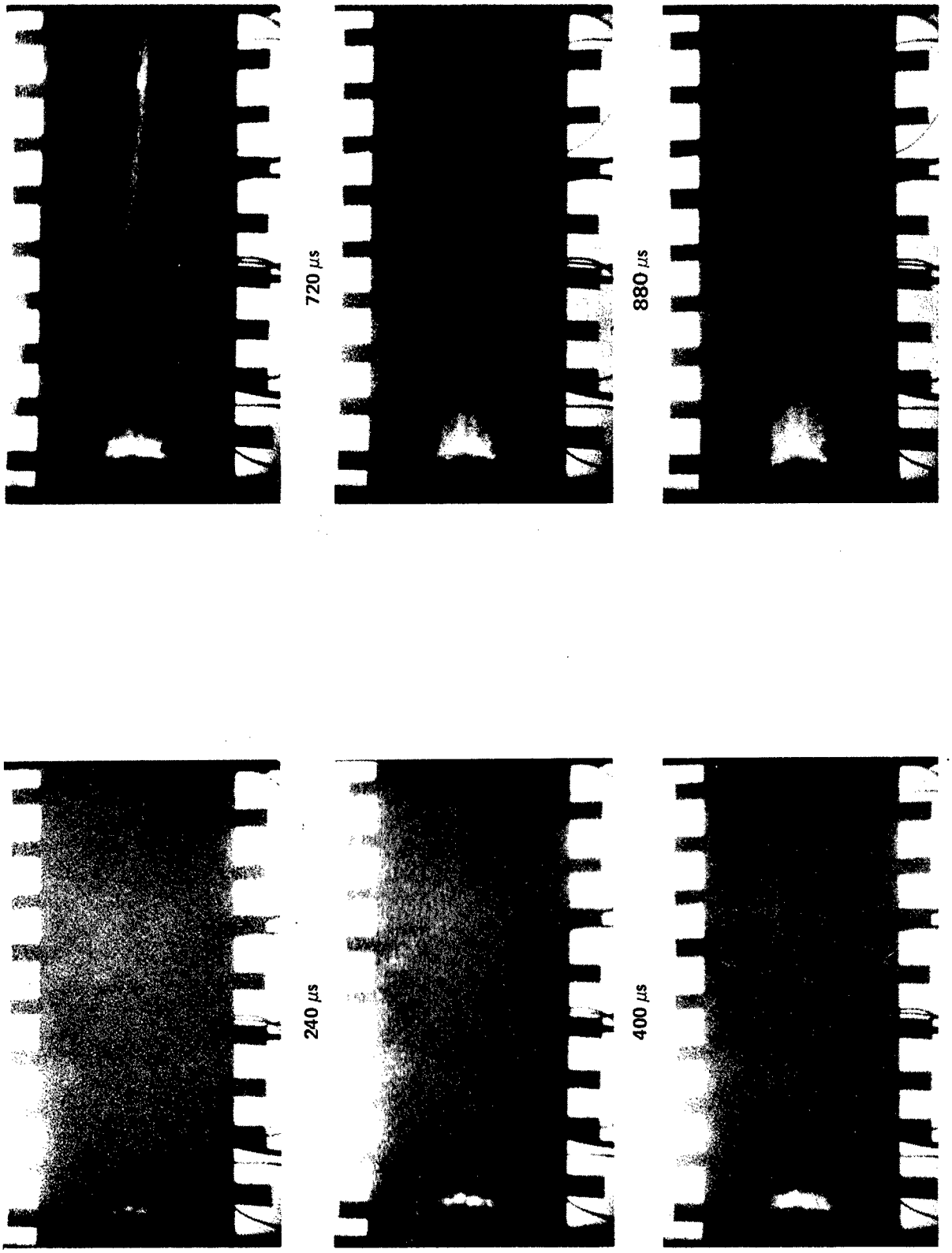

FIGURE 18a PHOTOGRAPHS OF BURNING IN 94/6 RDX/WAX (69.8% TMD), SHOT S37, SHEET 1 OF 2

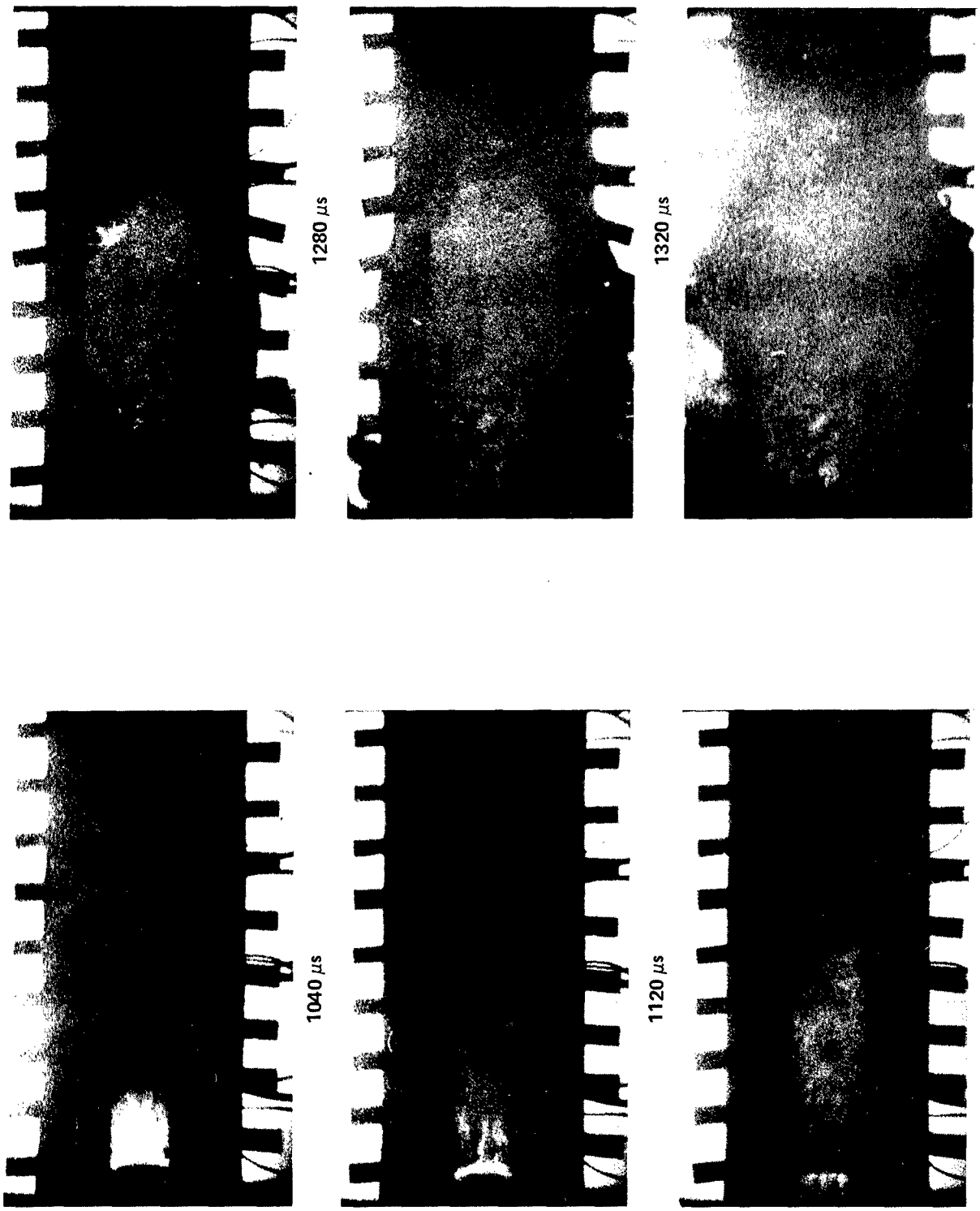

FIGURE 18b PHOTOGRAPHS OF BURNING IN 94/6 RDX/WAX (69.8% TMD), SHOT S37, SHEET 2 OF 2

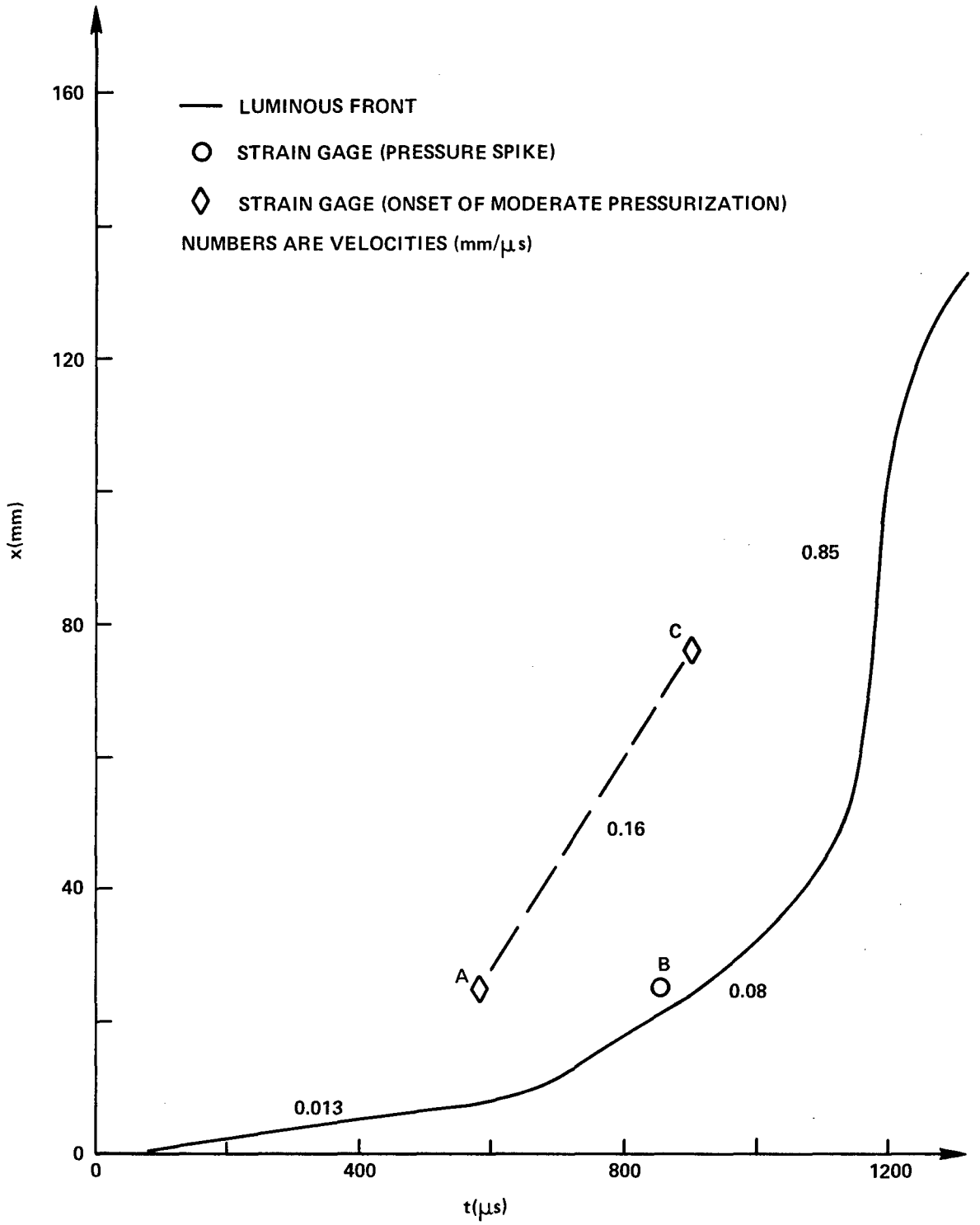

FIGURE 19 DISTANCE-TIME DATA FOR 94/6 RDX/WAX (69.8% TMD), SHOT S37

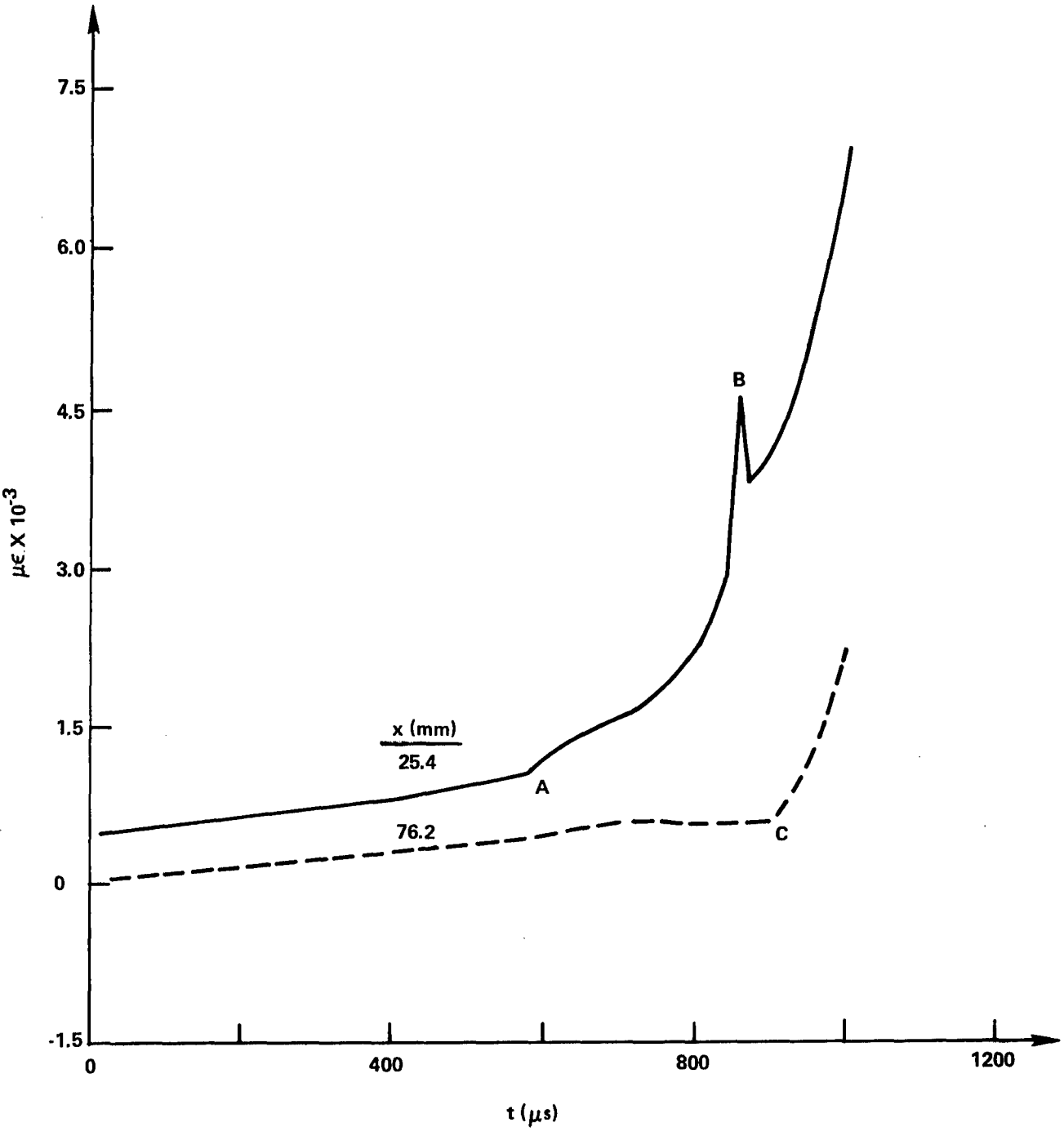

FIGURE 20 STRAIN VERSUS TIME FOR 94/6 RDX/WAX (69.8% TMD), SHOT S37

(KEY OF FIGURE 5)

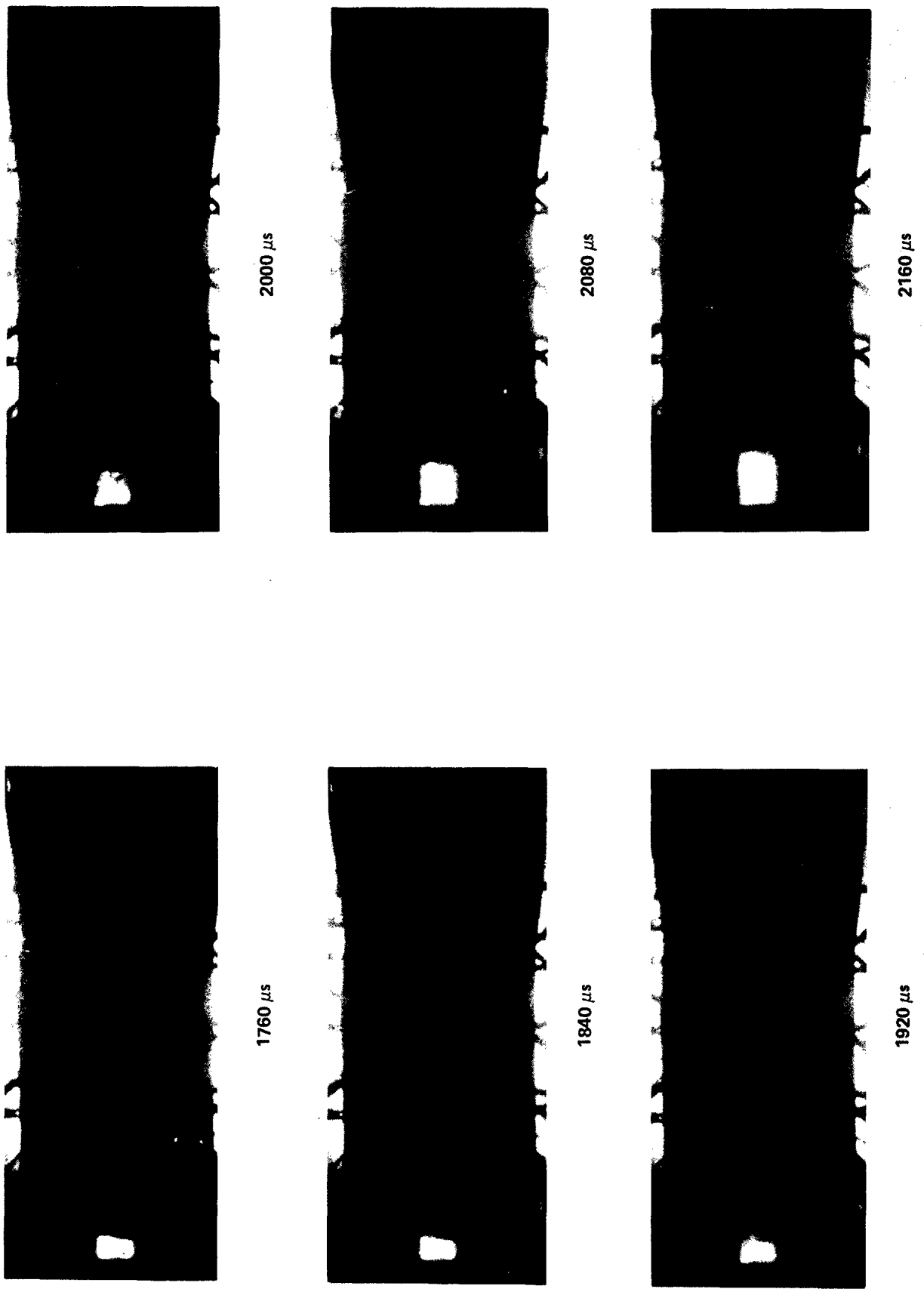

FIGURE 21a PHOTOGRAPHS OF BURNING IN 94/6 RDX/WAX (69.8% TMD), SHOT S40, SHEET 1 OF 3

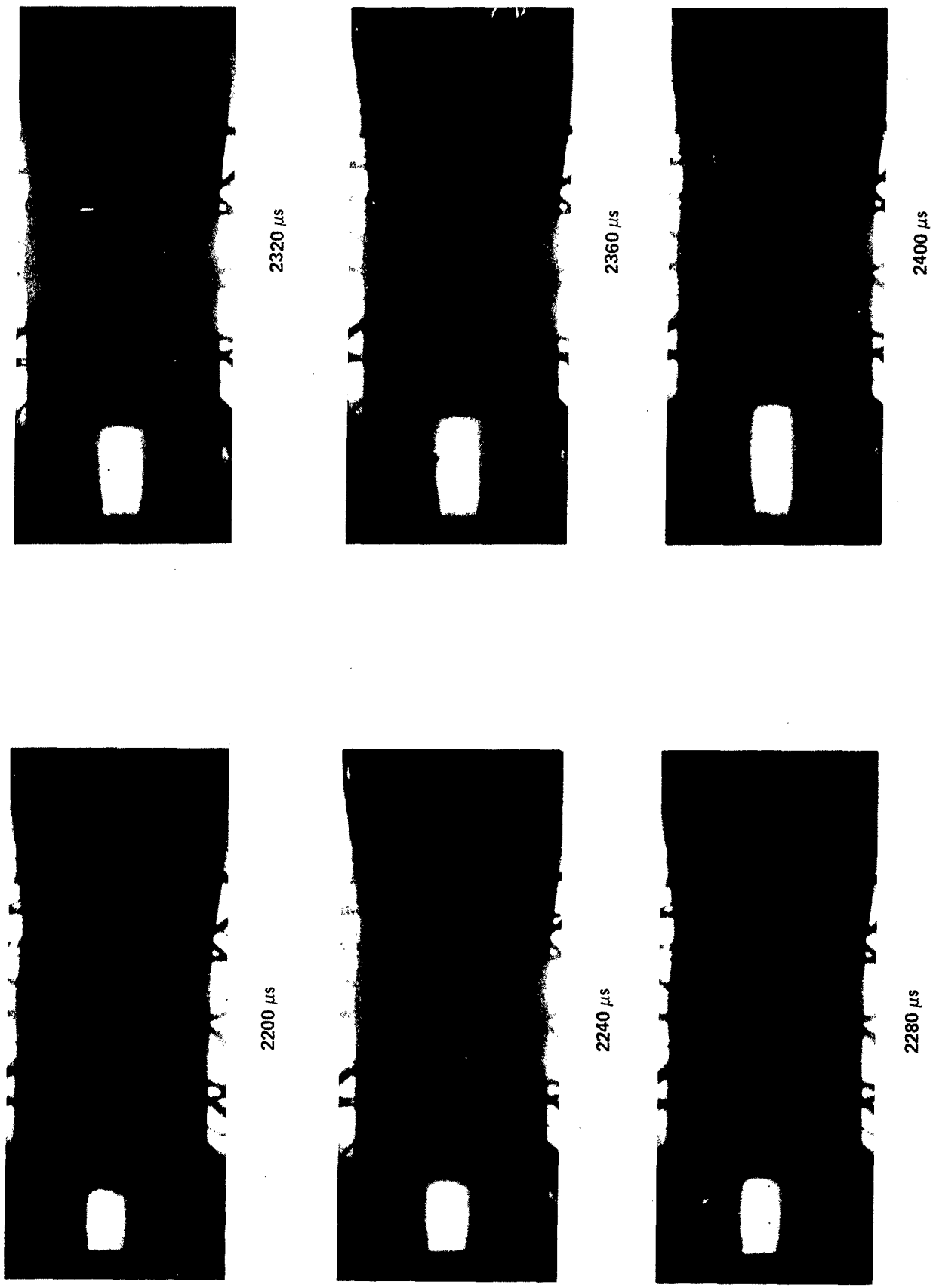

FIGURE 21b PHOTOGRAPHS OF BURNING IN 94/6 RDX/WAX (69.8% TMD), SHOT S40, SHEET 2 OF 3

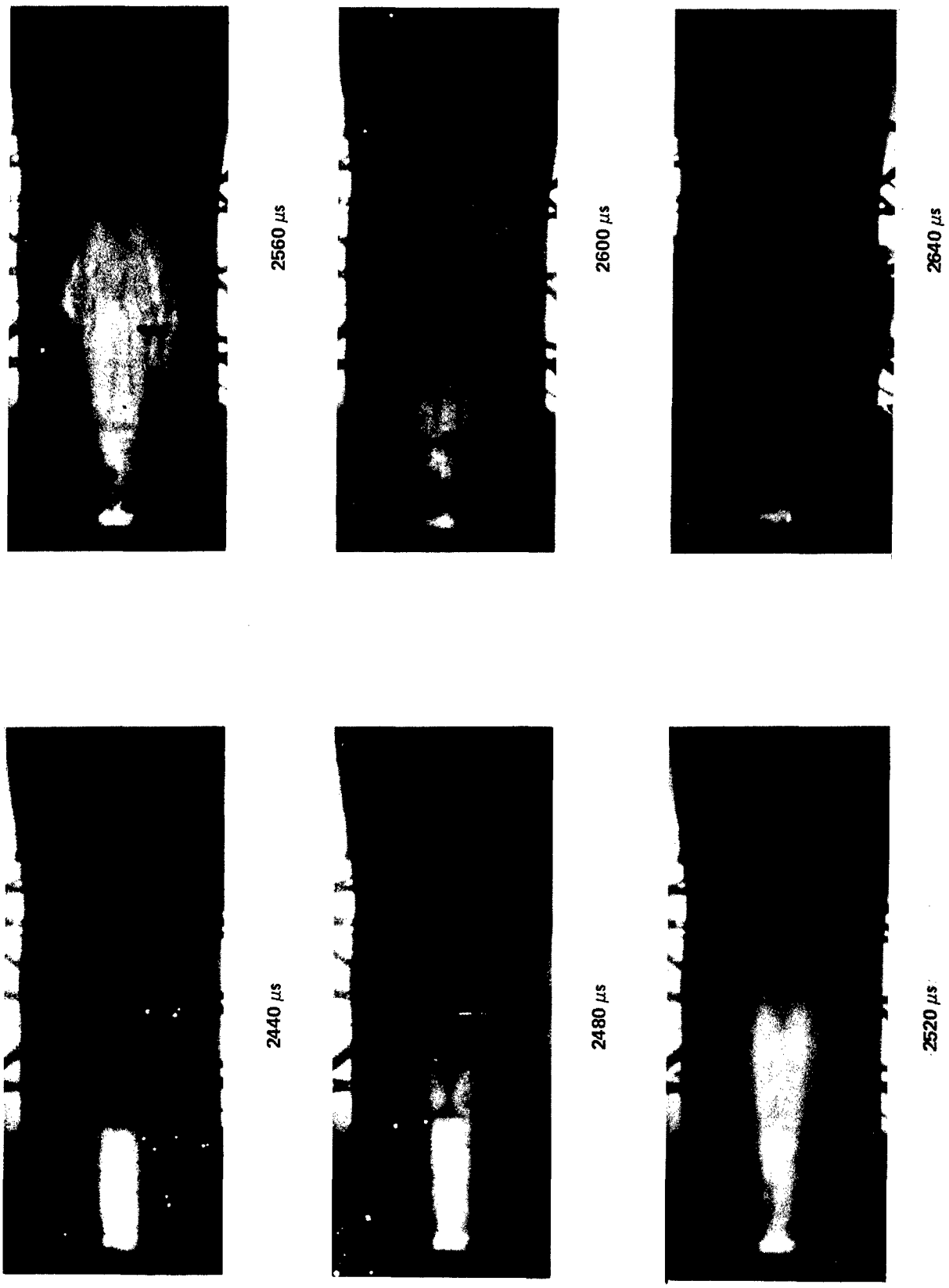

FIGURE 21c PHOTOGRAPHS OF BURNING IN 94/6 RDX/WAX (69.8% TMD), SHOT S40, SHEET 3 OF 3

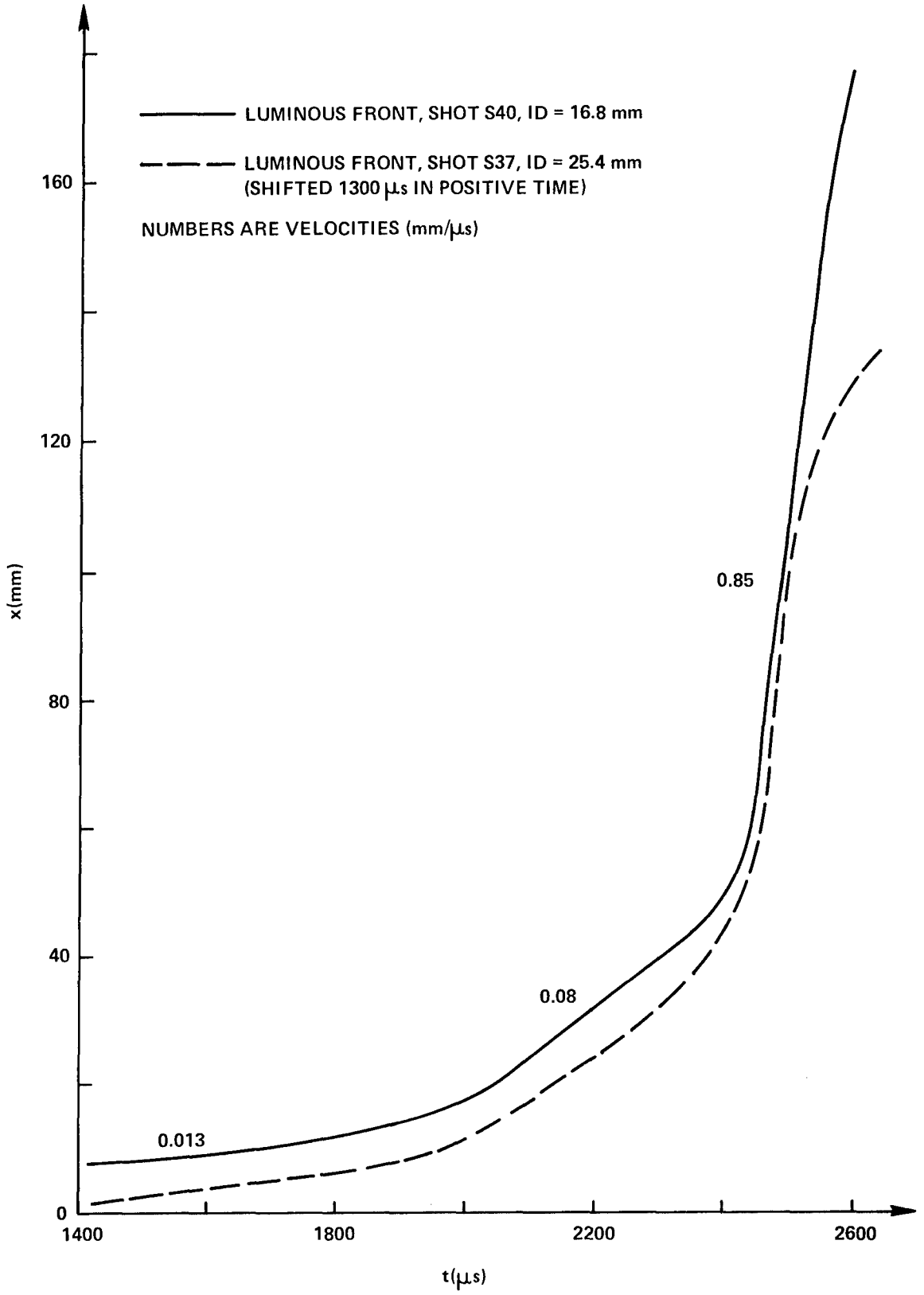

FIGURE 22 DISTANCE-TIME DATA FOR 94/6 RDX/WAX (69.8% TMD), SHOTS S40 AND S37

same region of the tubes, the convective front in the steel tube did not appear as a luminous front in the Lexan tube. However, the rapid burning (behind the 0.85 mm/μs luminous front), which caused the rupture of the Lexan tube, is characteristic of the accelerated burning behind the postconvective wave in the steel tube.

Since in the steel tube the postconvective wave originated near the same location, but about 100μs later than the convective front, it first appears that the convective front was simply not visible in the Lexan tube. The convective flame front may have propagated along only the central core of the charge; the ionization pins in the steel tube which detected the convective front were 40% of the charge diameter from the tube wall, whereas the luminous fronts in the Lexan tube are at the tube wall. Even if the convective front propagated over the entire charge cross-section, the 6% wax may have reduced the luminosity enough to prevent exposure of the camera film. If so, this was not the case for the 97/3 RDX/wax experiment discussed next.

2. 97/3 RDX/WAX AT 65.3% TMD (SHOT S52). In previous studies with the steel tube system, charges of 97/3 RDX/wax at 70.9% TMD underwent DDT with a predetonation column length of 72 mm (Shot 404)[8]. The shorter predetonation column than for 94/6 RDX/wax at the same porosity (ℓ=130 mm, Shot 401)[8] was expected to increase the possibility of transiting to detonation in a Lexan tube. However, a standard Lexan tube handpacked at 65.3% TMD with 97/3 RDX/wax ruptured at nearly the same location as a standard Lexan tube loaded with 94/6 RDX/wax at 69.8% TMD (Shot S37).

The enlargements (10X) from the framing camera film are shown in Figures 23 a, b; the corresponding distance-time data are shown in Figure 24. The first light on the film record is a planar, 0.010 mm/μs ignitor front which propagates for about 1500μs. At this time the luminous front quickly accelerates to a nearly steady 0.06 mm/μs, becomes less luminous and is less planar. At about 1700μs, just prior to the acceleration of the luminous front, the strain gages record a pressure front with a moderate rate of pressure rise behind it that propagates down the charge at 0.30 mm/μs (points A, B, C, D, E on Figure 24). The change in luminous front velocity and the propagation of a pressure front indicate increased reaction which is probably due to ignition of the explosive. The ignited explosive would be conductively burning on the exposed end of the column. In addition, reaction in larger pores ahead of the end of the column may be responsible for the front being less luminous and less planar than the preceding ignitor front.

About 300μs after the 0.06 mm/μs luminous front began propagating, a flame peninsula, first seen in the 217μs frame, appears. From this peninsula a weakly luminous, 0.40 mm/μs front develops and propagates until the Lexan tube ruptures about 200μs later. The pressures along this front have exceeded the elastic limit of the tube and are in the nominal range of 0.3-0.5 kbar. The strain gage responses on Figure 24 which are shown as solid diamonds are essentially an isobar (0.10-0.12 kbar) and, as shown in Figure 25, do not indicate a distinctive change in strain rate. This isobar as well as the strain gage responses showing the beginning of moderate pressurization (points A, B, C, D, E) are roughly parallel the 0.40 mm/μs luminous front.

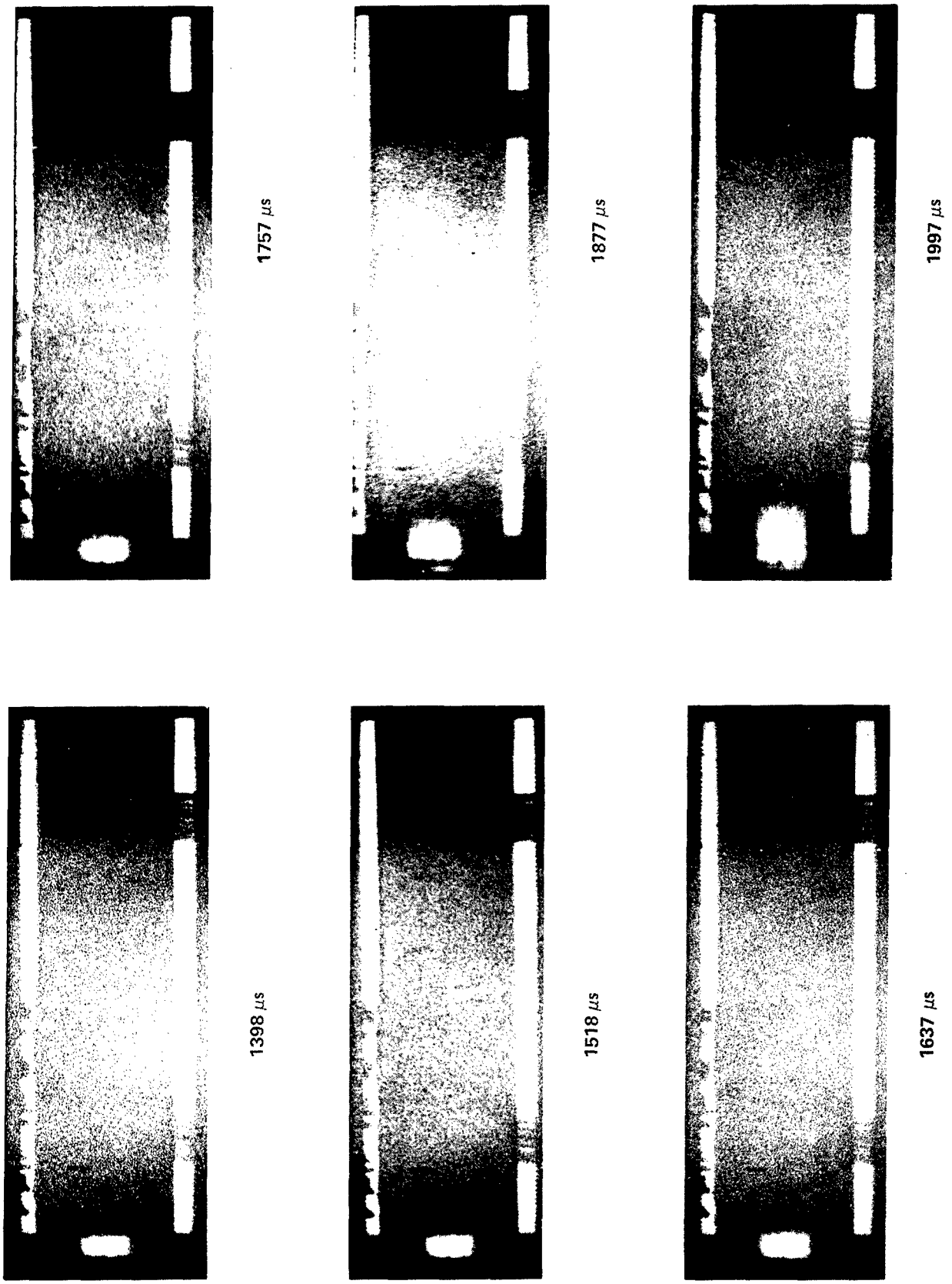

FIGURE 23a PHOTOGRAPHS OF BURNING IN 97/3 RDX/WAX (65.3% TMD), SHOT S52, SHEET 1 OF 2

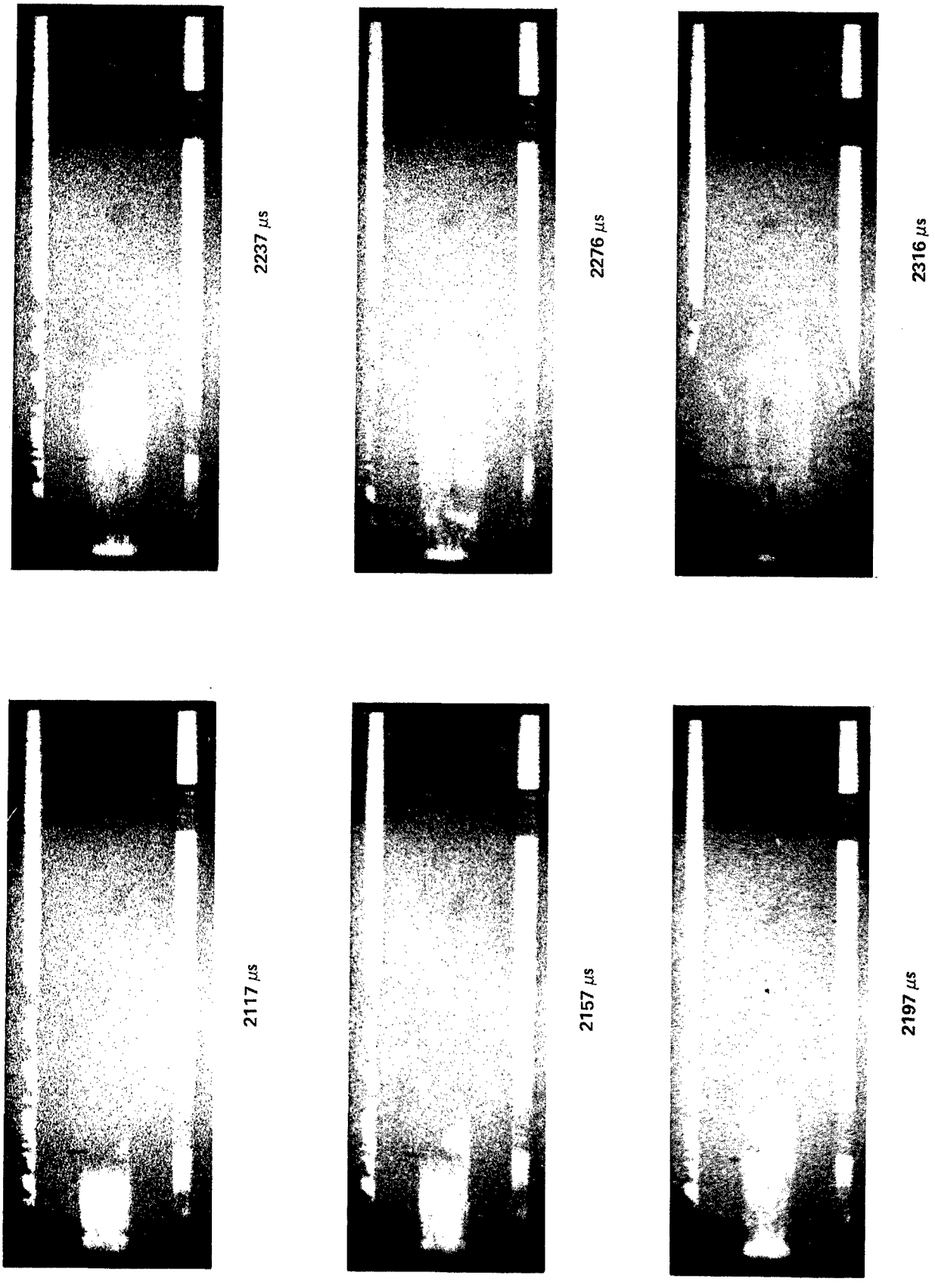

FIGURE 23b PHOTOGRAPHS OF BURNING IN 97/3 RDX/WAX (65.3% TMD), SHOT S52, SHEET 2 OF 2

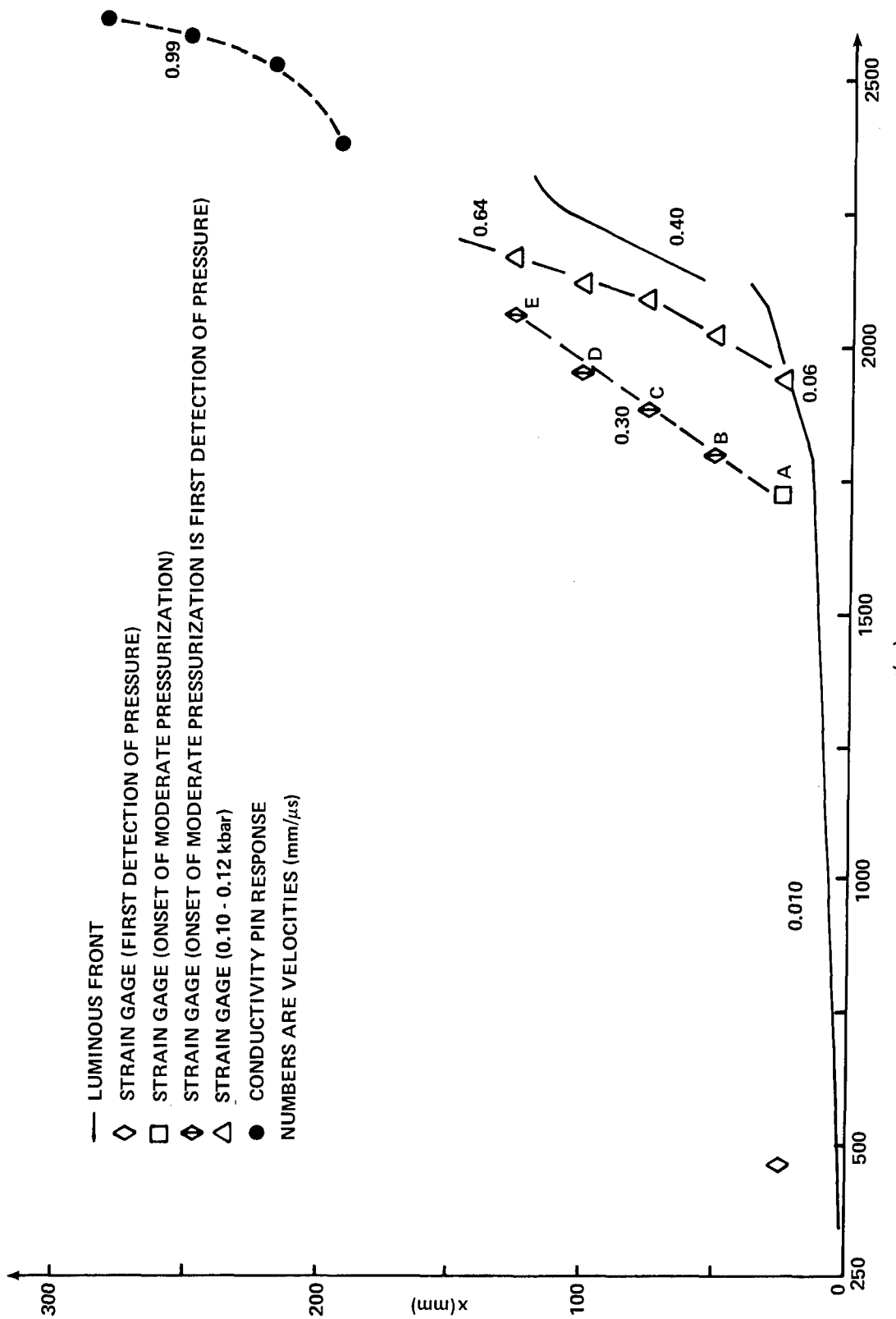

FIGURE 24 DISTANCE-TIME DATA FOR 97/3 RDX/WAX (65.3%TMD), SHOT S52

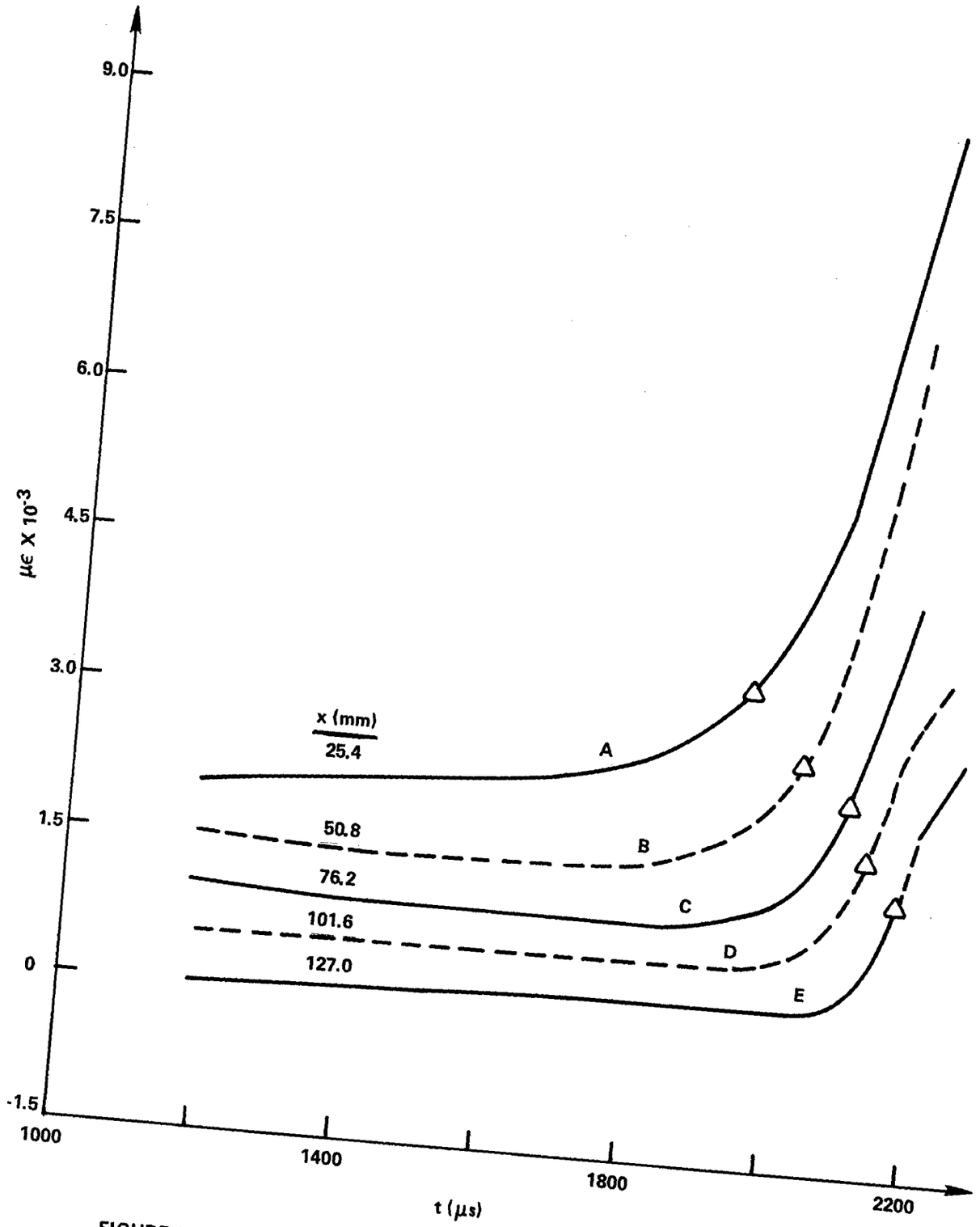

FIGURE 25 STRAIN VERSUS TIME FOR 97/3 RDX/WAX (65.3% TMD), SHOT S52

(KEY OF FIGURE 5, △ PRESSURE = 0.10 - 0.12 kbar)

Thus, the 0.40 mm/μs luminous front is preceded by a gradual increase in pressure (~0.001 kbar/μs) as a convective ignition front would be. This luminous front even has about the same velocity as the ~0.47 mm/μs convective front detected by ionization pins in steel tube Shot 404.[8]

If the 0.40 mm/μs luminous front is not a convective front it is at least associated with one. In the last three frames of Figure 23b there is obvious tube deformation which is blocking some of the backlighting from the electronic flash. The position in each of these frames where tube deformation appears to begin is close to the luminous front. The observed luminosity may be from gases between the deforming tube and the explosive column, but reaction following the passage of the convective front would be causing the tube deformation.

Following tube rupture at about 2316 μs, there was no luminous front recorded on the framing camera film; but as shown on the distance-time plot in Figure 24, the conductivity pins downstream from the last position of the luminous front detected an accelerating disturbance. The response of the first pin appears to be due to the pressure disturbance which originated near the ignitor and propagated ahead of the 0.40 mm/μs luminous front. The average velocity between the last two pins was 0.99 mm/μs, which is a reasonable postconvective wave velocity for this charge density. This disturbance and any subsequent reaction did not damage the steel plate on the downstream end of the charge. A postconvective wave could not have been detected by the strain gages since the tube was already yielding with the passage of the convective front. It is possible that the accelerated burning following a postconvective wave started tube rupture.

CHAPTER 4

DISCUSSION

A. DDT MECHANISM(S) FOR POROUS CHARGES

Generalized models of the DDT mechanism for porous explosive charges have been proposed by Belyaev et al.[16] and Bernecker and Price[4]. As discussed recently[1], the two proposed models are generally similar, the main difference between them being the origin of the driving force for accelerated (compressive) burning. Since the mechanism of Belyaev et al. is based upon photographic observations (made chiefly with metallic tubes containing a transparent plastic wedge), detailed discussions and observations presented in Reference 16 are very pertinent to the following discussions of the present experimental data.

In Figure 26 is shown a generalized DDT mechanism (for both cast and porous charges) as discussed in Reference 1. Four regimes are present following ignition: conductive burning; convective burning; compressive burning; and detonation. However, the ignition process can play an important role in the establishment of later stages, e.g., convective burning, and has not been adequately discussed in either Reference 16 or 4. It is important to note that the type and amount of ignitor material used can be important in comparing experimental results from different laboratories; in fact, its importance in influencing the early stages of DDT may approach that of the confinement.

To correlate the various luminous fronts (from any photographic coverage of DDT experiments) with the various stages of the DDT mechanism, it is important to have some knowledge of the velocity of propagation associated with the various reaction fronts. With the exception of the conductive burning regime and the detonation regimes, very little systematic information is available about the other (i.e., highly transient) regimes of convective burning and compressive burning, under conditions of closed tube experiments. Detailed studies have been made of convective burning under steady state conditions for porous charges or for a single pore (see Reference 16) but there is no satisfactory way to extrapolate these data to closed tube experiments. On the other hand, compressive burning velocities can be estimated from knowledge of the sound velocity and/or Hugioniot data for porous charges. Unfortunately, in these areas too, very little applicable information is available. Consequently, such items as the delineation between convective and compressive burning fronts is uncertain at present and will be resolved only as the result of extensive DDT studies and companion measurements.

[16] Belyaev, A. F., Bobolev, V. K., Korotkov, A. I., Sulimov, A. A., and Chuiko, S. V., Transition from Deflagration to Detonation in Condensed Phases, Izdatel'stvo "Nauka", Moscow, 1973. English translation by Israel Program for Scientific Translations, 1975.

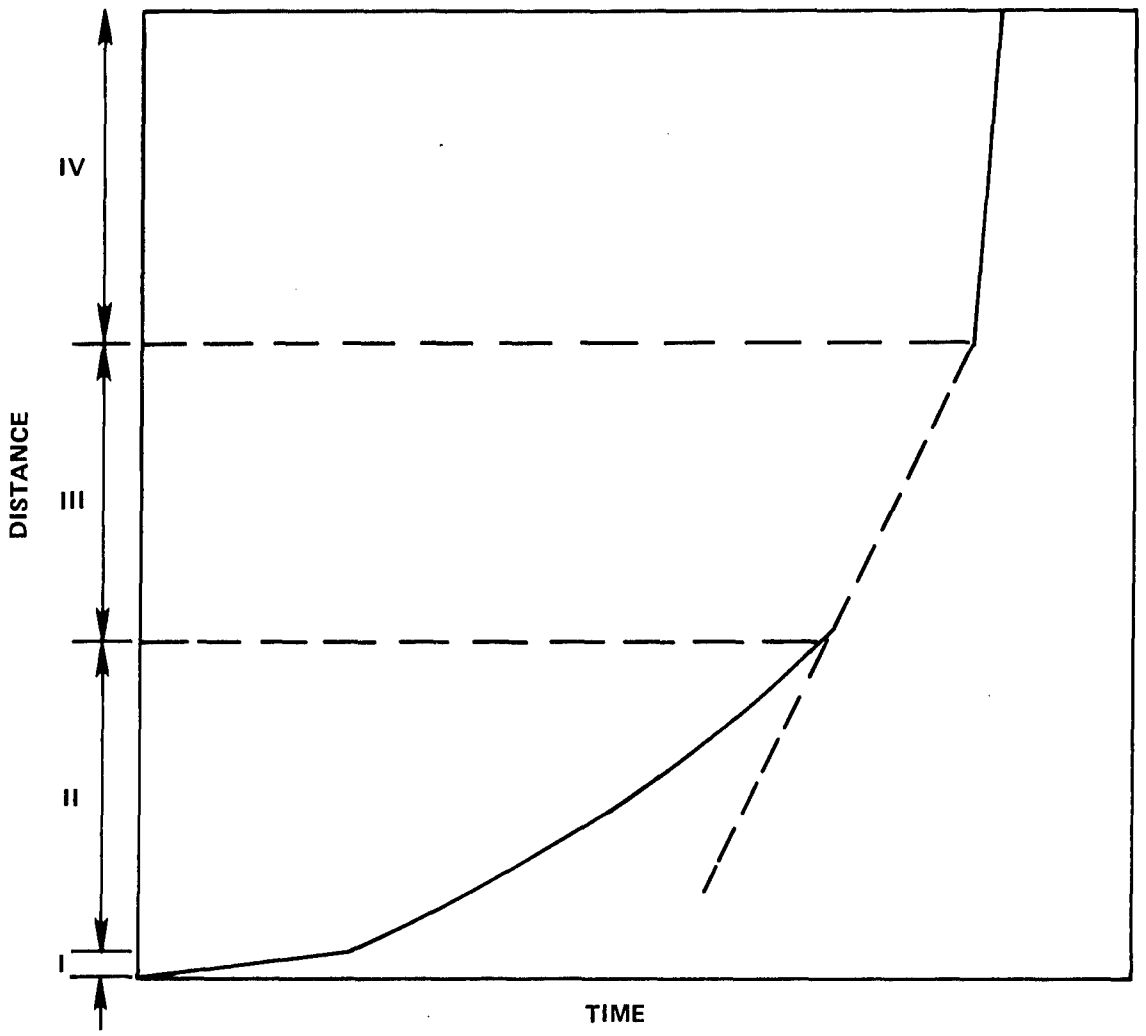

REGIME	STAGE
CONDUCTIVE BURNING	I
CONVECTIVE BURNING	II
COMPRESSIVE BURNING	II AND III
DETONATION	IV

FIGURE 26 PROPOSED GENERALIZED DDT MECHANISM (REF. 16)

B. IGNITION AND CONDUCTIVE BURNING

Ignition of the explosive and the resulting conductive (laminar) burning are the slowest processes in the DDT mechanism. A study of steady state ignition of HMX by radiant heating, for example, found ignition times of tens of milliseconds at a pressure of ~17 bars and heat fluxes of 20 to 500 cal/cm^2/s.[17] The ignition time for an explosive in a transparent tube in this system is faster, 0.5 to 3.5 ms for the explosives studied in this report, but the process is more complicated than heating the exposed surface of the explosive column initially adjacent to the ignitor. If the B/KNO3 products are in equilibrium at a pressure of 69 bar, there are 0.28 grams of solids and 0.47 grams (6.9×10^{-3} moles) of gases at a temperature of 2335°K. In addition to the ignitor products radiatively and conductively heating the exposed surface of the explosive, some of the gases and even the smaller particles can penetrate and heat the porous explosive column. These products escaping from the ignitor reduce its pressurization and burning rate. Thus, the porosity of the explosive influences the gas generating ignition source, unlike ignition by externally controlled radiant heating.

Early in the study several supplementary experiments aided in characterizing the ignitor. As discussed in Appendix A, ignitors were heavily confined with a 12.7 mm thick PMMA disc across their exposed surface in order to view flame break through with a framing camera. Even though the confining arrangement permitted gas leakage, the pressure from B/KNO_3 combustion would break the PMMA disc. Likewise, an explosive column would have to be quite permeable or the pressure from B/KNO_3 combustion would compact it. It was known from earlier studies in steel tubes[3] that an inert material, melamine, was compacted by an ignitor.[5]

As discussed in Appendix B, the dynamic compaction of 58 μm melamine packed in a transparent tube at 70% TMD was observed with a framing camera. Following the first detection of luminance by an optical fiber/photocell at the ignitor/melamine interface there was a 80 μs delay before the framing camera began to record light. This delay, which is discussed in Section 2.C.5.b., also occurs in experiments with explosives. The light on the framing film then propagated at about 0.013 mm/μs for 1 ms, and as discussed in Appendix B, corresponds to the formation of a 11(±3) mm long gas void between the ignitor and dynamically compacting charge. This luminous front is called the "ignitor front", and is the initial luminous front observed in all the explosive charges tested in this study.

The ignitor front velocity represents the particle velocity of a compaction front, which has been nonluminous in these experiments. The velocity of the compaction front is estimated to be 0.1 to 0.2 mm/μs; the exact value will be measured in future studies using flash radiography. The velocity of the compaction front will determine, 1) the length of the compacted region at any time, and 2) the time that the compaction front reaches the far end of the porous bed.

[17] Chan, M. L., Eisel, J. L., Zurn, D. E., Boggs, T. L., "Analysis of Preignition Pyroylsis Products of High Energy Propellants", 16th JANNAF Combustion Meeting, Monterey, California, 11 September 1979.

Besides the ignitor front, several other events are often observed in an explosive before sustained ignition* is achieved. The measurement of strain (pressure) along the length of the transparent tube sometimes revealed a pressure front originating with the ignitor front. In two of the explosives, the ignitor quickly forced the "burning" of a small amount of the explosive without achieving sustained ignition of the bulk; the associated luminous front is called a "transient ignition front". When sustained ignition is achieved, the end of the explosive column burns conductively and the rate of compaction increases; ignition is manifested in the photographic data as an increase in propagation rate of the luminosity (i.e., from the ignitor front velocity to the "conductive burning interface" velocity). These events are summarized in Table 3 for each explosive charge and the inert melamine charge.

1. PRE-IGNITION EVENTS. The ignitor front velocity is a function of the permeability and compressibility of the porous explosive, the friction between the inner tube wall and the porous explosive, and the ignitor pressure. The ignitor pressure is the driving force for the compaction until the explosive ignites. The compressibility, which is the mechanical strength of the porous explosive, and the wall friction resist the compaction. The gas pressure generated by the ignitor is reduced by the flow of gas into the permeable explosive and by dynamic compaction itself, which increases the volume of the gas void between the ignitor and end of the explosive column. Any influence on the pressure environment in turn influences the pressure sensitive ignitor burning rate and hence its rate of generating gas and pressure.

Relative to the 0.013 mm/μs ignitor front velocity of melamine, the RDX/wax charges have nearly identical velocities while picric acid and tetryl exhibit substantially higher velocities. It appears that the initial event in the RDX/wax mixtures is, like that of the melamine, compaction of the porous bed without ignition of the explosive. Since the particle sizes for picric acid and melamine are quite comparable (67 μm and 58 μm, respectively) the 30% porosity beds of melamine and picric acid should have similar permeabilities. However, the ignitor front velocities listed in Table 3 for the three picric acid charges are nearly four times greater than that for melamine and, more significantly, do not appear to be influenced by the permeability of the porous beds. Melting of the picric acid (122°C) by the initial products from the burning ignitor mix can possibly explain these two observations.

If the layer of picric acid adjacent to the ignitor is being melted, it is likely the ignitor products are more quickly cooled than in a porous bed without melting. The cooler ignitor products will be less luminous as they flow over the optical fiber in the ignitor sleeve (see Figure 1). As a consequence, the photocell which terminates the optical fiber and the framing camera may be delayed in detecting the initial efflux of ignitor products relative to other explosives. This delay allows sufficient time for the layer of picric acid adjacent to the ignitor to have melted and formed an impermeable plug. The pressure of the confined ignitor products increase until first, the optical/fiber photocell detects them and second, within an additional 200 μs, the melt layer ruptures. From the

*Sustained ignition does not necessarily imply steady state ignition. The selection of ignition time for each experiment is discussed in Section 4.B.2.

TABLE 3

SUMMARY OF PRE-IGNITION AND IGNITION EVENTS

SHOT NUMBER	MATERIAL	DENSITY (g/cc)	DENSITY (% TMD)	V_{IF} (mm/μs)	V_{PF} (mm/μs)	V_{TIF} (mm/μs)	τ_{IGN} (ms)	$X_{IF,max}$ (mm)	V_{CBI} (mm/μs)
S41	Picric Acid	1.05	59.7	0.041*	0.62		f	48	
351	Picric Acid	1.20	68.2	0.023*			3.0-3.5	32	
S43	Picric Acid	1.23	69.9	0.037*	1.20	0.14	1.4-1.6	~30	
S42	20 μm Tetryl	0.80	46.2	0.056	0.20	0.17-0.21	1.0-1.2	~65	
S49	470 μm Tetryl	1.00	57.8	0.038	0.22		0.45-0.50	14	0.10
S37	94/6 RDX/wax	1.20	69.8	0.013			0.50-0.60	8	0.08
S40	94/6 RDX/wax	1.20	69.8	0.013			~1.8	12	0.08
S52	97/3 RDX/wax	1.15	65.3	0.010			1.7-1.8	14	0.06
S7+	Melamine (inert)	1.10	70.0	0.013				11	

V_{IF} = Ignitor front velocity

V_{PF} = Velocity of pressure front originating with ignitor front

V_{TIF} = Transient ignition front velocity

τ_{IGN} = Time to achieve sustained ignition

$X_{IF,MAX}$ = Maximum displacement of ignitor front

V_{CBI} = Conductive burning interface velocity

f = Failure
* = Initial value, front decelerated at later times
+ = This experiment is discussed in Appendix B

rupturing melt layer 0.62 and 1.20 mm/μs compressive waves (in, respectively, the 60 and 70% TMD shots listed in Table 3) propagate the full length of the charges. Simultaneously, a luminous ignitor front appears which propagates at velocities four times greater than that for melamine. This high velocity arises because the ruptured melt layer still partially plugs the charge cross-section and compaction of the charge results from the pressure gradient across a "leaky piston".

The ignitor front and following events in the two tests with tetryl, 20 μm tetryl at 46.2% TMD and 470 μm tetryl at 57.8% TMD, were quite different from each other primarily due to their different particle sizes and, therefore, permeabilities. For example, the pressure gradient for equal flow velocities should be about 500 times higher in the 20 μm tetryl charge based on the Darcy equation*. The relatively lower permeability of the 20 μm tetryl charge should result in a higher pressure in the continuously expanding void next to the ignitor which will generate a higher ignitor front velocity, as is the case.

Although the melting point of tetryl (129°C) is quite similar to that of picric acid (123°C), there was no evidence of melting in tetryl. For example, in both tetryl charges the approximately 0.20 mm/μs pressure fronts originating with the ignitor fronts appear to be subsonic, indicating a continuous flow of gases into the porous bed. On the other hand, the sonic fronts originating with the ignitor fronts in the picric acid charges have been attributed to the sudden start of gas flow from the rupture of a melt layer.

The ~0.20 mm/μs pressure fronts in the tetryl charges are quite different despite their nearly equal velocities. The higher permeability of 470 μm tetryl permits ignitor products to flow more easily throughout the cross-section of the porous bed. The thermal energy of the ignitor products is dissipated over a significant bed volume thus inhibiting any immediate reaction and the appearance of light beyond the ignitor front. Conversely, in the 20 μm tetryl charge the low permeability of the porous bed could force more of the gas flow from the core to near the inner tube wall, as discussed later. This concentration of heated gas flow causes the tetryl adjacent to the tube wall to react, creating the "transient" 0.17-0.21 mm/μs luminous front which closely follows the pressure front.

For any charge, the permeability near the inner tube wall is greater than that of the core for two reasons. First, the ram which originally packs the explosive in the tube is about 250 μm smaller than tube inner diameter, and therefore, small particles (<125μm) next to the tube wall do not receive the same packing pressure as those in the core. This may be significant for a depth of only several particle diameters from the face of the ram. Second, even if the bed is uniformly packed, Schwartz and Smith[18] found a peak mass flux 30% to 100%

*The use of the Darcy equation for these charges is not valid because of the turbulent flow conditions here. Nevertheless, it does give an indication of trends and relative values.

[18]Schwartz, C. E. and Smith, J. M., "Flow Distribution in Packed Beds," Industrial and Engineering Chemistry, Vol. 45, No. 6, 1953, p. 1209.

greater than the mass flux at the axis of the bed occurred within one particle diameter from the wall. As an example of this effect from our own studies (see Appendix B), it was observed that melamine was discolored by ignitor products up to 94 mm along a 1 mm annulus adjacent to the inner tube wall.

The 0.17-0.21 mm/μs luminous front in the 20 μm tetryl charge is called a "transient ignition front" because sustained ignition of the bulk of the explosive was not achieved. The evidence for the failure of ignition is the decline in the rate of pressurization following the passage of the front. Also, the pressures associated with this front (0.01-0.05 kbar) are a factor of ten lower than those observed for the convective ignition fronts listed in Table 4. The 0.14 mm/μs luminous front which failed at 50 mm in the 70% TMD picric acid charge is also probably a transient ignition front. It has about the same velocity as the 0.17 mm/μs transient ignition front in the 20 μm tetryl charge, and it also originated with the onset of the ignitor front. Unlike the tetryl charge, this front failed as the ignitor burned out, which is consistent with the difficulty of establishing a convective ignition front in picric acid. The subsonic pressure front which should have preceded the luminous front was probably masked by the 1.20 mm/μs compressive wave which also originated with the onset of the ignitor front.

2. IGNITION EVENTS. When the B/KNO_3 is consumed (in 1-2 ms), the ignitor front will stop propagating if the explosive has not been ignited, as observed in the picric acid charges. It follows that a sustained velocity increase in an established ignitor front is from increasing pressure in the void due to ignition and burning of the explosive. The luminous front resulting from conductive burning and displacement of the end of the explosive column is called a "conductive burning interface".

As illustrated in Figure 24 for 97/3 RDX/wax, at ~1800 μs the 0.010 mm/μs ignitor front changes to a 0.06 mm/μs conductive burning interface while at about the same time, ~1700 μs, a 0.30 mm/μs pressure front originates near the ignitor. It is postulated that at ~1700 μs the free end of the compacted explosive column ignited, thereby increasing the pressure in the gas void, which caused the penetration of gas into the explosive (the pressure front) and increased the luminous front velocity. The data in Figure 19 from one of the 94/6 RDX/wax experiments suggests an ignition time of ~500 μs from the strain gage data and ~600 μs from the camera film. These times are listed in Table 3 as the time of ignition, τ_{IGN}.

For the 20 μm tetryl charge, ignition probably occurs with the onset of the 0.32 mm/μs pressure front that originates at ~1000 μs (see Figure 13). Unlike the RDX/wax charges, the ignitor front velocity does not increase at ignition possibly because the charge is already significantly compacted at this time making additional compaction more difficult. The ignition of the 470 μm tetryl charge is similar to that in the RDX/wax mixtures; however, the 0.70 mm/μs pressure front which originated at ignition in 470 μm tetryl charge is estimated to be propagating at about the local sound speed versus subsonic speeds for the pressure fronts in the RDX/wax mixtures and in 20 μm tetryl. The 0.70 mm/μs appears to be, therefore, a weak compressive front requiring more energy to drive it than a subsonic front. This, in addition to the relatively high conductive burning interface velocity, suggests a stronger ignition in the 470 μm tetryl charge than in the 20 μm tetryl charge and may be the difference between the two particle sizes of tetryl in achieving DDT within the transparent tube apparatus.

Only in picric acid was the B/KNO_3 ignitor apparently consumed before ignition was achieved. Following the failure of the ignitor front, ignition was not established in the 60% TMD charge and was established in the 70 and 68% TMD charges only after delays of ~1 and 3 ms, respectively. Ignition of the explosive by a gas generating ignitor may be due primarily to convective heating much like closed bomb studies of conductive burning changing to convective burning, as studied by the Margolin and Chuiko[19]. Listed below from their Table 2 are a variety of explosives and the critical pore size required for transition to convective burning at a pressure of 100 bars. This table shows that TNT,

Explosive	Critical Pore Size (μm)[19]
TNT	108
Nitrocellulose	100
Picric Acid	90
PETN	55
Tetryl	48
RDX	21
Ammonium perchlorate	20
Mercury fulminate	4.3

nitrocellulose, and picric acid require a relatively large pore size for the transition to convective burning at 100 bars or, conversely, for the same pore sizes, higher pressures are required for the transition in these three explosives. This may explain the difficulty of igniting picric acid with a gas generating ignitor as well as the faster ignition of the 470 μm tetryl charge versus the 20 μm tetryl charge, which has smaller pores. Future tests are planned with TNT and nitrocellulose to see if they exhibit a failing ignitor front as observed for picric acid.

C. CONVECTIVE BURNING

Convective burning is a term used to describe the propagation of an ignition front through the pores of a granular charge and the subsequent conductive burning of the pore walls after ignition. Convective burning has been extensively studied, under controlled or steady state conditions, by Russian workers; a review of their work is contained in Reference 16. Some of the interesting features that they have found which are pertinent to the understanding of our experimental data are: 1) the hot combustion gases (or products), which heat the pores walls and which in turn are cooled, produce a mildly pressurized porous bed ahead of the propagating convective ignition front (CIF); and 2) convective ignition occurs preferentially first in the larger pores ahead of the front and then spreads laterally into the interconnecting smaller pores. In addition, in an early paper discussing their interpretation of the DDT mechanism in porous

[19]Margolin, A. D. and Chuiko, S. V., "Combustion Instability of a Porous Charge with Spontaneous Penetration of the Combustion Products into the Pores," Fizika Goreniya i Vzryva, Vol. 2, No. 3, 1966, p. 119, English translation, Combustion, Explosion and Shock Waves, Vol. 2, No. 3, 1969, p. 72.

charges, Obmenin and coworkers[20] concluded that convective heat transfer contributed not only to ignition within the pores but also to ignition on the lateral surface of the porous bed as the confining tube expanded.

Although the literature contains extensive data and correlations on the onset and propagation of a convective ignition front (CIF) under controlled conditions (see Reference 16), much less systematic information is available for the onset and propagation under transient conditions as they pertain to our DDT tube experiments. Consequently, until sufficient experimental documentation is accumulated, much conjecture is involved in analyzing the data from DDT tubes in terms of convective burning. A systematic compilation of "convective ignition front velocities" has been made for steel tubes using ionization pins (IPs)(6-8). However, there are several areas which must be understood better before these steel DDT tube data are used quantitatively to characterize convective fronts. Specifically, more must be learned about, 1) the level of ionization associated with the convective ignition front and the total convective ignition wave (that part of the ignited bed behind the front), and 2) the extent of deformation of the IPs, in the higher porosity charges, before the arrival of the convective ignition front.

The externally mounted strain gages on a Lexan tube, unlike a steel tube, are sensitive enough to detect the mild pressurization from combustion gases which convectively preheat a porous bed in preparation for ignition. As discussed in the last section, the propagation of these gases, started by the ignitor, is supplemented by ignition of the explosive. Except in the picric acid charges, the B/KNO_3 ignitor is still generating pressure at this stage. The rate of propagation of the mild pressurization is designated as V_{pp} (mm/μs), and the time interval between the pressure front and the CIF at some bed location is designated as τ_{CIF}(μs). These and the other parameters associated with CIF's in the transparent tube apparatus are summarized in Table 4. The velocities and pressures associated with the luminous CIF's are listed as V_{CIF} (mm/μs) and P_{CIF}(kbar). For P_{CIF} the first tabulated value is associated with the luminous CIF as shown in a distance-time plot while the second value arises if the luminous data is shifted in positive time to account for the synchronizing error between the strain gage and film data (see Section 2.C.5.b.).

CIF velocities obtained by ionization probes in steel tube experiments with the same explosives at similar densities are listed in Table 4 for comparative purposes. In steel tube experiments the pressures associated with the CIF's are consistent with the pressures (0.3-0.5 kbar) observed in Lexan tube experiments. However, the comparison cannot be quantitative because of the low sensitivity of strain gages on steel tubes and the plastic deformation of Lexan tubes at about 0.28 kbar. For the same reason no quantitative comparison of τ_{CIF} between the Lexan and steel tube experiments is justified.

[20] Obmenin, A. V., Korotkov, A. I., Sulimov, A. A., and Dubovitskii, V. F., "Propagation of Predetonation Regimes in Porous Explosives," Fizika Goreniya i Vzryva, Vol. 5, No. 4, 1969, p. 461. English translation, Combustion, Explosion and Shock Waves, Vol. 5, No. 4, 1972, p. 317.

TABLE 4

SUMMARY OF CONVECTIVE IGNITION FRONT (CIF) PARAMETERS

MATERIAL	TRANSPARENT TUBE EXPERIMENTS						STEEL TUBE EXPERIMENTS			
	SHOT NUMBER	DENSITY (%TMD)	V_{pp} (mm/μs)	τ_{CIF} (μs)	V_{CIF} (mm/μs)	P_{CIF} (kbar)	SHOT NUMBER	DENSITY (%TMD)	V_{CIF} (mm/μs)	REFERENCE
Picric Acid	S41	59.7	f				1504	61.9	0.20	7
Picric Acid	S51	68.2		750±125	0.33	0.3-0.45	916	68.9	~0.16	7
Picric Acid	S43	69.9	0.31	440±40	0.23-0.52	0.3-0.5	1108	70.9	~0.19	7
20μm Tetryl	S42	46.2	0.32	275±25	0.42	0.3-0.45	1208	45.8	0.3	6
470μm Tetryl	S49	57.8	0.70	225±95	0.45	~0.7	607 612	63.2 69.5	0.20 *	6
94/6 RDX/Wax	S37	69.8	0.16		*		401	70.3	0.34	8
	S40	69.8			*					
97/3 RDX/Wax	S52	65.3	0.30	295±10	0.40	0.3-0.5	404	70.9	~0.47	8

V_{pp} = Velocity of Pressure Front Preceding Luminous CIF

τ_{CIF} = Time Interval Between CIF and Preceding Pressure Front

V_{CIF} = Velocity of CIF

P_{CIF} = Pressure (SG) Associated with Luminous CIF

f = Failure

* = No CIF observed

In those Lexan tube experiments in which a CIF was observed the parameters describing the CIF in Table 4 are similar, except for perhaps τ_{CIF} which ranged from 100 to 900 μs. Within a factor of two, CIF velocities from similar steel and Lexan tube experiments are in agreement. Also, the framing camera records for these experiments often showed relatively weak luminance from the convective combustion zone, as can be observed with photographic records published in the literature[16,20]. These similarities exist over a range of different explosive compositions packed into charges with at least an order of magnitude variation in permeability.

From our data, the most straight forward example of a CIF occurred in the 97/3 RDX/wax shot. The strain gages detected mild pressurization (points A-E on Figure 24) well ahead (295±10μs) of a luminous CIF. Each succeeding downstream strain gage had a more rapid build-up in pressure following the first detection of pressure (see Figure 25). Also, the weakly luminous 0.40 mm/μs CIF propagated at nearly the same velocity as the 0.47 mm/μs discharge of ionization pins associated with the CIF in a steel tube experiment.[8]

For a similar composition, 70% TMD 94/6 RDX/wax, data from two experiments show no luminous CIF before the onset of a weakly luminous 0.85 mm/μs compressive wave. However, in steel tube Shot 401,[8] ionization probe discharges indicate that a 0.34 mm/μs CIF propagated to 105 mm before intersecting with a 0.9 mm/μs compressive wave. From the data for Lexan tube Shot S37 in Figure 19, it would be expected from previous results that a CIF originates near the onset of the 0.08 mm/μs front and follows a path approximately parallel to the first detection of pressure (points A and C). If this is the case, then luminosity at the Lexan/explosive lateral interface is not always indicative of in-depth reaction.

In-depth reaction which eventually spread over the cross-section of the 470 μm tetryl charge (see Figure 16) may have been responsible for the delayed appearance of the 0.45 mm/μs luminous front, whether this front is associated with convective or compressive ignition. Compressive ignition may be suspected for two reasons. First, if the preceding 0.70 mm/μs pressure front (points D, E, G, J of Figure 16) is a weak compressive wave, it may have ignited the tetryl, Second, the pressures associated with the luminous front (~0.7 kbar) are higher than those associated with CIF's in other explosives tested in this study, but they are not as high as those associated with the luminous 0.85 mm/μs compressive waves in Shots S37 and S40 with 94/6 RDX/wax according to the tube expansion visible on the framing camera records. The luminous 0.45 mm/μs front in the 470 μm tetryl charge may be a CIF or a manifestation of a thermal explosion near 75 mm.* In either case, the presence of this luminous front may explain why 470 μm tetryl is the only explosive in this study to have transited to detonation.

In the 20 μm tetryl experiment the first luminous front to propagate beyond the ignitor front is termed a transient ignition front, but there is evidence of a CIF. It is the 0.42 mm/μs luminous front, shown in Figure 13b

*The 1.14 mm/μs front outlined by the strain gages could also be associated with this thermal explosion.

that begins to propagate at about 300 μs after the passage of a pressure front, points B, D, F, G. The pressures associated with this front are nearly the same as those observed for CIF's in the 97/3 RDX/wax and picric acid transparent tube experiments, and the velocity is within a reasonable range although somewhat higher than the 0.3 mm/μs CIF velocity in steel tube shot 1208[6].

The 0.42 mm/μs luminous front may instead be a manifestation of a thermal explosion in a small zone of the charge, as was just suggested for the 0.45 mm/μs luminous front in the 470 μm tetryl charge. However, the shock wave from a thermal explosion which would precede the luminous front, like the 1.14 mm/μs pressure front in the 470 μm tetryl charge, does not appear or could not be detected in the 20 μm tetryl charge. It is possible that such a pressure front was responsible for the violent reaction at the far end of the 20 μm tetryl charge.

The picric acid experiments demonstrated the difficulty of establishing a CIF in picric acid, as discussed in the previous section. Once a CIF was established in the 68 and 70% TMD charges, the parameters describing the CIF's in Table 4 (V_{PP}, V_{CIF}, τ_{CIF}, P_{CIF}) were quite comparable with those for 97/3 RDX/wax despite the differences in permeability and ignitability. However, for just a 2% change in density, it is surprising that the 68% TMD charge had a constant 0.33 mm/μs CIF velocity while the 70% TMD charge had two distinct velocities, 0.23 and 0.52 mm/μs. Considering that the average CIF velocity for the 70% TMD charge is about 0.3 mm/μs, the two distinct velocities may be due to the delayed appearance of core ignition. Also, it may be that the region of the charge in which the 0.52 mm/μs CIF propagated was more highly compacted by earlier burning. Higher CIF velocity as initial packing density increased was observed for picric acid in steel tube experiments. As noted in Section 3.A.3., the gas leak at the ignitor plate in the 70% TMD charge probably had some influence on the CIF propagation.

Conductivity probes were located in the predetonation column of only the 20 μm tetryl, 470 μm tetryl and 97/3 RDX/wax charges. The probe responses in the 97/3 RDX/wax charge are discussed in the next section. For the tetryl charges, the probes responded to neither the 0.20 mm/μs luminous transient ignition front in the 20 μm charge nor to the 0.45 mm/μs luminous front in the 470 μm charge. If the transient CIF propagated along only the annulus of the 20 μm tetryl charge near the tube wall as postulated, then it would not be expected to trigger the conductivity probes. However, the gases associated with the accelerating pressure before and behind the 0.45 mm/μs luminous front in 470 μm tetryl should have been propagating across the entire cross-section of the charge and would be expected to trigger the conductivity probe before rather than after the onset of detonation.

This limited conductivity probe data is another indication that luminous fronts observed at the explosive/tube lateral interface are not indicators of in-depth reaction. Hence, there is need for simultaneous measurements of luminosity and/or ionization level at the lateral surface and within the granular bed.

D. COMPRESSIVE BURNING

Compressive burning is defined as the decomposition or reaction which results from the propagation of weak "shock" waves through the reactive bed. Compressive burning is governed by wave properties instead of the transport properties which govern convective burning. Consequently, compressive burning is associated with subsonic waves. (A sonic wave velocity is defined as the longitudinal sound velocity for the initial porous bed). Compaction, which precedes the propagation of sonic waves, naturally will affect the sound velocity of the porous bed during the dynamic measurements.

One of the areas of initial interest in this study was the detection of luminosity associated with compressive burning. Compressive burning may be a luminous or nonluminous reaction as seen at the lateral surfaces of a DDT charge. Unfortunately a problem exists in distinguishing between compressive burning and convective burning; there are very limited data currently available on sound velocities in porous charges (particularly at the higher porosities). In this work we distinguish between the velocity of nonluminous sonic waves as outlined by strain gage data (designated V_C) and the velocity of luminous compressive waves (V_{LC}) which occur some time after the passage of these sonic (supersonic) waves.* In earlier steel tube DDT experiments with 91/9 RDX/wax, the first compressive wave was detected by strain gages after the propagation of a CIF; the velocity of this wave was defined as V_{PC}. We will not equate, a priori, V_{PC} with V_C for several reasons. First, the threshold for detecting compressive waves is much less in a Lexan tube relative to a steel tube because of the relative Young moduli. Hence V_{PC} might be erroneously associated with a local bulk sound velocity. Second, the term PC implies a compressive wave propagating after a convective wave; this situation is not always observed in all explosives (in either steel or Lexan tubes) and hence can be a "confusing" terminology now based on our expanded knowledge of the variability of DDT events in porous charges.

In Table 5 are listed the compressive wave velocities determined by strain gage data from Lexan and steel tube experiments as well as the velocities of accompanying luminous fronts from the Lexan tube experiments. Only in the 94/6 RDX/wax experiments were luminous compressive fronts definitely observed, and the 0.85 mm/μs velocity closely agreed with the 0.9 mm/μs postconvective wave velocity in steel tube Shot 401. The observation of the luminous compressive fronts may have been possible in 94/6 RDX/wax because no convective ignition front was observed; that is, the preceding luminous CIF in other experiments may mask the compressive fronts, which in the 94/6 RDX/wax experiments were only weakly luminous and therefore could have been easily masked.

The transition to detonation in the 470 μm tetryl experiment indicates the existence of compressive waves in the predetonation column, and the strain gage data in Figure 16 does show a 0.70 mm/μs pressure wave followed by a higher velocity, 1.14 mm/μs, pressure wave. These velocities are certainly higher than that expected from a CIF, and the faster wave has a velocity similar to V_{PC} from steel tube Shot 607. The slower wave, because of its low pressure, would never

*The velocity associated with the low velocity detonation in Reference 16 corresponds to V_{LC}, as described here.

TABLE 5

SUMMARY OF COMPRESSIVE BURNING AND DETONATION PARAMETERS

MATERIAL	TRANSPARENT TUBE EXPERIMENTS					STEEL TUBE EXPERIMENTS			
	SHOT NUMBER	DENSITY (%TMD)	V_C (mm/μs)	V_{LC} (mm/μs)	D (mm/μs)	SHOT NUMBER	DENSITY (%TMD)	V_{PC} (mm/μs)	REFERENCE
Picric Acid	S41	59.7	0.62			1504	61.9		7
Picric Acid	S51	68.2				916	68.9	1.0	7
Picric Acid	S43	69.9	1.20			1108	70.9	1.1	7
20μm Tetryl	S42	46.2				1208	45.8	1.4	6
470μm Tetryl	S49	57.8	1.14		5.44	607	63.2	1.3	6
94/6 RDX/wax	S37	69.8		0.85		401	70.3	0.9	8
	S40	69.8		0.85					
97/3 RDX/wax	S52	65.3	~1.0*			404	70.9	~1.0	8

V_C = Compressive Pressure Front Velocity

V_{LC} = Luminous Compressive Front Velocity

D = Detonation Velocity

V_{PC} = Postconvective Wave velocity (see Reference 3)

*Implied from conductivity probe data

have been detected in a steel tube. With these pressure waves preceding the 0.45 mm/μs luminous front in Figure 16, it might be assumed that the luminous front is associated with compressive ignition. As discussed in the previous section, the 0.45 mm/μs luminous front is most likely a CIF. If a luminous compressive wave followed the 0.45 mm/μs front, it may have been masked by the existing luminance or it may have existed for less than the interframe time (40μs) of the camera before the onset of detonation.

Because a Lexan tube will expand in response to much lower amplitude compressive waves than a steel tube, the first compressive waves detected by strain gages in a Lexan tube are generally not accompanied by ignition of the explosive, as was just discussed for the 470 μm tetryl experiment. However, these weak compressive waves do deposit energy in and compact the porous bed. This is the case for the weak compressive waves detected in the picric acid experiments almost simultaneously with the first detection of light on the camera film.

In the 97/3 RDX/wax experiment the accelerating compressive wave detected by conductivity pins beyond the position of tube rupture was probably igniting the explosive and yet was not luminous. Similar to convective ignition which sometimes appears to propagate in the core of the charge, weak compressive ignition may manifest itself in the core of the charge and so is not visible to the camera. This is another area which may be aided by making in-depth measurements of luminance.

E. EFFECT OF CONFINEMENT ON THE DDT MECHANISM(S)

While all the explosives studied here underwent DDT in steel tubes[6,7,8], only 470 μm tetryl underwent a transition in this Lexan system. The lower confinement of the Lexan tube illustrates a variation in the DDT mechanism for tetryl. The earlier steel tube study of tetryl[6] (470 μm in particular) showed clearly that the accelerating pressure build-up preceding the onset of detonation occurred much closer to the onset of detonation than for other explosives, such as the RDX/wax series and picric acid. Thus, confinement is expected to have a lesser effect on the susceptibility of tetryl to transit to detonation. Even so, the Lexan tube surrounding the predetonation column in 470 μm tetryl was significantly expanded prior to the transition to detonation; the expanding tube reduced the pressure build-up causing the predetonation column to be twice that in a steel tube.

For the other explosives, such as the RDX/wax series and picric acid which follow the DDT mechanism in Reference 4, the onset of accelerated burning originates near the ignitor and must propagate the length of the predetonation column. Even for an energetic explosive, such as 70% TMD 94/6 RDX/wax, accelerated burning was already well established when the Lexan tube ruptured from the rapid pressure build-up. The pressures associated with accelerated burning are an order of magnitude greater than the yield strength of the Lexan tube. The Lexan tube can confine accelerated burning for only a brief time (<50 μs) because of the inertia of the tube wall as well as the flexibility of Lexan (the advantage of Lexan's high impact strength). Therefore, the region of the predetonation column in which accelerated burning originates is a major factor in determining the susceptibility for DDT in the present Lexan system.

The lower confinement of the Lexan tube arrangement can also prevent even the establishment of accelerated burning and thereby prevent DDT. The pressure build-up during convective combustion is one of the postulated driving forces for compressive fronts and the associated accelerated burning. Especially for the slower burning materials such as picric acid, expansion of the inner tube wall may negate the otherwise increasing pressure during convective combustion.

A possible example of this is provided by comparing data from picric acid in Lexan and steel tubes. For 70% TMD picric acid (Shot S43) a 0.14 mm/μs luminous front ahead of the ignitor front failed at about 50 mm followed by a delay of about 1 ms when a CIF began propagating to the end of the charge. In the steel tube arrangement picric acid exhibited an apparent CIF which, at very low densities, failed to propagate much beyond the first third of the charge[7]. Then after about a 500 μs delay, a compressive front (onset of accelerated burning) began propagating and there was a transition to detonation. The difference between a CIF in the Lexan tube and a compressive wave in the steel tube following the failure of the first burning front in picric acid may be a manifestation of the effect of confinement.

For achieving DDT in a low confinement system, it is an advantage to maintain lower pressures in the ignitor region until accelerated burning begins. For example, the initial decomposition of tetryl is believed to be a lower pressure and temperature reaction than for other explosives[8], which may partly contribute to the DDT of tetryl in a Lexan tube. A similar conclusion can be inferred from the study of Calzia and Carabin[21]. For low density charges of RDX and an RDX/wax mixture, they reported that a hole had to be placed in the ignitor plate "to prevent the premature bursting of the tube [in order to observe a transition to detonation]." Consequently, in future work we will explore the effect of controlled venting on inducing DDT in low confinement systems.

[21] Calzia, J. and Carabin, H., "Experimental Study of the Transition from Burning to Detonation," Fifth Symposium (International) on Detonation, ACR-184, Office of Naval Research, U. S. Government Printing Office, Washington, D. C., 1970; pp. 231-236.

CHAPTER 5

CONCLUSIONS AND SUMMARY

An experimental study of DDT in a low confinement arrangement (transparent Lexan tube) has been made of several explosives which had undergone DDT, in earlier studies, in a high confinement arrangement (thick-walled steel tube). The photographic recordings (taken at the lateral surface of the charge in the transparent tube) and simultaneous strain gage measurements yield results which are reasonably consistent with data from the steel tube arrangement. However, the transparent tube data for tetryl suggest gas flow around the porous bed (i.e., in an annulus between the Lexan tube inner wall and the porous material). Hence, the interpretation of the present transparent tube data must be considered to be tenative until the flash radiography system is available to detect any annular spaces and instrumentation is such that simultaneous comparison of internal and external luminosities can be made.

The transparent tube has outlined the early processes occurring after ignition of the B/KNO_3 ignitor. In all cases, the first luminous front observed was an 0.01-0.06 mm/μs ignitor front representing the displacement of the free end of the explosive column by the B/KNO_3 ignitor products. That is, the ignitor gases compact the adjacent porous bed; the extent and rate of the compaction process depends upon the permeability of the explosive column and the compressibility of the porous explosive medium.

Following the first detection of ignitor products at the ignitor/explosive interface, there was a delay of 0.5 to 3.5 ms before the explosive itself was ignited (except for 60% TMD picric acid which failed to ignite). The gas products from the reacting explosive increased the rate of displacement of the near end of the explosive column for the RDX/wax mixtures and 470 μm tetryl to 0.06 to 0.10 mm/μs. Also, during the process of igniting the explosive, an appreciable quantity of gases began penetrating into and preheating the porous bed. These gases conditioned the porous bed for the propagation of a convective ignition front, as best exemplified by a 65% TMD 97/3 RDX/wax charge.

For most charges the luminous fronts observed, except for the ignitor front, were complicated and difficult to interpret primarily because it was uncertain whether the observed luminosity was just at the inner tube wall or was representative of the charge cross-section. There were also cases in which the strain gages indicated the probable propagation of a reaction front and no luminosity was observed. Most of this uncertainty will be eliminated when flash radiography is available to check the condition of the tube and the explosive column, and when more probes are inserted into the core of the charge to measure the rate of reaction there. For the very porous charges ($\leq$70% TMD) observed in Lexan tubes, the convective ignition fronts were often irregular with both dark and

very luminous zones behind them. Compressive burning was observed only for 70% TMD 94/6 RDX/wax possibly because it was not masked by a preceding convective ignition front.

One of the objectives in this study was to define more precisely the nature of the early combustion processes in picric acid since at low porosities in the steel tube arrangement an apparent CIF failed to propagate much beyond the first third of the charge. The transparent tube data (photographs, strain gage traces, and an extinguished charge) suggest the presence of a melt layer during the pre-ignition phase. No evidence of a melt layer appeared in the other explosives tested. In picric acid the postulated melt layer 1) affected the rate of compaction during the pre-ignition phase, 2) lengthened the time to ignition, and 3) led to the formation of a transient luminous front which failed followed by a 1 ms delay before the appearance of a CIF. This differs from the steel tube experiments in that a compressive burning front followed the failure of the first reaction front after a comparable delay; however, this is probably due to the greater confinement of a steel tube.

In the low confinement of a Lexan tube the pressures from convective burning are sufficient to initiate plastic deformation of the Lexan tube, especially for a slower burning explosive such as picric acid, and thereby negate the pressure rise that is the probable driving mechanism for accelerated burning. If accelerated burning was attained, as it was for 94/6 RDX/wax and 470 μm tetryl, the resulting higher pressures permit confinement of the charge by the Lexan tube for only about 50 μs. For explosives such as 94/6 RDX/wax, in which accelerated burning originates near the ignitor and propagates the length of the predetonation column[4], the Lexan tube most likely ruptures before DDT can be attained. For tetryl, in which the origin of accelerated burning is nearer the onset of detonation[6], the charge has a greater probability of attaining DDT. Even so, the only charge to attain DDT in a Lexan tube, 470 μm tetryl at 58% TMD, had a predetonation column length about twice that in a comparable steel tube experiment[6].

BIBLIOGRAPHY

1. Bernecker, R. R., "Experimental Techniques and Results for DDT of Propellants and Explosives," ONR/AFOSR Workshop on Deflagration to Detonation Transition, CPIA Publication 299, Sep 1978, pp. 187-216.

2. Bernecker, R. R. and Price, D., "Studies in the Transition from Deflagration to Detonation in Granular Explosives. I. Experimental Arrangement and Behavior of Explosives which Fail to Exhibit Detonation," Comb. and Flame, Vol. 22, 1974, p. 111. See also Reference 14.

3. Bernecker, R. R. and Price, D., "Studies in the Transition from Deflagration to Detonation in Granular Explosives. II. Transitional Characteristics and Mechanisms Observed in 91/9 RDX/wax," Comb. and Flame, Vol. 22, 1974, p. 119. See also Reference 14.

4. Bernecker, R. R. and Price, D., "Studies in the Transition from Deflagration to Detonation in Granular Explosives. III. Proposed Mechanisms for Transition and Comparison with Other Proposals in the Literature," Comb. and Flame, Vol. 22, 1974, p. 161. See also Reference 14.

5. Price, D. and Bernecker, R. R., "Sensitivity of Porous Explosives to Transition from Deflagration to Detonation," Comb. and Flame, Vol. 25, 1975, p. 91. See also NOLTR 74-186.

6. Bernecker, R. R., Price, D., Erkman, J. O., and Clairmont, A. R., Jr., "Deflagration to Detonation Transition Behavior of Tetryl," Sixth Symposium (International) on Detonation, ACR-221, Office of Naval Research, U. S. Government Printing Office, Washington, D. C., 1978; pp. 426-435. See also Reference 13 and NSWC/WOL TR 77-175.

7. Bernecker, R. R. and Price, D., "Burning to Detonation Transition in Picric Acid," Proceedings of 17th Symposium (International) on Combustion, Combustion Institute, 1979; pp. 55-62. See also Reference 13 and NSWC/WOL TR 77-175.

8. Price, D. and Bernecker, R. R., "Effect of Wax on the Deflagration to Detonation Transition of Porous Explosives," Proceedings of Symposium (International) on High Dynamic Pressure in Paris, CEA, Saclay, France, 1978; pp. 149-159. See also NSWC/WOL TR 77-96.

9. Beckstead, M. W., et. al, "Convective Combustion Modeling Applied to Deflagration-to-Detonation Transition," 12th JANNAF Combustion Meeting, Newport, Rhode Island, 11 Aug 1975.

10. Krier, H. and Cokhale, S. S., "Modeling of Convective Mode Combustion Through Granulated Solid Propellant to Predict Possible Detonation Transition," AIAA/SAE 13th Joint Propulsion Conference, Orlando, Florida, 11 Jul 1977.

11. Pilcher, D. T., Beckstead, M. W., Christensen, L. W., and King, A. J., "Comparison of Model Predictions and Experimental Results of Deflagration to Detonation Tests," AIAA/SAE 13th Joint Propulsion Conference, Orlando, Florida, 11 Jul 1977.

12. "Typical Properties of Lexan," General Electric, Publication CDC-570.

13. Price, D., Bernecker, R. R., Erkman, J. O., Clairmont, A. R., Jr., "DDT Behavior of Tetryl and Picric Acid," NSWC/WOL/TR 76-31, 31 May 1976.

14. Bernecker, R. R. and Price, D., "Transition from Deflagration to Detonation in Granular Explosives," NOLTR 72-202, 13 Dec 1972.

15. Phillips, D. W., et al., "Ultrasonic Studies of Polycarbonate, Polysulfone, and Polyether Sulfone," Journal of Applied Polymer Science, Vol. 21, 1977, p. 1859.

16. Belyaev, A. F., Bobolev, F. K., Korotkov, A. I., Sulimov, A. A., and Chuiko, S. V., Transition from Deflagration to Detonation in Condensed Phases, Izdatel'stvo "Nauka", Moscow, 1973. English translation by Israel Program for Scientific Translations, 1975.

17. Chan, M. L., Eisel, J. L., Zurn, D. E., Boggs, T. L., "Analysis of Preignition Pyroylsis Products of High Energy Propellants," 16th JANNAF Combustion Meeting, Monterey, California, 11 Sep 1979.

18. Schwartz, C. E. and Smith, J. M., "Flow Distribution in Packed Beds," Industrial and Engineering Chemistry, Vol. 45, No. 6, 1953, p. 1209.

19. Margolin, A. D. and Chiko, S. V., "Combustion Instability of a Porous Charge with Spontaneous Penetration of the Combustion Products into the Pores," Fizika Goreniya i Vzryva, Vol. 2, No. 3, 1966, p. 119. English translation, Combustion, Explosion and Shock Waves, Vol. 2, No. 3, 1969, p. 72.

20. Obmenin, A. V., Korotkov, A. I., Sulimov, A. A., and Dubovitskii, V. F., "Propagation of Predetonation Regimes in Porous Explosives," Fizika Goreniya i Vzryva, Vol. 5, No. 4, 1969, p. 461. English translation, Combustion, Explosion and Shock Waves, Vol. 5, No. 4, 1972, p. 317.

21. Calzia, J. and Carabin, H., "Experimental Study of the Transition from Burning to Detonation," Fifth Symposium (International) on Detonation, ACR-184, Office of Naval Research, U. S. Government Printing Office, Washington, D. C., 1970; pp. 231-236.

APPENDIX A

PHOTOGRAPHIC STUDY OF IGNITORS

The manner in which burning is initiated in a porous charge has definite effects on succeeding stages of the DDT mechanism. The ignitors used in this study (see Section 2.B.1.) generate hot gaseous and solid products which establish conductive burning at the adjacent explosive interface. To assess the uniformity of our ignition source, the flame breakthrough to the ignitor face (which is adjacent to the explosive in a DDT tube) was photographically observed. As will be discussed in Appendix B, the ignitors will also compact the highly porous explosive column in the vicinity of the ignitor while conductive burning of the explosive is being established.

In all, eleven ignitors were tested in various configurations. The camera used in these tests was the same one used to observe the transparent DDT tubes (see Section 2.C.5.a) . Most tests were observed at camera speeds of 25,000 fps, but several tests were observed at speeds of 8,000 to 10,000 fps in order to increase the total available filming time.

In the first configuration of the ignitors the ignitor face was unconfined. Of the three ignitors tested in this configuration, luminosity appeared on the camera film from only one test, even though all ignitors fired. For the one test in which luminosity was recorded, the luminosity persisted so long (>9 ms) that the rotating drum camera film was overwritten, and little could be learned from the film about the early stages of flame breakthrough. For the two tests in which the continuous access camera recorded no luminosity, possibly the early stages of burning in the bottom of the ignitor cup generated enough pressure to jetison the ignitor mix from the cup within the interframe time of the camera.

Therefore, for the next eight tests the ignitor mix was restrained from early ejection from the cup, and luminosity was recorded in all tests. The ignitor cup was recessed into a brass block so that the face of the ignitor was level with the brass, and then a 12.7 mm thick PMMA plate was positioned over the face of the ignitor and bolted to the brass block. The face of the ignitor was observed through the PMMA plate.

It was expected that a flame would first break through to the ignitor face near the center of the cup, because its is closest to the bridgewire, and then break through in an expanding circle from the center. However, the film records showed breakthrough was always along what appeared to be a crack, which was more often between the ignitor mix and the cup than somewhere on the face of the ignitor mix itself. Until the PMMA broke, the products would flow away from the ignitor between the tightly clamped PMMA and brass assembly often without the

central region of the ignitor face becoming luminous. This suggests that the ignitor mix near the center of the cup was tightly pressed against the PMMA by pressure in the bottom of the cup. Therefore, the observation of flame breakthrough next to the cup may be a consequence of the confining apparatus which confines the ignitor mix more than a porous explosive charge in a transparent DDT tube.

The time from application of bridgewire voltage to flame breakthrough, from 5 to 25 ms, is the same in these experiments as in the transparent DDT tube experiments. Although the position of flame breakthrough may be different in the two experiments, the consistent times for breakthrough suggest that the build-up to flame breakthrough is nearly the same.

There is additional evidence that suggests flame breakthrough at a crack. X-rays of ignitors show many fine cracks and voids throughout the ignitor mix which would contribute to crack burning rather than uniform flame propagation. No correlations could be made between the fine cracks and voids in ignitors and the film records of flame breakthrough to the ignitor face.

When the flame breaks through to the ignitor face, only a small fraction of the mix has been ignited and consumed. The subsequent ignition and burning of the rest of the mix should depend on the confinement of the ignitor mix. In order to study this, as well as examine the compaction of the adjacent porous explosive column by the ignitor products, ignitors were fired in transparent tubes in which all or most of the explosive was replaced by an inert, as discussed in Appendix B.

APPENDIX B

DYNAMIC COMPACTION EXPERIMENTS

In this section are recorded the earlier work done with a polymethyl methacrylate (PMMA) tube and some dynamic compaction experiments. The latter experiments were aimed at understanding the ignition front and all but one were conducted before the flash radiography equipment was available. Since the various types of instrumentation were under development, the amount of data successfully acquired varied from experiment to experiment.

The first transparent DDT tube experiment (Shot S4) utilized a relatively short, uninstrumented PMMA tube (25.4 mm I.D., 69.8 mm O.D. and 181 mm long) loaded with 70% TMD picric acid. The progress of the luminous fronts, as observed with the framing camera at 10,000 fps, is plotted on Figure B1. Because there was no backlighting, zero time corresponds with the first appearance of light on the film.

The first light was a luminous zone next to the ignitor which expanded at a rate of 0.02 mm/μs for about 1000 μs. As discussed in Section 4.B, this is defined as an ignitor front. At 1300 μs a point of light appeared 63 mm from the ignitor. The convective ignition front which appeared to develop from that point of luminosity had advanced only to 120 mm when the tube ruptured. From this first test it was realized that 1) the higher impact resistance of Lexan would be required for future transparent tubes, and 2) that the ignition front was several orders of magnitude too fast for conductive burning and an order of magnitude too slow for convective burning.

In a later test, 70% TMD picric acid was packed in a Lexan tube (Shot S43) as reported in Section 3.A.3. The film records from both Shots S4 and S43 show an ignitor front and a convective ignition front which first appears $\geq$40 mm downstream of the stagnated ignitor front. However, the film record from Shot S43 also shows a 0.14 mm/μs transient ignition front which originated with the ignitor front and stagnated before the onset of normal convective burning. More tests are required first to determine if consistent results can be obtained from one DDT tube configuration (e.g., the Lexan tube configuration) and second to determine what effect confinement (PMMA versus Lexan versus steel tubes) has on the build-up to DDT.

Because the ignitor was suspected of being responsible for the ignitor front in Shot S4, another PMMA tube of identical dimensions was loaded with a porous inert material, 70% TMD melamine ($\bar{\delta}$=58 μm). The 20,000 fps camera film from this

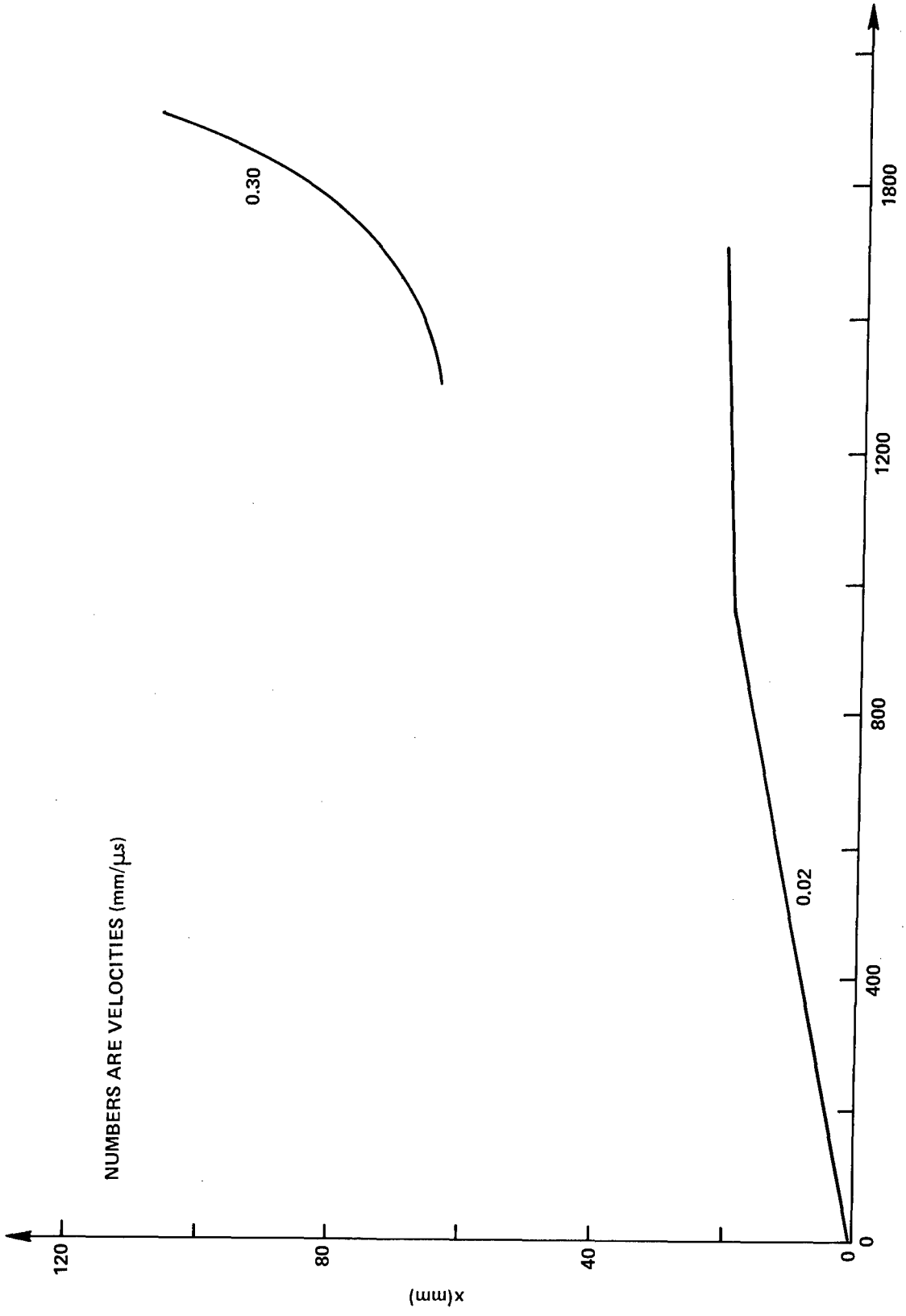

FIGURE B1 LUMINOUS FRONTS FOR 70% TMD PICRIC ACID IN PMMA TUBE, SHOT S4

test (Shot S7) showed a similiar luminous 0.013 mm/μs ignition front which propagated 11.3 mm before stagnating (see Figure B2). Since the tube was undamaged, it was observed after the experiment that the melamine column was uniformly displaced 10.5 mm from the ignitor. Therefore, within experimental error, the final position of the luminous front corresponds to the final displacement of the melamine interface.

An x-ray of the recovered tube did not reveal any variation in film density along the length of the melamine column, indicating that the column was uniformly compacted. It is possible that some compaction occurred after the luminosity of the ignitor front declined and so the state of the recovered melamine column may not have been the same as, for example, 1400 μs after the first detection of light.

The melamine in the recovered tube was discolored by ignitor products at up to 94 mm just along a 1 mm annulus adjacent to the inner tube wall. There was essentially no dark material within the recovered column. Thus the ignitor products were able to penetrate along the inner tube wall more easily than into the central core of the melamine column. It is well known that the pressure drop in a uniformly packed bed is lowest in the region from the container wall to a depth of several particle diameters. Also, since the ram diameter is about 0.25 mm less than the inner tube wall diameter, there was probably an annulus of melamine that was not uniformly packed, which would only enhance the normal wall effect. Therefore, there is a definite possibility that convective combustion in transparent DDT tube tests would tend to propagate along the wall rather than uniformly over the cross-section of the explosive column. The framing camera alone would not be able to determine if a flame propagated primarily along the wall.

In a steel tube experiment[5] with 74.5% TMD melamine (1.17 g/cc) the ignitor compacted the charge only 2-3 mm and created a short, small channel within the charge. In a steel tube the inner diameter is 16.27 mm versus 25.4 mm for the transparent tube; however, the diameters of the ignitors are scaled so that the ignitor face is 35% of the charge cross-sectional area for both tubes. In addition, the depth of the ignitor mix is the same for both tubes; therefore, ignitors in both tubes should generate identical pressure-time histories at the ignitor/explosive interface. The somewhat greater initial packing density in the steel tube, 74.5% TMD versus 70% TMD in the transparent tube, and perhaps the greater wall friction in the steel tube both contributed to the shorter void in the steel tube.

Although compaction of a porous charge may be initially caused by the ignitor products, some of the early luminosity and compaction should be from conductive burning of the charge. To check this, another PMMA tube (Shot S12) was loaded with a 25 mm column of 70% TMD picric acid adjacent to the ignitor and a 130 mm column of 70% TMD melamine between the picric acid and closure plate. With a relatively small amount of picric acid it was hoped to preserve the compaction characteristics of a pure melamine column (Shot S7) and still have a contribution from conductive burning of picric acid. The distance-time data from the camera film on Figure B2 shows that the ignition front propagated more rapidly than in Shot S7 but that the ignitor front had propagated only 1.4 mm further before

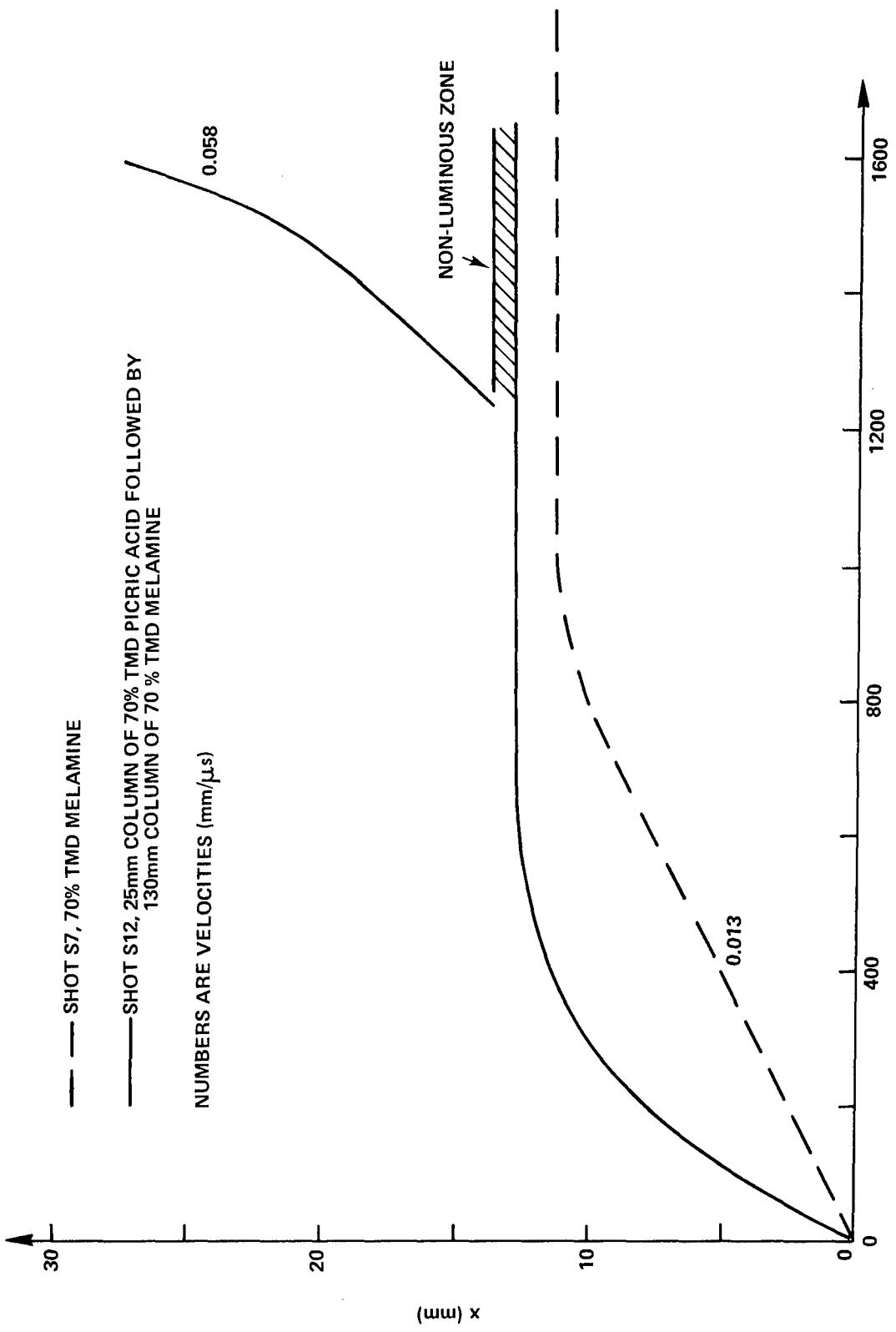

FIGURE B2 LUMINOUS FRONTS IN PMMA TUBES DURING DYNAMIC COMPACTION TESTS

stagnating. Differences between ignitors may have been just as responsible for the relatively minor differences between ignitor fronts in Shots S7 and S12 as the contribution of picric acid burning in Shot S12. Even for essentially identical charges of 70% TMD picric acid, Shot S4 in a PMMA tube and Shot S43 in a Lexan tube, the ignitor front velocities were 0.02 and 0.037 mm/μs, respectively.

In Shot S12 there was a less luminous 0.058 mm/μs front which began propagating just beyond where the ignitor front stagnated. There was a non-luminous zone (as in Shot S51 with 68.2% TMD picric acid, Figure 7b, c) between the end of the ignitor front and the beginning of the second front that remained until the tube ruptured at 1600 μs. The existence of this stationary, non-luminous zone indicates that the 0.058 mm/μs luminous front was not associated with further movement of the explosive interface by compaction caused by conductive burning on the end of the picric acid column. Since the 0.058 mm/μs velocity is too low for a convective ignition front, this front is probably a transient ignition front (see Section 4.B.). However, sustained ignition of the picric acid was somewhere attained in order for the tube to rupture.

Further testing, with the aid of flash radiography, would aid in understanding the non-luminous zone and the 0.058 mm/μs front in Shot S12. However, for the purpose of identifying the ignitor front, the data from Shots S4, S7 and S12 demonstrate that the ignitor front is associated primarily with compaction. With respect to confinement, Shot S12 demonstrated definitely that PMMA is too weak a material for these tests since the "burning" of just a short column of picric acid led to rupture of the tube.

In the next series of compaction experiments the downstream end of a 76.2 mm long charge was not rigidly restrained. Instead, a 25.4 mm hole, matching the inner diameter of the transparent tube, was located in the closure plate. A loose fitting steel cylinder (25.3 mm diameter by 19.05 mm long) filled the opening in the closure plate and was in contact with the end of the charge. In the first three tests, the steel cylinder was weakly seated into the closure plate with silicon rubber. With this arrangement the pressure in the tube was released by expelling the charge before the strength of the tube was exceeded.

The five shots listed on Table B1 were conducted with the same tube. In two shots the charge was inert while in the other three shots there was a short column of explosive between the ignitor and inert. Since the previous compaction tests in this study, the instrumentation of transparent DDT tubes had expanded. When using the framing camera the tubes were backlighted so that the motion of the steel cylinder could be observed. Three pairs of strain gages at 1, 26, and 52 mm were used to record pressure build-up. In the last test, a flash x-ray of the compacting charge column was obtained.

For the 70% TMD melamine charge observed by the framing camera (Shot S30) the ignitor end of the melamine column was displaced 8 mm in about 1000 μs, (see Figure B3), about 3 mm less than in Shot S7 (Figure B2). Then there was a 1500 μs delay between the end of visible compaction and movement of the steel cylinder, but the strain gages still recorded increasing pressure at nearly the same rate.

TABLE B1

DYNAMIC COMPACTION EXPERIMENTS OF 76.2 MM LONG

POROUS CHARGES WITH THE FAR END UNRESTRAINED

SHOT	MATERIAL	INSTRUMENTATION*
S30	70% TMD Melamine	FC, SG's
S31	12.7 MM of 65% TMD Picric Acid followed by 63.5 MM of 70% TMD Melamine	FC, SG's
S32	12.7 MM of 70% TMD 85/15 RDX/wax followed by 63.5 MM of 70% TMD Melamine	FC, SG's
S34	25.4 MM of 70% TMD 85/15 RDX/wax followed by 50.8 MM of 70% TMD Melamine	FC
S39	Alternating 12.7 MM Increments of 70% TMD Melamine and 70% TMD 50/50 Aluminum/Melamine	Flash X-ray, SG's

*FC = Framing Camera
SG's = Strain Gages

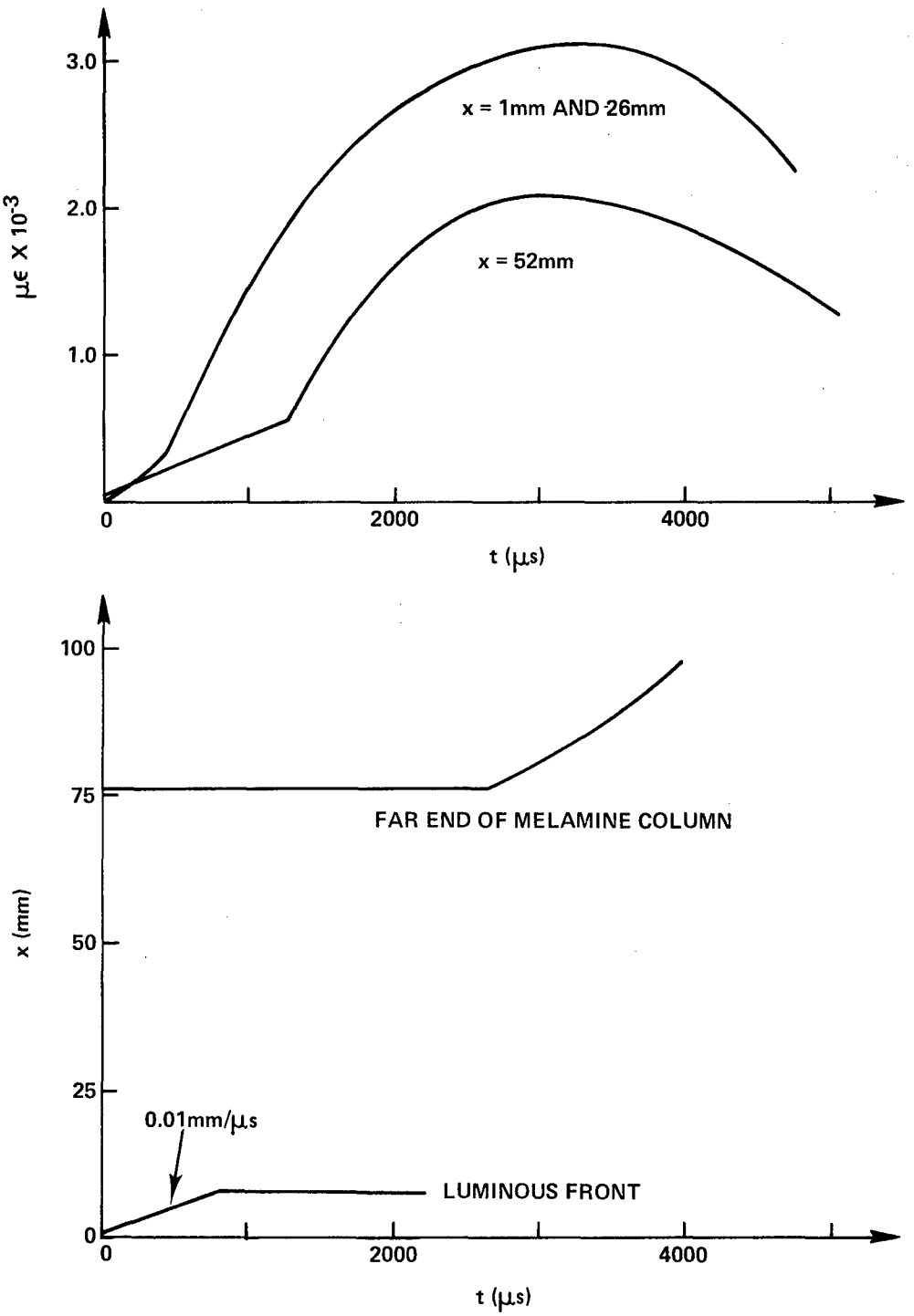

FIGURE B3 DYNAMIC COMPACTION AND MOVEMENT OF 76.2mm COLUMN OF 70% TMD MELAMINE, SHOT S30

(As indicated on Figure B3, the 26 mm strain gage had almost identically the same response as the 1 mm strain gage.) Even after the far end of the melamine column began to move, the strain gages recorded a small increase in pressure before a decline. The continued pressurization of the tube after the luminous ignitor front stopped suggests that the ignitor continued to generate gas but that there was not enough pressure gradient to compact the melamine column further.

For another test with inert powders, Shot S39, increments of melamine and 50/50 aluminum/melamine, both at 70% TMD, were loaded alternately in order to enhance the visibility of compaction on the flash radiograms. Based on the results of Shot S30, flash radiograms were preset to be taken at 1000 and 3000 μs. The x-ray heads and cassette were arranged so that both exposures would be adjacent on a single x-ray film. Unfortunately the x-ray showed that the charge column had begun to move out of the tube before 1000 μs and was completely expelled before 3000 μs. The shorter time for the onset of bed movement for Shot S39 may have resulted from the steel cylinder not being sealed in the closure plate with silicon rubber or from a faster burning ignitor. The 1000 μs radiogram shows that the interface of the inert column (which was originally at the ignitor), was displaced almost evenly 19 mm downstream and the column was approximately uniformly compacted to 78% TMD.

For the three tests in which a short column of explosive preceded an inert column of 70% TMD melamine, the results were similar. After the first detection of light the charge interface would be displaced about 10 mm from the ignitor before the steel cylinder would begin to move at about 1000 μs. Once it started to move, the steel cylinder and the luminous front in the tube both would propagate at the same velocity, which ranged from 0.06 to 0.10 mm/μs, indicating that the charge was expelled as a single unit. The consistent results (for ignitor and ignitor plus picric acid or 85/15 RDX/wax) suggest that the first 1000 μs following flame breakthrough to the ignitor surface is largely controlled by the ignitor. However, only slow burning explosives, e.g., picric acid and 85/15 RDX/wax, were tested.

These first tests suggest that compaction is significant during the build-up of DDT in porous explosives because if the ignitor can compact the charge then the more sustained burning of the explosive should compact it further. The mathematical models of DDT should include the role of compaction, both during the ignition/conductive burning stage as well as during later stages. This will require quantitative experiments of dynamic compaction to provide parameters for and to guide the mathematical description of compaction mechanisms.

APPENDIX C

PROBE SEQUENCE AND TIME INTERVAL RECORDER

Cleaver, H., Vogel, N. C., Erkman, J. O., and Rosenthal, L. (Rutgers Univ.)

INTRODUCTION

The Probe Sequence and Time Interval Recorder is designed to record the order of a sequence of eight signals and to measure and record the time intervals between successive signals. Information is stored in digital format and presented on a digital readout display panel.

As shown in Figure C1., the probe recorder is connected to the output of a probe signal generator circuit that leads to ionization probes in the explosive charge. The probe recorder is designed to accept a variety of signal configurations that could be generated by using one of the various types of probe signal generator circuits listed in the figure. Note that some of the probe recorder requirements are also listed in Figure C1 .

Information captured by the probe recorder is presented in a display shown in Figure C2. There are 36 seven-segment digital readouts in the display panel. The sequence in which the probe signals occured is displayed across the top of the panel. The seven time interval measurements are displayed in rows and columns under the SEQUENCE row. Should the interval between two consecutive probe signals exceed the time allowed for the particular range selected, a COUNTER OVERFLOW indicator light for that channel will be turned on.

The pattern shown in Figure C2 illustrates an internally generated test sequence where the circuits are triggered 400 microseconds apart in order from 1 to 8.

A summary of the Probe Sequence and Time Interval Recorder Specifications is shown in Table C1.

BASIC OPERATION

Each analog signal from the probe signal generator circuit goes through a separate pulse shaping circuit designed to produce a digital logic level pulse for driving the logic circuits in the recorder. A pulse from the shaping circuits is used to do three things in the system. First, the pulse generates its own identifying coded signal using an encoder, second, the pulse generates a clock pulse to store its coded signal in a memory location, and third, the pulse controls a set of counters used to measure time intervals by counting pulses from the system clock.

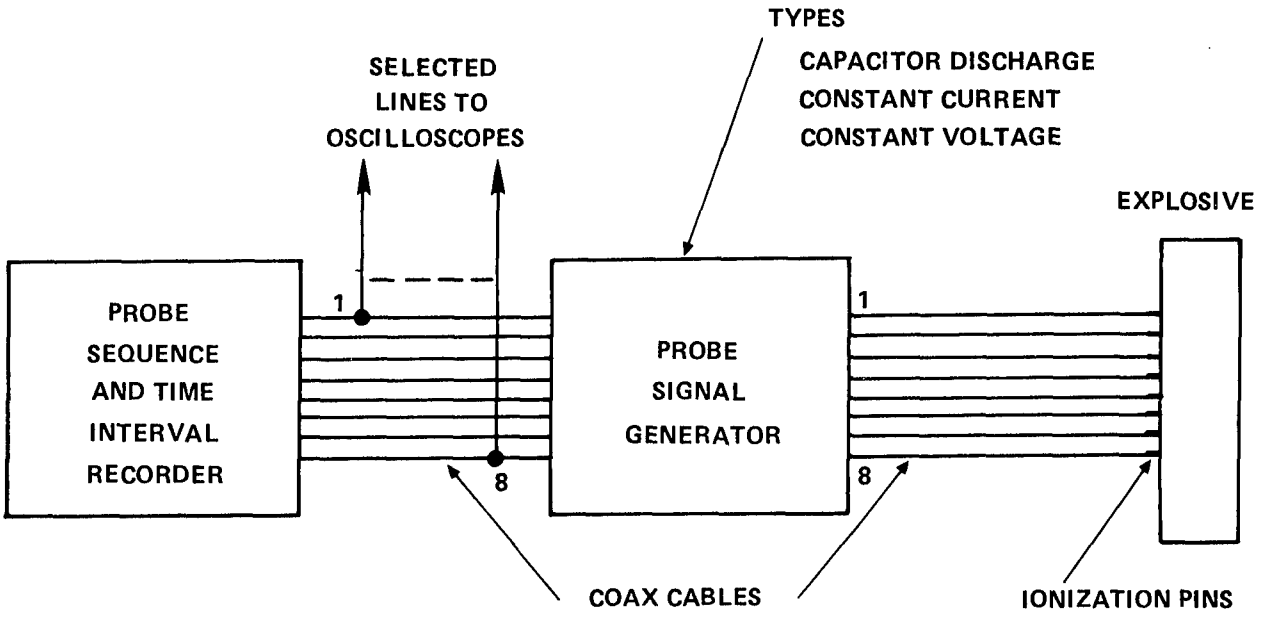

PROBE RECORDER REQUIREMENTS

1. TRIGGER AT VARIABLE VOLTAGE LEVELS
2. RESPOND ONLY TO FIRST SIGNAL FROM PROBE
3. RECORD SEQUENCE
4. MEASURE TIME INTERVALS
5. CAPTURE SIGNALS FROM 0.5 μs TO 1 ms APART

FIGURE C1 PROBE RECORDER SYSTEM DIAGRAM

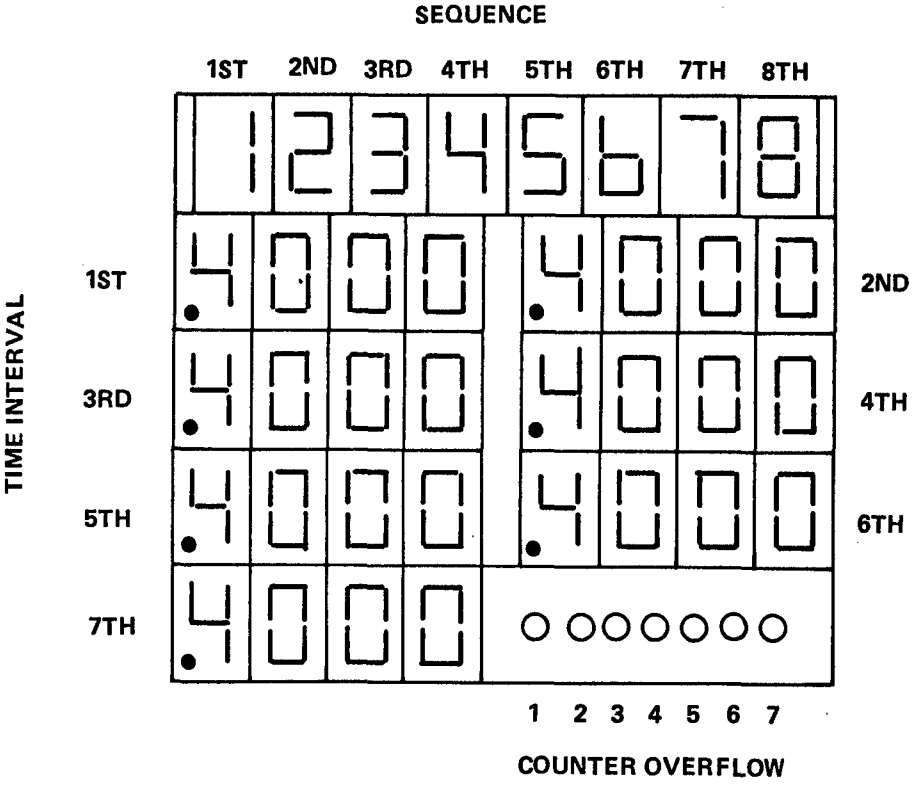

FIGURE C2 DISPLAY PANEL

TABLE C1 PROBE RECORDER SPECIFICATIONS

INPUTS – 8 CHANNELS

OUTPUTS – 8 MONITOR POINTS, NEGATIVE GOING 5 VOLTS
1 OSCILLOSCOPE TRIGGER PULSE, POSITIVE 5 VOLTS

INPUT RANGE = ± 13 VOLTS

REFERENCE VOLTAGE RANGE = ± 3 VOLTS

MINIMUM TIME BETWEEN PULSES = 0.5 μs

RESOLUTION = 0.1 μs, ± 1 COUNT

DISPLAY RANGE = .9999 ms MAX
9.999 " "
99.99 " "

MASTER CLOCK: VECTRON LABS
10 MHz ± 0.001%, ± 0.0025% 0 – 70°C

SINGLE RESPONSE PER CHANNEL

INTERNAL TEST CIRCUIT FOR OPERATIONAL CHECK

A block diagram of the probe recorder is shown in Figure C3. Eight input lines pass through individual pulse shaping circuits out onto eight lines to the encoder and to a logic gate performing an OR function. The first probe signal to occur on any input line will cause a pulse from the shaping circuit to be impressed on the encoder. The encoder will generate, for the duration of the input pulse, a binary coded decimal (BCD) output code corresponding to whichever input line was pulsed. The BCD code goes on a four line bus connected to eight temporary memory locations called latches. While it is still impressed on the encoder, the pulse passes through the GATE to the circuit block that generates latch clock pulse signals. A clock pulse is sent to the first latch to store the BCD code put on the bus by the encoder. Each latch can receive only one clock pulse during a recording cycle. Thus, the first latch stores the BCD code corresponding to the line pulsed by the first probe signal, the second latch stores the BCD code of the second line pulsed, and so on for eight signals.

At the instant the first latch clock pulse signal is generated, the first set of decade counters is turned on to count pulses from the system clock. When the second latch clock pulse signal is generated, the first set of counters is turned off and the second set is turned on. The time interval between the first and second probe signals is stored as the BCD code that remains on the output of the first set of counters. The third pulse detected stops the second set of counters and starts the third set. This start-stop operation continues in response to the input pulses until the time intervals are stored as BCD codes on seven sets of decade counters.

All BCD coded information in the latches and counters goes through decoding and multiplexing to the digital readouts on the display panel. All information stored in the recorder will remain in storage until the circuits are cleared through the use of a manually operated RESET switch.

A 10 MHz squarewave oscillator is the master clock in the recorder. The master clock frequency is divided by circuits in the system clock generator to provide the three different time bases used.

The test signal generator section uses the system clock frequency to send synchronized signals to the pulse shaping circuits. These signals simulate probe signal firings and test for correct operation of the entire recorder circuits with the exception of the input voltage comparators. The test signal generator is manually triggered and the recorder must be manually reset after its use.

INPUT CIRCUITS

In order to get from the analog world of the probe signals into the digital world of the recorder, a circuit called a voltage comparator is used. A voltage comparator is a device whose output state is dependent upon the relative magnitude of one input compared to the other. By carefully selecting which voltage signals are connected to the two input terminals, the comparator can be made to operate with a variety of input signal polarities and transistions. The comparator shown in Figure C4 has an output signal compatible with the 7400 series transistor-transistor logic (TTL) family used in the recorder. In order for the recorder

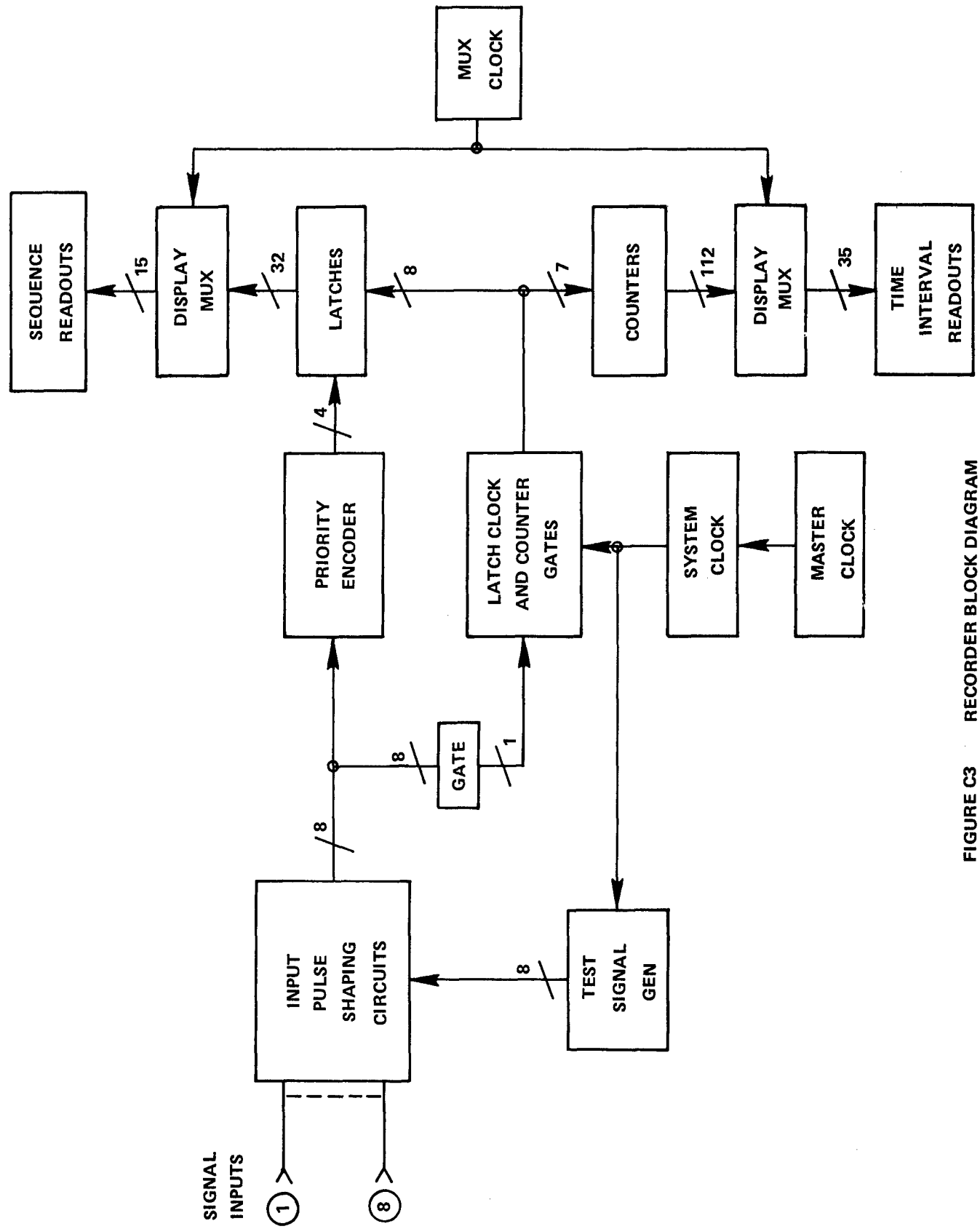

FIGURE C3 RECORDER BLOCK DIAGRAM

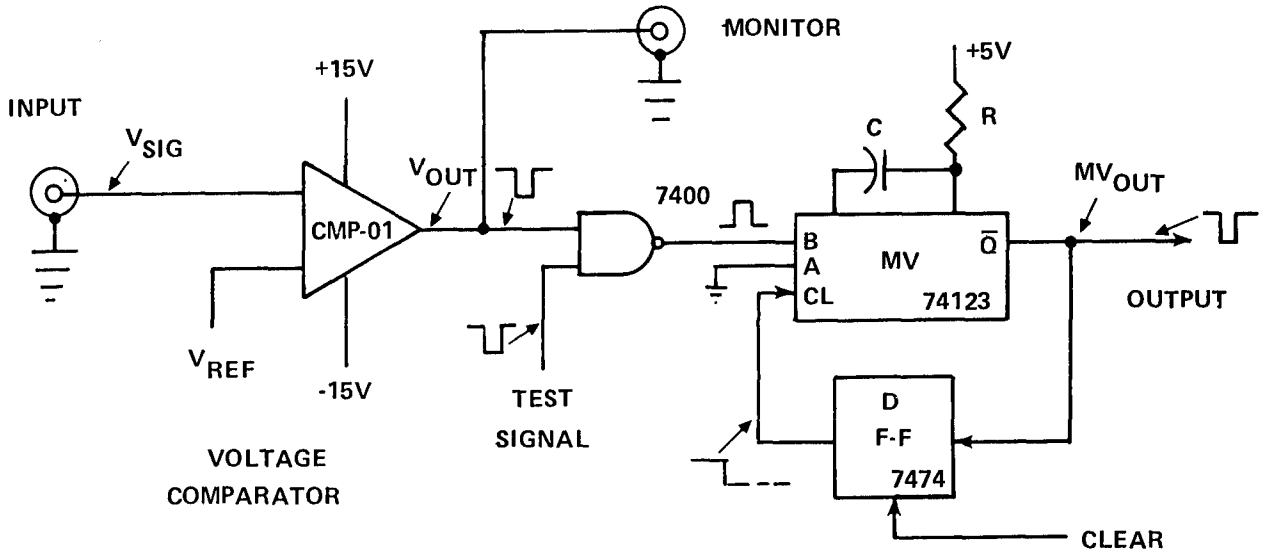

CIRCUIT DIAGRAM

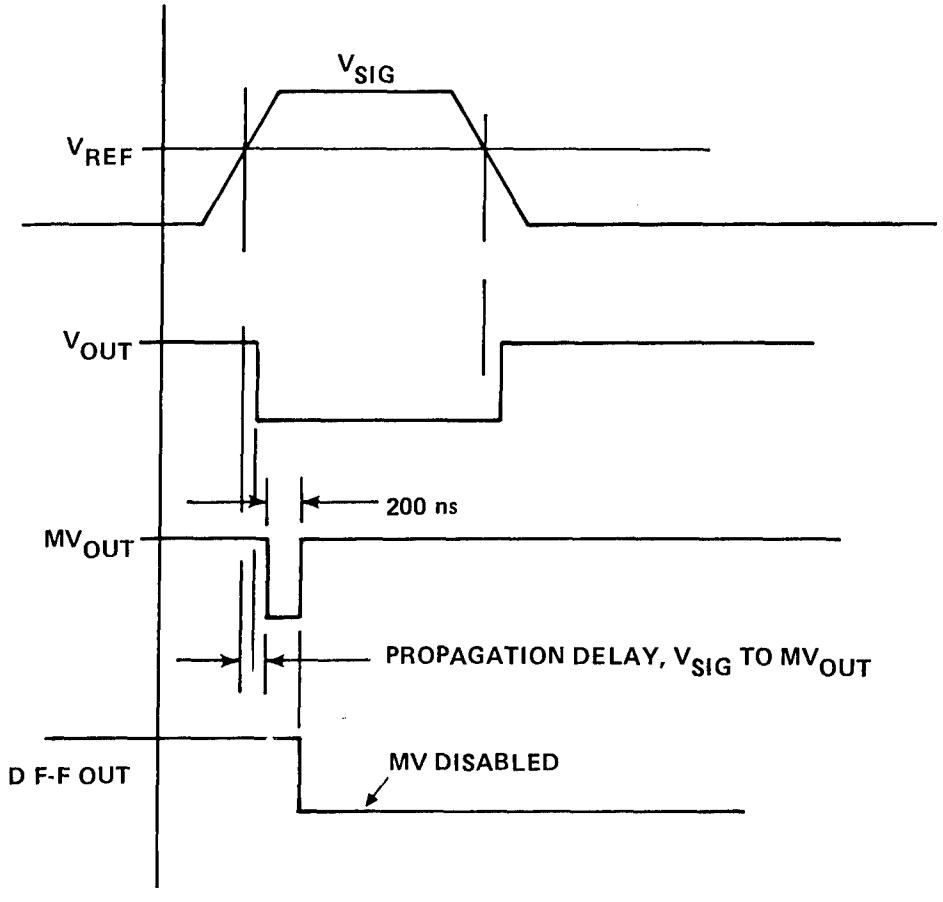

TIMING DIAGRAM

FIGURE C4 INPUT PULSE SHAPING CIRCUIT

to function properly, the input configuration selected for the comparator must be one that results in the output being at a logic HIGH during the standby state.

The timing diagram in Figure C4 shows that when the signal from the probe circuit V_{sig} rises above the voltage on the reference terminal V_{ref}, the output of the comparator changes logic states from a HIGH to a LOW. This level transition passes through a 7400 NAND gate to trigger a 74123 multivibrator. The multivibrator (MV) generates a 200 nanosecond wide negative-going pulse that is the output signal from the pulse shaping circuit. This pulse is sent on to the encoder and counter circuits.

The trailing edge of the MV output pulse triggers a D-type flip-flop. Upon tirggering, the flip-flop outputs change state to disable the MV and prevent it from being retriggered by any multiple signals that might come from the probe signal generator circuit. Thus the MV is locked out after one output pulse until the recorder circuits are cleared using the manual reset operation. Note that the signal from the test circuit passes through the NAND gate also and triggers the multivibrator during a test sequence. In either case the flip-flop must be manually reset before another cycle can be initiated.

ENCODER AND COUNTER CIRCUITS

Pulses from the shaping circuits enter the encoder and counter circuits at the point shown in the top left corner of Figure C5, The first incoming pulse causes the 74147 encoder to set up the BCD code identifying that particular input line on the bus going to the eight 74175 latches. The same pulse also passes through a 7430 8-input NAND gate that performs the logic OR function already mentioned. The pulse passes through a control gate and an inverter to increment a 74192 decade counter to a count of one. BCD codes from the counter are operated on by a 7442 BCD-to-decimal decoder.

When the counter is incremented to a count of one, output line 1 of the 7442 decoder goes to a logic HIGH and line 2 goes from HIGH to LOW. Positive-going transitions on the decoder's output lines are used for clock pulse signals to the eight latches. The positive transition on line 1 clocks the BCD information on the latch bus into the first latch. The transition to LOW on line 2 opens the first 7402 NOR gate allowing clock pulses from the system clock to be counted by the first set of four 7490 decade counters. When the second incoming pulse arrives at the decade counter-decimal decoder stage, the counter is incremented to a count of two. Decoder output line 2 goes back to HIGH and line 3 goes LOW. The positive-going transition on line 2 causes the new BCD code on the latch bus to be stored in latch 2 and also closes NOR gate 1 to stop the first set of counters. The transition to LOW on line 3 opens NOR gate 2 and starts the second set of four 7490 decade counters.

The decoder output signals control the latching and counting in this manner until the eighth probe signal. When the eighth input signal arrives, decoder output line 8 goes HIGH storing the BCD code on the latch bus in latch 8 and stopping the seventh set of 7490 counters. When line 8 goes HIGH, line 9 goes LOW. The LOW on line 9 disables the 7400 NAND gate preventing signals from reaching

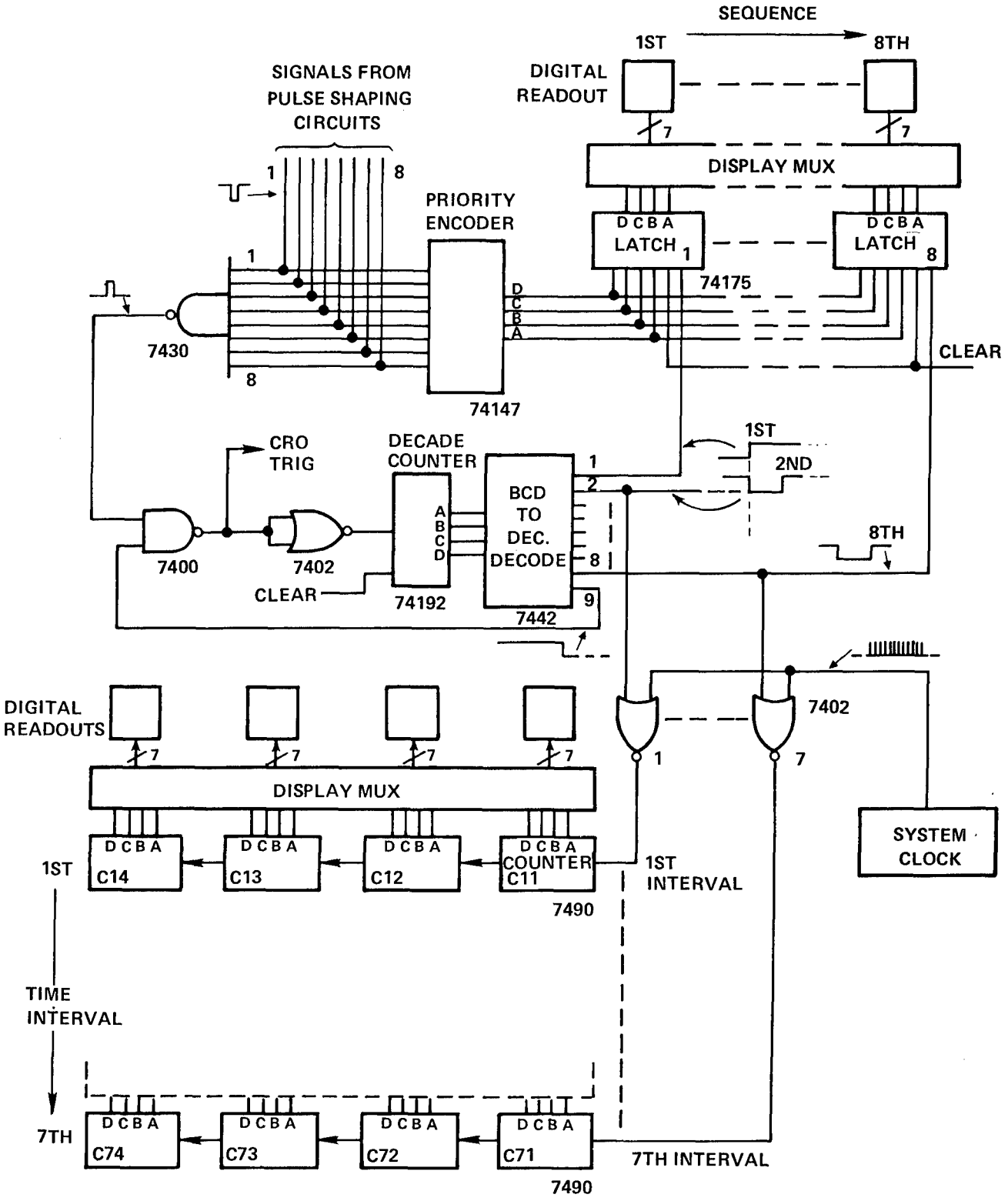

FIGURE C5 ENCODER AND COUNTER SCHEMATIC

the 74192 decade counter. Thus the counter-decoder stage is locked out until the counter is cleared during manual reset of the recorder. This lock-out feature is in addition to the multivibrator lock-out for added protection of the stored BCD codes.

All BCD codes on the latches and counters go through multiplexing and decoding circuits to seven-segment light emitting diode (LED) digital readouts. Multiplexing is used to reduce power consumption and parts count in the system. For brevity's sake, a discussion of the multiplexer, status, system clock, and reset circuits has been omitted.

OPERATING INSTRUCTIONS

Figure C6 shows the front and back panels of the recorder. The INPUT connectors, numbered 1 to 8, are located on the top left corner of the back panel. Below them are eight MONITOR output connectors. The MONITOR signal is a high-to-low transition of five volts when the corresponding INPUT channel is triggered by a probe signal. A CRO-OUTPUT connector produces a 200 nanosecond wide positive five volt pulse when any of the eight channels is triggered either externally, by a probe signal, or internally, by the test circuit.

To set up operation of the recorder, connect the eight input cables and any monitor cables desired. Turn ON the POWER switch on the front panel. When power is turned on, transient voltages in the recorder will cause the display to present meaningless numbers, the STATUS lights to go OFF, and the COUNTER OVERFLOW lights to go ON. Check that all overflow lights are in working condition.

Use the RESET switch to clear the recorder and establish initial conditions. The SEQUENCE display should be blank and the TIME INTERVAL display should read all zeros. The COUNTER OVERFLOW lights should be OFF and the STATUS lights should be ON indicating the circuits can be triggered.

A channel is triggered when its input signal crosses the channel reference voltage level. Each channel's triggering point can be independently adjusted using the REFERENCE VOLTAGE LEVEL controls on the front panel.

Connect a voltmeter to the reference MONITOR terminal and select the channel to be adjusted using the selector dial. While monitoring the reference voltage level, make any adjustments required using a screwdriver to turn the appropriate ADJUST screw. When all adjustments are made, return the selector dial to the OFF position and disconnect the voltmeter.

Select the time base desired using the rotary switch to the right of the RESET button. The decimal point location in the display panel indicates the range selected. At maximum count the range will be .9999, 9.999, or 99.99 milliseconds.

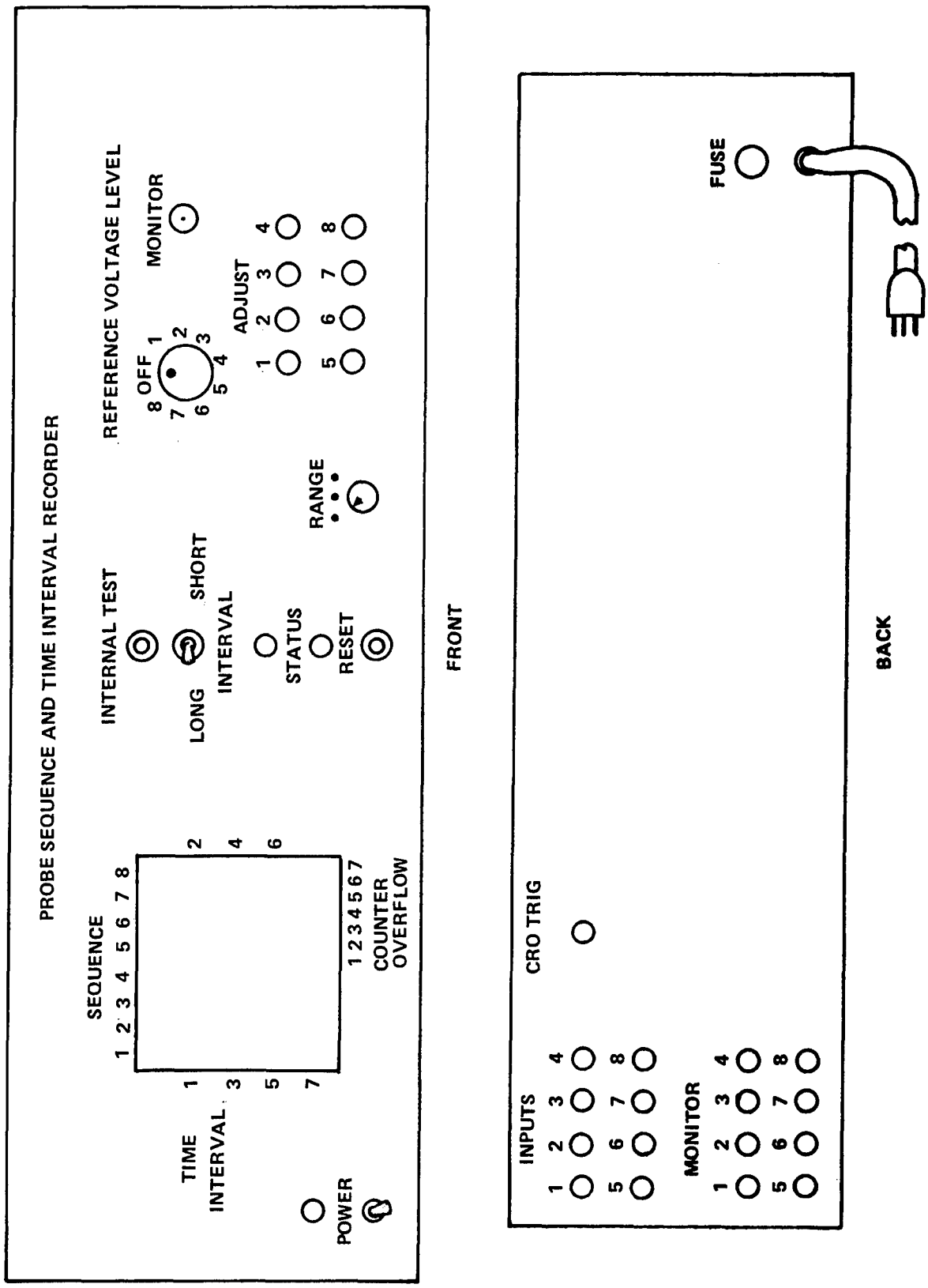

FIGURE C6 RECORDER PANEL LAYOUT

To check operation of the recorder, first clear the circuits using the RESET switch. Select a LONG or SHORT INTERVAL and press the INTERNAL TEST swtich. The internally generated SEQUENCE display reads in order from 1 to 8. ALL TIME INTERVAL readings should be 4000 for LONG intervals and 0004 for SHORT intervals, ± 1 count. The decimal point location will be determined by the range selected. The COUNTER OVERFLOW lights are not triggered during an internal test sequence. After a test, the recorder must be manually RESET to allow the system to accept external signals.

DISTRIBUTION

	Copies
Chief of Naval Material Washington, DC 20360	
Commander Naval Air Systems Command Attn: AIR-350 AIR-330 Department of the Navy Washington, DC 20361	
Commander Naval Sea Systems Command Attn: SEA-09G32 SEA-03B SEA-62R SEA-62R2 SEA-62R3 SEA-62R32 SEA-64E Department of the Navy Washington, DC 20362	2
Director Strategic Systems Project Office (PM-1) Attn: SP-273 (R. M. Kinert) SP-27311 (E. L. Throckmorton, Jr.) John F. Kincaid Department of the Navy Washington, DC 20376	
Office of Naval Research Attn: Rear Admiral A. J. Baciocco, Jr. ONR-473 (R. Miller) ONR-200B (J. Enig) ONR-741 (Technical Library) Department of the Navy Arlington, VA 22217	

DISTRIBUTION (Cont.)

Copies

Commander
Naval Weapons Center
Attn: Code 556
Technical Library
H. D. Mallory
Code 3264
Code 3205 (C. Thelin)
Code 32052 (L. Smith)
Code 388 (R. L. Derr, T. Boggs)
Code 383 (H. D. Mallory)
China Lake, CA 93555

Director
Naval Research Laboratory
Attn: Technical Information Section 2
Washington, DC 20375

Office of Chief of Naval Operations
Operations Evaluation Group (OP03EG)
Washington, DC 20350

Director
Office of the Secretary of Defense
Advanced Research Projects Agency
Washington, DC 20301

Commanding Officer
Naval Weapons Station
Attn: R&D Division
Code 50
Yorktown, VA 23691

Commanding Officer
Naval Propellant Plant
Attn: Technical Library
Indian Head, MD 20640

Commanding Officer
Naval Explosive Ordnance Disposal Facility
Attn: Information Services
Indian Head, MD 20640

McDonnell Aircraft Company
Attn: M. L. Schimmel
P. O. Box 516
St. Louis, MO 63166

DISTRIBUTION (Cont.)

Copies

Commanding Officer
Naval Ammunition Depot
Crane, IN 47522

Commanding Officer
Naval Underwater Systems Center
Attn: LA 151-Technical Library
Newport, RI 02840

Commanding Officer
Naval Weapons Evaluation Facility
Attn: Code AT-7
Kirtland Air Force Base
Albuquerque, NM 87117

Commanding Officer
Naval Ammunition Depot
Attn: QEL
Concord, CA 94522

Superintendent Naval Academy
Attn: Library
Annapolis, MD 21402

Naval Plant Representative Office
Strategic Systems Project Office
Lockheed Missiles and Space Company
Attn: SPL-332 (R. H. Guay)
P. O. Box 504
Sunnyvale, CA 94088

Hercules Incorporated
Allegany Ballistics Laboratory
Attn: Library
P. O. Box 210
Cumberland, MD 21502

AMCRD
5001 Eisenhower Avenue
Alexandria, VA 22302

Redstone Scientific Information Center
U. S. Army Missile Command
Attn: Chief, Documents 2
Redstone Arsenal, AL 35809

DISTRIBUTION (Cont.)

Copies

Commanding Officer
Army Armament Research and
Development Command
Energetic Materials Division
Attn: Louis Avrami, DRDAR-LCE
Dover, NJ 07801

Commanding General
Attn: BRL Library
DRDAR-BLT (P. Howe)
Aberdeen Proving Ground, MD 21005

Commanding Officer
Harry Diamond Laboratories
Attn: Library
Keith Warner
2800 Powder Mill Road
Adelphi, MD 20783

Armament Development & Test Center
DLOSL/Technical Library
Eglin Air Force Base, Florida 32542

Commanding Officer
Naval Ordnance Station
Louisville, KY 40124

Director
Applied Physics Laboratory
Attn: Library
Johns Hopkins Road
Laurel, MD 20810

U. S. Department of Energy
Attn: DMA
Washington, DC 20545

Director
Defense Nuclear Agency
Washington, DC 20305 2

Research Director
Pittsburgh Mining and Safety
Research Center
Bureau of Mines
4800 Forbes Avenue
Pittsburgh, PA 15213

DISTRIBUTION (Cont.)

Copies

Director
Defense Technical Information Center
Cameron Station
Alexandria, VA 22314 — 12

Goddard Space Flight Center, NASA
Glenn Dale Road
Greenbelt, MD 20771

Lawrence Livermore National Laboratory
University of California
Attn: M. Finger
E. James
E. Lee
P. Urtiew
C. Tarver
P. O. Box 808
Livermore, CA 94551

Sandia Laboratories
Attn: R. J. Lawrence, Div. 5166
P. O. Box 5800
Albuquerque, NM 87115

Director
Los Alamos Scientific Laboratory
Attn: Library
L. C. Smith
B. G. Craig
H. Flaugh
C. Forest
P. O. Box 1663
Los Alamos, NM 87544

Chairman
DOD Explosives Safety Board
Attn: Dr. T. A. Zoker
2461 Eisenhower Avenue
Alexandria, VA 22331

Aerojet Ordnance and Manufacturing
Company
9236 East Hall Road
Downey, CA 90241

DISTRIBUTION (Cont.)

	Copies
Hercules Incorporated Research Center Attn: Technical Information Division B. E. Clouser Wilmington, DE 19899	
Thiokol/Huntsville Division Attn: Technical Library Huntsville, AL 35807	
Shock Hydrodynamics Division Whittaker Corporation Attn: Dr. L. Zernow 4716 Vineland Avenue North Hollywood, CA 91706	2
Stanford Research Institute Attn: D. Curran 333 Ravenswood Avenue Menlo Park, CA 94025	
Thiokol/Wasatch Division Attn: Technical Library P. O. Box 524 Brigham City, UT 84302	
Thiokol/Elkton Division Attn: Technical Library P. O. Box 241 Elkton, MD 21921	
Teledyne McCormick Selph P. O. Box 6 Hollister, CA 95023	
Lockheed Missiles and Space Co., Inc. P. O. Box 504 Sunnyvale, CA 94086	
R. Stresau Laboratory, Inc. Star Route Spooner, WI 54801	
Rohm and Haas Huntsville, Defense Contract Office Attn: H. M. Shuey 723-A Arcadia Circle Huntsville, AL 35801	

DISTRIBUTION (Cont.)

Copies

U. S. Army Foreign Service
and Technology Center
220 7th Street, N.E.
Charlottesville, VA 22901

Princeton Combustion Research Laboratories, Inc.
1041 U. S. Highway One North
Attn: M. Summerfield
N. Messina
Princeton, NJ 08540

Pennsylvania State University
Department of Mechanical Engineering
Attn: K. Kuo
University Park, PA 16802

Ballistic Research Laboratories
Attn: N. Gerri
P. Howe
R. Frey
D. Kooker
Aberdeen Proving Ground, MD 21005

Paul Gough Associates
1048 South Street
Portsmouth, NH 03801

Hercules Incorporated, Bacchus Works
Attn: B. Hopkins
Library 100-H
D. Caldwell 2
P. O. Box 98
Magna, UT 84044

Professor H. Krier
A & A Engineering Department
101 Transportation Building
University of Illinois
Urbana, IL 61801

Chemical Propulsion Information Agency
The Johns Hopkins University
Applied Physics Laboratory
Johns Hopkins Road
Laurel, MD 20810

DISTRIBUTION (Cont.)

	Copies
ITT Research Institute Attn: H. S. Napadensky 10 West 35th Street Chicago, IL 60616	
Erion Associates, Inc. Attn: W. Petray 600 New Hampshire Avenue, Suite 870 Washington, DC 20037	
Brigham Young University Department of Chemical Engineering Attn: Dr. M. W. Beckstead Provo, UT 84601	
Library of Congress Attn: Gift and Exchange Division Washington, DC 20540	4

NDW-NSWC(W)-5605/1 (Rev. 5-78)

TO AID IN UPDATING THE DISTRIBUTION LIST FOR NAVAL SURFACE WEAPONS CENTER, WHITE OAK TECHNICAL REPORTS PLEASE COMPLETE THE FORM BELOW:

TO ALL HOLDERS OF NSWC/TR 79-79
by Harold W. Sandusky, Code R13
DO NOT RETURN THIS FORM IF ALL INFORMATION IS CURRENT

A. FACILITY NAME AND ADDRESS *(OLD) (Show Zip Code)*

NEW ADDRESS *(Show Zip Code)*

B. ATTENTION LINE ADDRESSES:

C.

☐ REMOVE THIS FACILITY FROM THE DISTRIBUTION LIST FOR TECHNICAL REPORTS ON THIS SUBJECT.

D.
NUMBER OF COPIES DESIRED _____

GPO 930-764